Degree-2 Spherical Harmonics of the Earth's Gravity field from Earth Rotation Parameters and SLR measurements to LAGEOS

Craig Matthew Hancock

Thesis Submitted for the Degree of

Doctor of Philosophy

School of Civil Engineering and Geosciences

University of Newcastle Upon Tyne

January 2012

Degree-2 Spherical Harmonics of the Earth's Gravity field from Earth Rotation Parameters and SLR measurements to LAGEOS

Craig Matthew Hancock
Newcastle University, Doctor of Philosophy, July 2011

Abstract

The gravity field of the Earth is fundamental to subjects such as geodesy and geophysics. Many observations within geodesy refer directly or indirectly to gravity. Geodetic techniques provide information regarding the Earth and the processes that act on it. Mass and angular momentum are, according to physics, conserved in a closed system. The Earth interacts very little with components outside of it and can be thought of as a closed system. Mass components in one reservoir of the Earth system are exchanged with others. Mass redistribution within the Earth system is caused by geophysical processes. This movement of geophysical fluid (mass) causes variations in the Earth's rotation, gravity field and geocentre. The improvement of geodetic techniques over the last few decades allows us to measure the effects of these processes on the Earth to an unprecedented accuracy.

Earth rotation parameters (ERPs) are excited by variations in the mass distribution on the Earth's surface and the exchange of angular momentum between the atmosphere and oceans and the solid Earth. The same mass redistribution causes temporal changes in the gravity field coefficients with the second degree harmonics related to the rotational deformation and hence to changes in the Earth's inertial tensor. If precise models of the atmospheric and oceanic angular momentum are available solution for polar motion and degree-2 Stokes harmonics can be unified. In this study we utilise SLR tracking of LAGEOS to compare (i) degree-2 harmonics from ERPs and gravitation, and (ii) LAGEOS excitation functions and geophysical data (mass + motion). To what extent a unified approach is possible with current models for AM data and gravity mass change estimated from ERP within orbit determinations is investigated. Finally, the ability of SLR to calculate the motion of the Earth's geocentre is also investigated.

Keywords: SLR, Earth Rotation, Gravity Field, Mass Redistribution

Acknowledgements

This has taken a long time and at times it has been a struggle to get to the end! Due to this I have numerous people that I need to thank for their time, expertise, patience, encouragement and support.

Firstly I thank my supervisor, Professor Philip Moore, for his help and guidance throughout my PhD studies. Without his support this would not have been possible.

I also need to thank my current employers, the University of Nottingham, for allowing me time to work on my PhD during work. My special thanks go to Professor Gethin Roberts for his continued encouragement throughout my time in Nottingham.

I would also like to thank all my fellow PhD students and staff at Newcastle University who provided advice and help throughout my PhD in numerous ways. Special thanks must go to Dr Qiang Zhang for his advice, Dr David Lavellee for the use of his TANYA software and to Dr Nigel Penna for the use of his Ocean Tide Loading Algorithm. I would also like to thank Dr Matt King and Professor Peter Clarke for their UNIX support and for not shutting down the UNIX before I had finished!

Finally I would like to express my appreciation to my family and friends who have continued to support and encourage my efforts to finish and submit my PhD thesis. They are too many to mention all by name but I appreciate all the help myself and my family have received to enable me to have the time and peace of mind to complete my studies. I would like to thank my parents, my brothers Jared and Ben and my sister Amy.

To those who have suffered the most I give the most thanks. Without the love, support and patience of my wife Frances and our 3 children, Joshua, Leah and Jacob I would not have been able to finish this study. I am grateful that they have gone almost without having a husband or father for the last 3 months (my wife would say 6 years!) so that I would have the time to finish. Thank you!

Contents

List of Figures

List of Tables

Acronyms

AU	**Astronomical Units**
CSR	**Centre for Space Research**
DORIS	**Doppler Orbitography and Radio positioning Integrated by Satellite**
ECCO	**Estimating the Circulation and Climate of the Ocean**
ECMWF	**The European Centre for Medium-Range Weather Forecasts**
ENSO	**El Niño/La Niña-Southern Oscillation**
ENVISAT	**Environmental Satellite**
ERP	**Earth Rotation Parameters**
FAUST	**Newcastle University's in House Precise Orbit Determination Software**
GAST	**Greenwich Apparent Sidereal Time**
GMST	**Greenwich Mean Sidereal Time**
GNSS	**Global Navigation Satellite Systems**
GPS	**Global Positioning System**
GRACE	**Gravity Recovery and Climate Experiment**
HAM	**Hydrological Angular Momentum**
HAMF	**Hydrological Angular Momentum Function**
IB	**Inverted Barometer**
IERS	**International Earth Rotation Service**
ILRS	**International Laser Ranging Service**
ITRF	**International Terrestrial Reference Frame**
IVS	**International VLBI Service**
JD	**Julian Date**
JMA	**Japanese Metrological Agency**
JPL	**Jet Propulsion Laboratory**
LAGEOS	**Laser Geodynamics Satellites**
LOD	**Length of Day**
MIT	**Massachusetts Institute of Technology**
NASA	**National Aeronautics and Space Administration**
NCAR	**National Center for Atmospheric Research**

NCEP	**National Centers for Environmental Prediction**
OAM	**Oceanic Angular Momentum**
OAMF	**Oceanic Angular Momentum Function**
OTL	**Ocean Tide Loading**
PM	**Polar Motion**
POD	**Precise Orbit Determination**
PRARE	**The Precise Range and Range-Rate Equipment**
SINEX	**Solution Independent Exchange Format**
SLR	**Satellite Laser Ranging**
SO	**Southern Oscillation**
TAI	**International Atomic Time**
TDB	**Barycentric Dynamical Time**
TT	**Terrestrial Time**
UKMO	**United Kingdom Met Office**
UT1	**Universal Time**
UTC	**Coordinated Universal Time**
VLBI	**Very Long Baseline Interferometry**
XP	**X Pole**
YP	**Y Pole**

Chapter 1

1 Introduction

1.1 Introduction

Over the past few decades there have been great advances in the quality and quantity of geodetic technology and data availability. This advancement was driven partly by the need to improve knowledge and understanding of the rotational dynamics of the Earth system.

The causes of variations in Earth rotation can be divided into two main categories, 1) the gravitational interaction between the Earth and other celestial bodies (such as the Sun, Moon and other major planets) and 2) interactions of the Earth's geophysical fluids (atmosphere, oceans, water storage, core etc). The drive to understand these interactions more, led to the development of better techniques to observe these phenomena and soon routine daily determinations of Earth Rotation Parameters (ERPs) were being determined using Very Long Baseline Interferometry (VLBI) (Carter et al., 1985, Robertson, 1991), Satellite Laser Ranging (SLR) (Tapley et al., 1985) and Lunar Laser Ranging (LLR) (Dickey and Eubanks, 1985). In addition to these Earth Rotation Parameters even higher frequency time series are routinely derived using Global Navigation Satellite Systems (GNSS) such as the Global Positioning System (GPS) (Herring et al., 1991; Lichten et al., 1992).

Rotational variations have been linked to a number of geophysical phenomena, such as fluid dynamic processes in the atmosphere, oceans and core as well as the exchange of mass between the atmosphere, oceans and the "solid Earth". Earth orientation data provides valuable information on the processes of mass redistributions within the Earth system on a global scale which is typically poorly determined from other techniques. The variations of the Earth are not easily understood in isolation but can be better understood by the use and understanding of theory and data from other areas of geophysics and thus makes the science of Earth rotation a multi-disciplinary science encompassing geodesy, meteorology, oceanography, geomagnetism, hydrology and others (Eubanks, 1993).

The movements of mass within the Earth system that affect rotational dynamics are the same processes that affect the variations of the Earth's gravity field, and hence the geoid. Knowledge of the Earth's gravity field is important for many subject areas such as surveying, geodesy, oceanography, hydrology, and geophysics and satellite orbit determination. It is important in geodesy as it contributes to knowledge about the size and shape of the Earth and therefore aids in the understanding of how the Earth is changing on a global scale.

The temporal variations of the gravity field are important in the study of many scientific fields. They are regarded as important for understanding the Earth's interior structure and characteristics, as well as providing valuable information about the redistribution of mass around the Earth. This thesis will concentrate on the links between observed parameters of the rotation of the Earth and how these relate to models of the Earth's geophysical fluids and gravity.

The relationship between ERPs and the low degree spherical harmonics of the Earth's gravity field J2, C21 and S21 has been described in Wahr (1982) and Gross and Lindqwister (1992) has been utilised to compare these low degree harmonics derived from geodetic sources, SLR, GPS and GRACE, from geophysical models and from ERPs. Good agreement has been found between the different sources.

Newcastle University's Precise Orbit Determination (POD) software, *FAUST*, (Boomkamp, 1998) is a multi-satellite, multi arc satellite orbit determination software. It uses a least squares process to minimise the sum of the residuals to obtain the best position of the satellite at a specific epoch. *FAUST* can process data from Doppler Orbitography and Radio positioning Integrated by Satellite (DORIS), the Precise Range and Range-Rate Equipment (PRARE) and SLR as well as satellite altimetry (raw heights and crossovers), Gravity Recovery And Climate Experiment (GRACE) inter-satellite range-rate data and Cartesian positioning derived independently from say GNSS tracking.

FAUST has been improved, by the author, by bringing it in line with the IERS conventions 2003 (McCarthy and Petit, 2003) as well as adding to the functionality of

the software by adding the ability of the software to estimate the Earth orientation parameters XP, YP and Length of Day (LOD).

In this thesis *FAUST* has been used to process SLR data to the geodetic satellites LAGEOS I and LAGEOS II from 1996 – 2007, estimating the low degree spherical harmonics of the Earth's gravity field, ERPs and station coordinates. These results have been used to assess the agreement between the low degree harmonics of the gravity field derived directly from the orbit of LAGEOS and the same harmonics estimated from the ERP values also estimated from the same SLR defined orbit and geophysical models.

However, the typically low sensitivity of orbits to gravity field variability or the high correlation between the harmonics means that there is little possibility of space geodetic techniques providing accurate measurements of mass change, even at low spatial resolutions, at intervals of less than a few days/weeks (e.g. SLR, GPS) or months (e.g. GRACE). However, the disparity in temporal resolutions raises the possibility of simultaneously recovering and using higher frequency degree-2 harmonics from the ERP data (on utilizing angular momentum data from geophysical models) within an orbital determination procedure. High correlations are also found between the harmonics which have an effect on the overall fit of the orbit and the accuracy of the harmonics themselves.

FAUST has been modified to utilise the relationship and relatively good agreement between the low degree harmonics derived from SLR orbit determination to LAGEOS and ERPs to solve for J2, C21 and S21 on a daily basis, as well as solving for one correction over a 15 day period to mimic what is currently done within the normal gravity estimating process. The main aim of this thesis is to investigate to what extent this integrated orbit determination process is useful in determining the low degree harmonics and whether the models and ERP estimates are accurate enough to obtain good estimates of the corrections to J2, C21 and S21 to glean more information about the high frequency variations in the Earth's gravity field from space geodetic techniques. This will be done by comparing the same orbital period processed while estimating different sets of parameters.

Finally, as mass redistribution within the Earth system also contributes to the movement of the centre of mass of the Earth with relation to the centre of the Earth coordinate system, SLR orbits produced by *FAUST* have also been used to investigate how SLR determines geocentre motion when compared with the same estimates derived from GPS and from loading models.

1.2 Thesis Overview

This thesis will investigate the relationship between the temporal variations in the Earth's gravity field, the ERPs and the geophysical models derived from collected geophysical data. The main themes of this thesis are the Earth's Gravity field and its estimation from SLR, ERPs and their estimation from SLR and the usefulness of using ERP-derived gravity field estimates in a combined orbit determination solution.

1.2.1 Chapter 2

This chapter describes the fundamental theory of the Earth's gravity field that is the underlying subject of this thesis. It also describes how the Earth's gravity field can be described in terms of spherical harmonics. Finally it gives a brief introduction to computing the gravity field from precise orbit determination.

1.2.2 Chapter 3

This chapter reviews the theory of Earth rotation. It very briefly addresses and describes the main three areas of Earth rotation, the theories of precession, nutation and polar motion. The theory of rigid body rotation is treated initially as it provides the background theory before the theory of non-rigid body rotation can be introduced. This provides the equations that relate the variations of rotation in the Earth to the Earth's inertia tensor and therefore the excitation functions that describe how the rotation of the Earth can be excited by geophysical processes. This mathematical theory will be used in subsequent chapters to relate the variations of rotations within the Earth system, to the observations of gravity field variations, various loading and angular momentum models and Earth rotation computed in *FAUST*.

1.2.3 Chapter 4

Chapter 4 gives discussion and analysis of the available geophysical models from various organisations that provide data on how mass in the atmosphere, oceans and continental water storage change as a function of time. It gives a review of each of the possible sources of variations in the rotation of the Earth and gravity field and estimates of the sizes of these. The mathematical theory described in Chapter 3 is expanded to show how estimates of geophysical processes in the atmosphere, oceans and continental water storage can be expressed as excitation functions of the Earth's rotation.

Plots of the excitation functions (atmospheric, oceanic and hydrological) are given and comment is made about the contributions of each excitation function to the variations in the rotation of the Earth from published literature.

Finally an analysis of the excitation functions of the atmosphere computed by various different organisations is presented.

1.2.4 Chapter 5

This chapter gives a description of the precise orbit determination software *FAUST* and gives an overview of the amendments made to the software by the author for the purposes of bringing it in line with the IERS conventions 2003 (McCarthy and Petit, 2003) and also for the purpose of the research within this thesis and future research on Earth rotation and gravity. The methods for computing the corrections for the orbit determination process are described.

The orbit determination strategy is then described in full showing which models were used in the process as well as showing the rejection criteria that was used for processing the data. This is followed by an analysis of the fit of several different orbit determination strategies that will be used for comparison purposes later in the thesis.

1.2.5 Chapter 6

Chapter 6 describes the method for computing corrections to the low degree spherical harmonics of the Earth's gravity field using excitation functions for motion computed from geophysical models, described in Chapter 4 and the ERPs computed within *FAUST*.

Following on from this theory, comparisons between excitation functions estimated from the different sources and gravity field harmonics estimated from different sources are compared to see how well they agree with each other. The aim of this analysis is to analyse whether estimating low degree spherical harmonics in this manner is good enough to expect an improvement in the orbit.

1.2.6 Chapter 7

Chapter 7 describes a novel method of estimating gravity field harmonics in an iterative orbit determination process using geophysical models and ERPs. It presents and discusses the results of using gravity field harmonics estimated from ERPs. The RMS values from the orbits presented in Chapter 5 of this thesis are compared to the RMS values of the orbits using the new method.

In addition to this the improvements and deteriorations of the orbits at specific epochs are analysed in more detail to try to identify the reason why some epochs show improvements while other show deterioration.

1.2.7 Chapter 8

Chapter 8 describes analysis of the variation of the geocentre of the Earth from SLR, GPS and loading models. The methods of processing the data and the different models used have been described.

Estimates of geocentre motion from SLR orbits determined using *FAUST* are validated by comparing with the same estimates from International Laser Ranging Service (ILRS) combination SLR contribution to ITRF2005. These results show good agreement. The

geocentre estimates from SLR, GPS and the loading models are then analysed to gain an understanding of how well the estimates from different techniques agree with one another.

1.2.8 Chapter 9

Chapter 9 provides a review of the thesis and a discussion of the results that have been described in previous chapters. It also gives recommendations for future research in this particular subject area.

Chapter 2

2 Gravity Field Theory

2.1 Introduction

Understanding the gravity field of the Earth is fundamental to subjects such as geodesy and geophysics. Many observations within geodesy refer directly or indirectly to gravity and thus modelling of these observations requires knowledge of the gravity field or geopotential. The common approach for representing the global gravity field of a planetary body is through the use of spherical harmonics, which will be discussed further in this chapter. The gravity field is one of the key issues discussed in this thesis and therefore is explained separately. This thesis will however cover only the key aspects of gravity field theory relevant to the study; for a more in depth discussion of the subject see Bomford (1980), Torge (2001) and Heiskanen and Moritz (1967).

2.2 The Earth's Gravity field

The analysis of the external gravity field of the Earth gives information regarding the internal structure of the Earth (Torge, 2001). If gravity is known on the Earth's surface then the shape of the Earth can be determined. The geoid, which is the equipotential surface of the Earth's gravity field and coincides on average with mean sea level, is important for height referencing. Knowledge of the gravity field of the Earth is also required for orbit determination of Earth satellites.

The starting point for all discussions on gravity is Newton's Law of Gravitation (1687). The gravitational attraction between two point masses is given by

$$\underline{F} = -G\frac{m_1 m_2}{l^2}\underline{\ddot{\rho}} \qquad \textbf{(2.1)}$$

where $\underline{F}$ is the gravitational force (attractive force), m_1, m_2 are masses that are separated by distance l, $\underline{l^{\ddot{o}}}$ a unit vector from point one to point two and G is Newton's gravitational constant given as:

$$G = 6.673 \times 10^{-11} m^3 kg^{-1} s^{-2} \qquad \textbf{(2.2)}$$

We can connect the gravitational force F with the potential V by introducing the gradient vector.

$$GradV = \left(\frac{\partial V}{\partial x} \frac{\partial V}{\partial y} \frac{\partial V}{\partial z} \right) \qquad \textbf{(2.3)}$$

We can now consider the gravitational force acting between the Earth and an Earth orbiting satellite in a global Cartesian coordinate system (X, Y, Z) see Figure 2.1.

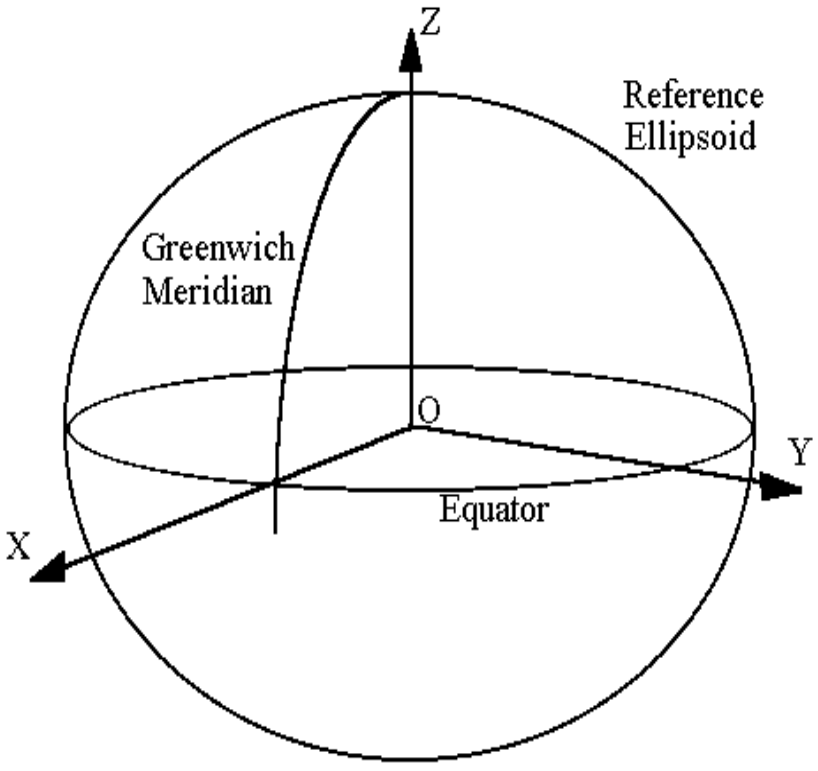

Figure 2.1 Cartesian coordinate system

For simplicity let $m_{2,}$ an elemental mass of the Earth, be equal to m and m_1 the mass of the satellite, be a unit mass. According to Newton's second law of motion, "The rate of change of momentum of the body is proportional to the force impressed and is in the same direction in which the force acts", an orbiting satellite with a gravitational force $\underline{F}$ will experience an acceleration $\underline{a}$ of magnitude.

$$\underline{a} = \frac{Gm}{l^2}\hat{\underline{l}} \qquad \textbf{(2.4)}$$

The representation of gravitational acceleration is simplified if expressed as a scalar quantity "potential" instead of the vector quantity "acceleration". This is because gravity is invariant to rotations (Torge, 2001). We can therefore express equation 2.4 as:

$$\underline{a} = GradV \qquad \textbf{(2.5)}$$

The gravitational potential at any point is the work done against the force of gravitation in moving a body from infinity to that point. The Earth is composed of an infinite number of these elemental masses, represented as m. To obtain the total gravitational attraction of the Earth to an object outside the Earth, such as an artificial satellite, it can be expanded as a triple integral over the whole Earth. Let δv be an elemental volume of the Earth centred at (x', y', z') with a density of ρ(x, y, z). The element then has mass δm = ρδv .The gravitational potential due to δm is

$$V = \frac{Gm}{l} \text{ with } \lim_{l\to\infty} V = 0 \qquad \textbf{(2.6)}$$

Therefore the gravitational potential over the whole earth is given by

$$V = G\iiint_{Earth}\frac{\delta m}{l} = G\iiint_{Earth}\frac{\rho}{l}\delta v \qquad \textbf{(2.7)}$$

We can now show that V in this case satisfies Laplace's equation at every point which is not occupied by matter (MacMillan, 1958).

$$\nabla^2 V = \frac{\partial^2 V}{\partial x^2}\frac{\partial^2 V}{\partial y^2}\frac{\partial^2 V}{\partial z^2} = 0 \qquad \textbf{(2.8)}$$

The density function of the Earth ρ = ρ(r') is not well determined. Therefore we cannot use Newton's Law of Gravitation to find the gravity potential of the Earth from equation 2.7. However it is possible to solve Laplace's differential equation (equation 2.8) as a convergent series expansion of V (Torge, 2001). This can be derived from the reciprocal of the distance *l* from equation 2.7 (Blakely, 1995).

$$\frac{1}{l} = (r^2 + r'^2 - 2rr'\cos\psi)^{-1/2} = \frac{1}{r}\left(1 + \left(\frac{r'}{r}\right)^2 - 2\frac{r'}{r}\cos\psi\right)^{-1/2}. \qquad \textbf{(2.9)}$$

Here r and r' are the position vectors of the attracted point P from Figure 2.1, ψ is the central angle from the origin of the coordinate system O to P and P' respectively. We can now expand 1/*l* in a series converging for r'< r (Heiskanen and Moritz, 1967; Blakely, 1995)

$$\frac{1}{l} = \frac{1}{r}\sum_{l=0}^{\infty}\left(\frac{r'}{r}\right)^l P_l(\cos\psi) \qquad \textbf{(2.10)}$$

Here

$$P_l(t) = \frac{1}{2^l \times l!} \times \frac{d^l}{dt^l}(t^2 - 1)^l \qquad \textbf{(2.11)}$$

The $P_l(\cos\psi)$ terms represent polynomials, known as Legendre polynomials of the l^{th} degree in cosψ. They are computed using equation 2.11, where $t = \cos\psi$.

We can now introduce a unit sphere with a spherical coordinate system, where r is the geocentric distance from the attracting body, θ is the co-latitude and λ the longitude.

Through the decomposition of Pl(cosψ) by introducing the longitude λ and geocentric latitude θ of point r as

$$x = r\sin\theta\cos\lambda$$
$$y = r\sin\theta\sin\lambda$$
$$z = r\cos\theta$$

we obtain

$$V = \frac{G}{r}\sum_{l=0}^{\infty}\sum_{m=0}^{l} k\frac{(l-m)!}{(l+m)!}\times$$
$$\frac{1}{r^{l}}\left(\begin{array}{l} P_{lm}(\cos\theta)\cos m\lambda \iiint_{Earth} r'^{l} P_{lm}(\cos\theta')\cos m\lambda^{l} dm \\ + P_{lm}(\cos\theta)\sin m\lambda \iiint_{Earth} r'^{l} P_{lm}(\cos\theta')\sin m\lambda^{l} dm \end{array}\right) \qquad \textbf{(2.12)}$$

where k equals 1 when m = 0 and 2 when m $\neq$ 0 (Torge, 2001).

Any solution of Laplace's equation is known as a harmonic function. The solution is given by separating the variables in spherical coordinates. The general solution of Laplace's equation in spherical coordinates is

$$V = \frac{Gm}{r}\left[1+\sum_{l=1}^{\infty}\sum_{m=0}^{l}\left(\frac{\mathrm{Re}}{r}\right)^{l}\left(C_{lm}\cos m\lambda + S_{lm}\sin m\lambda\right)P_{lm}\cos(\theta)\right] \qquad \textbf{(2.13)}$$

where C_{lm} and S_{lm} are coefficients of the Earth's gravity field (unnormalised) which describe the dependence on the Earth's internal mass distribution (Montenbruck and Gill, 2000), M is the mass of the Earth, Re is the equatorial radius of the Earth and P_{lm} are Legendre functions of the first kind given by

$$P_{lm}(t) = (1-t^2)^{\frac{m}{2}} \frac{d^m}{dt^m} P_l(t) \qquad \textbf{(2.14)}$$

The harmonic coefficients, also known as Stokes' coefficients, of the Earth's gravity field can now be written in spherical coordinates as

$$C_{lm} = C_l = \frac{1}{M} \iiint_{Earth} \left(\frac{r'}{\mathrm{Re}} \right)^l P_l(\cos\theta') \rho dv$$

$$\begin{Bmatrix} C_{lm} \\ S_{lm} \end{Bmatrix} = \frac{2}{M} \times \frac{(l-m)!}{(l+m)!} \iiint_{Earth} \left(\frac{r'}{\mathrm{Re}} \right)^l P_{lm}(\cos\theta') \rho dv \qquad \textbf{(2.15)}$$

$$dv = r'^2 \cos\theta' dr' d\theta' d\lambda'$$

These formulae link the gravity field of the Earth and the Earth's internal density ρ. As the coefficients tend to small values, partly because of the nature of the Earth's gravity field and partly because the associated Legendre functions tend to large values as the degree increases, it is convenient to write spherical harmonics in their unnormalised form rather than in their unnormalised state. Conversion from unnormalised to unnormalised harmonics is given by Torge (2001), Montenbruck and Gill (2000), and Lambeck (1980b).

$$\overline{P}_{lm} = \sqrt{\frac{(2-\delta_{0m})(2l+1)(l-m)!}{(l+m)!}} P_{lm}$$

$$\begin{Bmatrix} \overline{C}_{lm} \\ \overline{S}_{lm} \end{Bmatrix} = \sqrt{\frac{(l+m)!}{(2-\delta_{0m})(2l+1)(l-m)!}} \begin{Bmatrix} C_{lm} \\ S_{lm} \end{Bmatrix} \qquad \textbf{(2.16)}$$

2.3 Spherical Harmonics

To gain a better understanding of why we use spherical harmonics as a representation of the geopotential of the Earth, we need to understand some of the characteristics of spherical harmonics and what the harmonics themselves represent in the real world. Spherical harmonics are functions of two coordinates θ,λ on the surface of a unit sphere. Spherical Harmonics are orthogonal; this means that for each function, using different degree and order (l and m), they each contribute independent information. An advantage of using spherical harmonics as a representation of the Earth's gravity field is that they are easy to visualise.

Following on from equation 2.13 the functions

$$P_{lm}(\cos\theta)\cos m\lambda, \qquad P_{lm}(\cos\theta)\sin m\lambda, \tag{2.17}$$

depending on θ and λ are known as Laplace's surface harmonics. They characterise the behaviour of a function on a unit sphere (Torge, 2001).

Spherical harmonics when m = 0 are known as zonal harmonics. Zonal harmonics have no dependence on longitude and have *l* zeros between ±90° in latitude. This means that for even values of *l*, the zonal harmonics are symmetric about the equator and for odd value of *l*, they are asymmetric. As the degree increases so the number of zeros between ±90° in latitude also increases. This means that the higher the degree the smaller the scale of the latitudinal variations in the Earth's geopotential. Therefore if one is only interested in the large scale changes in the Earth's gravity field only low degree harmonics need be considered. The most important of the zonal harmonics is C20 which is of the order 10^{-3} in size and accounts for the oblateness of the Earth.

Another special case in spherical harmonics is when $m = l$. These are called sectorial harmonics and, in contrast to zonal harmonics, vary with longitude. As with the zonals, however, the higher the degree the finer the spatial representation is acquired from the

harmonics. All remaining harmonics are known as tesserals and are defined when m > 0 and m < l. Tesserals have the same properties as sectorial harmonics (Kaula, 1966; Torge, 2001).

The $P_{lm}(\cos\theta)$ up to l = 2 are given below according to Torge (2001).

$$P_0 = 1, \qquad P_0 = \cos\theta, \qquad P_0 = \frac{3}{2}\cos^2\theta \tag{2.18}$$

The degree one terms l = 1 are related to the centre of mass of the system. If we choose the origin of the reference frame to be the instantaneous centre of mass of the total Earth and atmosphere then, in this inertial reference frame, the degree-1 coefficients are zero. In an Earth fixed terrestrial reference frame this origin, often referred to as the geocentre, r moves in time and space due to the redistribution of mass within the Earth (Feissel-Vernier et al., 2006). The motion of the geocentre obeys the law of conservation of angular momentum in an Earth fixed reference frame. The degree-1 terms of the gravity field are related to the three coordinates of the geocentre; x_g, y_g, z_g in a terrestrial reference frame. The geocentre will be discussed in more detail in Chapter 8.

The second degree spherical harmonics are related to the Earth's inertia tensor I which describes how difficult it is to induce an angular rotation of an object around a particular axis. The relationship between the Stokes' coefficients and the inertia tensor of the Earth is given by:

$$\begin{aligned}
C20 &= \frac{-\left[I_{33} - \frac{1}{2}\left(I_{11} - I_{22}\right)\right]}{MR_e^{\,2}}, \\
C21 &= \frac{-I_{13}}{MR_e^{\,2}}, \qquad S21 = \frac{-I_{23}}{MR_e^{\,2}}, \\
C22 &= \frac{-\left(I_{11} - I_{22}\right)}{4MR_e^{\,2}}, \qquad S22 = \frac{-I_{12}}{2MR_e^{\,2}},
\end{aligned} \tag{2.19}$$

2.4 Precise Orbit Determination and Gravity

From the very beginning of space flight, ground based observations of artificial satellites have allowed scientists to infer the Earth's gravity field through the associated perturbations seen in the orbits of these satellites (Montenbruck and Gill, 2000). The LAGEOS satellites used in this research are especially good at determining the Earth's gravity field, more especially the very long wavelength part (i.e. very low degree and order) of this gravity field. These parameters can be determined from the normal equations in the many precise orbit determination packages that have been developed for this purpose. However gravity values can only be determined over the period of the orbit determination, typically a minimum of 7 days, using this method. One of the main aims of this project is to investigate whether it is possible to use a new method to determine the low degree gravity value to improve the resolution of this data.

2.5 Conclusion

Knowledge of the gravity field is of vital importance in geodesy and particularly in orbital dynamics, with which this thesis is primarily concerned. Knowledge of the basics of the gravity field, and how that gravity field affects the orbits of satellites, is of key importance in understanding the methods and purpose of this study. The methods employed for the gravity models and for solving for low degree harmonics will be discussed in Chapters 4 and 5.

Chapter 3

3 Earth Rotation Theory

3.1 Introduction

Space geodesy uses many kinds of space orientated techniques and measurements including VLBI, lunar, and satellite (Plag et al., 2009; Vanâiécek and Krakiwsky, 1986). These techniques provide information regarding the Earth and the processes that act on it. It is necessary therefore to have an understanding of the different forces that act on the Earth and how the Earth is affected by these processes. Since Earth rotation is fundamental to this thesis a discussion of the theory of the rotation of the Earth follows.

The theory of Earth rotation can be divided into three areas, the study of precession and nutation, the study of polar motion, also known as wobble, and the study of the length of time the Earth takes to spin round its axis, more commonly referred to as Length of Day. In this thesis we are primarily concerned with the latter two parts of Earth rotation theory and their links to gravity and geophysical models. To appreciate how these links come about it is necessary to understand the fundamental principles of firstly rigid body rotation and secondly non-rigid body rotation. This chapter discusses these principles in some detail and derives the important equations needed for first calculating Earth rotation within the orbit determination process and, then, using these Earth rotation values to derive low degree gravity harmonics of the Earth. For a more complete discussion of Earth rotation refer to Munk and MacDonald (1960) and Lambeck (1980b).

3.2 Precession, Nutation, Wobble and Length of Day

In geodesy we are primarily concerned with 1) the Earth's motion around the Sun or annual motion and 2) the movement of the Earth around its instantaneous axis of rotation or diurnal motion. The motion of the Earth around the Sun is perturbed by other planets so that it is not exactly elliptical. The effects of these perturbations are small compared with the orbital dimensions and, for most applications, can be neglected (Vanâiécek and Krakiwsky, 1986). When describing the motion of the Earth around its

instantaneous axis the dimensions of the motion are no longer negligible. The instantaneous axis of rotation of the Earth and the Earth's principal axis of inertia coincide in a rigidly rotating Earth but differ slightly in the presence of external torques. As stated previously, Earth rotation theory can be divided into three different sections, namely precession and nutation; polar motion and Length of Day (LOD). Each one will now be discussed briefly.

3.2.1 Precession

Consider the Earth to be a rigid body travelling around the Sun, and spinning around its own axis. In mechanics this is known as a gyroscope. If an external torque is applied to a spinning gyroscope then the gyroscope describes a circular cone with its vertex at the centre of mass of the gyroscope. For the external torques acting on the Earth the period of the motion around the circular cone is about 26,000 years. In the case of the Earth the external torque is the attraction of other celestial bodies. This motion is known as precession.

3.2.2 Nutation

The orbit of the moon is inclined with respect to the ecliptic by 5º 11´ (Mueller, 1969). The intersection of the lunar orbital plane with the Earth's ecliptic rotates every 18.6 years. This causes a periodic change, a rocking or swaying motion, in the orbital axis of the Earth. This is known as nutation.

3.2.3 Polar motion (Wobble) and Length of Day

In a non-uniform rotating Earth in an Earth fixed coordinate system the Earth's rotation axis varies slightly with time, this is called the Earth's Wobble. The wobble of the Earth, also known as free nutation, is a torque free nutation that accompanies any gyroscopic motion (Vanâiécek and Krakiwsky, 1986). The length of time it takes the Earth to rotate once in this reference frame also varies with time and is known as LOD. Changes in the rotation of the Earth are caused by the redistribution of mass within the Earth thus conserving the angular momentum of that body. This is the main subject of this thesis

and, therefore, will be explained in detail, starting with Earth Dynamics and then linking Earth Dynamics with mass redistribution calculated from geophysical models.

3.3 Earth Dynamics

The understanding of how the Earth moves with respect to different coordinate systems is fundamental to this thesis and will therefore be treated in some detail. Rigid Body rotation gives a basic understanding of the fundamental equations used in rotation theory and will be treated first. Secondly we will discuss non-rigid rotation of the Earth by building upon this knowledge.

3.3.1 Rigid Body Rotation

Before considering how the Earth rotates, i.e. non uniform body rotation, we must consider uniform body rotation. In the absence of internal energy and gravitational and mechanical forces and interactions with other celestial bodies, the Earth, both its solid (crust, mantle, inner core) and fluid (ocean, atmosphere, outer core) parts, would rotate together at a constant rate (Barnes et al., 1983). For a continuous distribution of particles situated throughout space we introduce the following expression for the moments and products of inertia (Rutherford, 1964). Notationally, A, B and C are called the moments of inertia about x_1, x_2, x_3; D, E and F are known as the products of inertia with reference to the axes (x_2, x_3), (x_3, x_1), (x_1,x_2).

$$\begin{aligned} A &= (x_2{}^2 + x_3{}^2)dM, & D &= (x_2x_3)dM, \\ B &= (x_1{}^2 + x_3{}^2)dM, & E &= (x_1x_3)dM, \\ C &= (x_1{}^2 + x_2{}^2)dM, & F &= (x_1x_2)dM, \end{aligned} \qquad \textbf{(3.1)}$$

We now consider a body rotating about a fixed point O, with an angular velocity of ω about an instantaneous axis of rotation Oω at any time t. Let $P(x_1, x_2, x_3)$ represent any fixed point on the body such that OP = $\underline{r}$ (see Figure 3.1).

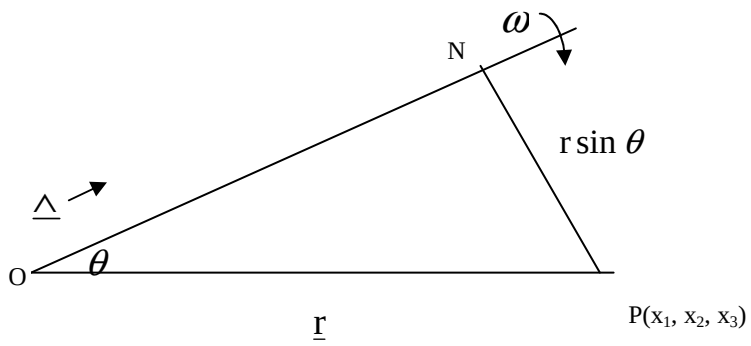

Figure 3.1 Diagram illustrating rigid body rotation

From Figure 3.1 we let PN be perpendicular to Oω and $\underline{\wedge}$ be the unit vector in the direction ON.

We now can show that the velocity of P is $r\sin\theta$ or vectorially

$$\underline{v} = \omega r \underline{\wedge} \wedge \underline{r} = \omega \underline{\wedge} \wedge r\underline{r} = \omega \wedge r \qquad \textbf{(3.2)}$$

where $\underline{\omega} = \omega_{\underline{i}} + \omega_{\underline{j}} + \omega_{\underline{k}}$ and $\underline{r} = x_{\underline{i}} + x_{\underline{j}} + x_{\underline{k}}$. Now if we know the velocity of P we can use this to find the vector angular momentum $\underline{H}$.

$$\underline{H} = \int_M \underline{r} \wedge \underline{v}\, dM \qquad \textbf{(3.3)}$$

Since $\underline{v} = \omega \wedge r$ we then have,

$$\underline{H} = \int_M \underline{r} \wedge (\_ \wedge \underline{r}) dM \qquad \textbf{(3.4)}$$

By expanding this vector triple product we obtain,

$$\underline{H} = \int_M \{\underline{\omega}(\underline{r} \cdot \underline{r}) - \underline{r}(\underline{r} \cdot \underline{\omega})\} dM \qquad \textbf{(3.5)}$$

Using the definition for $\underline{\omega}$ and $\underline{r}$ and remembering that $\underline{H}$ is a vector we can equate the components of $\underline{H}$ to give:

$$H_1 = \omega_1 \int_M (x_2^{\,2} + x_3^{\,2}) dM - \omega_2 \int_M x_1 x_2 dM - \omega_3 \int_M x_1 x_3 dM \qquad \textbf{(3.6)}$$

From our definition of moments and products of inertia (equation 3.1) we define H_1 as:

$$H_1 = A\omega_1 - F\omega_2 - E\omega_3 \qquad \textbf{(3.7)}$$

Similarly, when we equate for $\underline{j}$ and $\underline{k}$ we obtain

$$\begin{aligned} H_2 &= B\omega_2 - D\omega_3 - F\omega_1 \\ H_3 &= C\omega_3 - E\omega_1 - D\omega_2 \end{aligned} \qquad \textbf{(3.8)}$$

We now consider the matrix *I*, the inertia tensor, given as:

$$I = \begin{pmatrix} A & -F & -E \\ -F & B & -D \\ -E & -D & C \end{pmatrix} \qquad \textbf{(3.9)}$$

We note that $I_{11} = A$, $I_{22} = B$, $I_{33} = C$ and $I_{12} = I_{21} = -F$, $I_{13} = I_{31} = -E$, $I_{32} = I_{23} = -D$. Equations 3.7 and 3.8 become

$$\underline{H} = I \cdot \underline{\omega} \qquad \textbf{(3.10)}$$

For a rigid body with its axes fixed the inertia tensor I does not vary with time and thus the axes can be chosen such that the products of inertia, D, E and F are equal to zero. In this case we can rewrite equation 3.9 as

$$I = \begin{pmatrix} A & 0 & 0 \\ 0 & B & 0 \\ 0 & 0 & C \end{pmatrix} \qquad \textbf{(3.11)}$$

This can be even further simplified if the body being considered is rotationally symmetrical about the x_3 axis as, in this case, $A = B$. We can now write $\underline{H}$ as:

$$\underline{H} = A\omega_1 + A\omega_2 + C\omega_3 \qquad \textbf{(3.12)}$$

The fundamental equations that describe the rotation of a body are Euler's Dynamical Equations (Munk and MacDonald, 1960; Lambeck, 1980b). These equations describe the rotational response of a body to an applied torque L in an inertial reference frame. We can use our definition of $\underline{H}$ from equation 3.12 to determine Euler's equation.

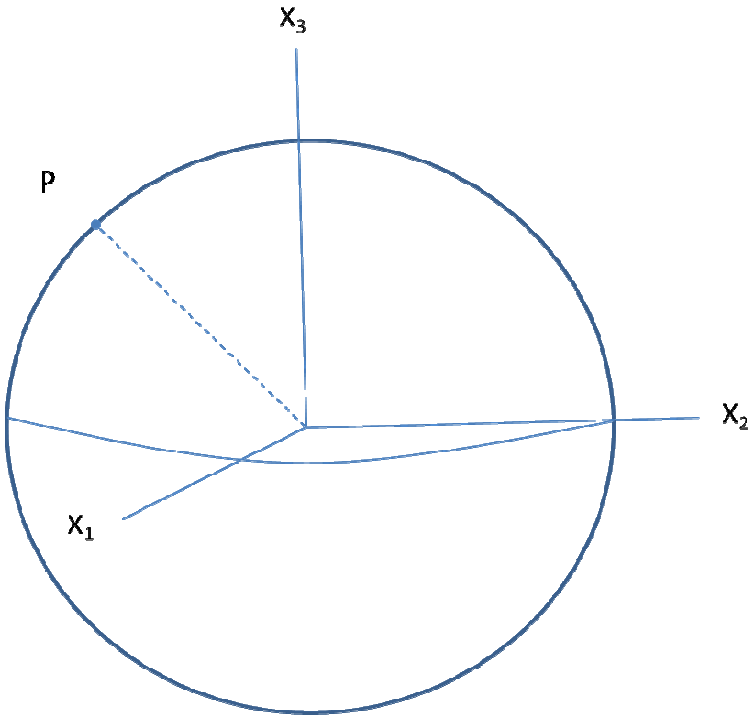

Figure 3.2 Point P, relative to reference frame X_1, X_2 and X_3

Figure 3.2 considers a point $P = (x_1, x_2, x_3)$ in space relative to the frame with origin O and axes $X_1\ X_2\ X_3$. The velocity of the point P relative to this frame is given by:

$$\begin{aligned} \underline{v} &= \frac{dr}{dt} = \frac{d}{dt}(x_1\underline{i} + x_2\underline{j} + x_3\underline{k}) = \\ &\dot{x}_1\underline{i} + \dot{x}_2\underline{j} + \dot{x}_3\underline{k} + x_1\frac{d\underline{i}}{dt} + x_2\frac{d\underline{j}}{dt} + x_3\frac{d\underline{k}}{dt} \end{aligned} \qquad \textbf{(3.13)}$$

In the above equation $\frac{d\underline{i}}{dt}$ is the velocity of the point (1, 0, 0) and is given by

$$\frac{di}{dt} = \underline{\omega} \wedge \underline{i} = (\omega_1\underline{i} + \omega_2\underline{j} + \omega_3\underline{k}) \wedge \underline{i} = \omega_3\underline{j} - \omega_2\underline{k} \qquad \textbf{(3.14)}$$

Similarly for $\underline{j}$ and $\underline{k}$

$$\begin{aligned} \frac{d\underline{j}}{dt} &= \omega_1\underline{k} - \omega_3\underline{i} \\ \frac{d\underline{k}}{dt} &= \omega_2\underline{i} - \omega_1\underline{k} \end{aligned} \qquad \textbf{(3.15)}$$

Now if we substitute back equation 3.14 and 3.15 into equation 3.13

$$\begin{aligned} \underline{v} = (\dot{x}_1\underline{i} + \dot{x}_2\underline{j} + \dot{x}_3\underline{k}) + x_1(\omega_3\underline{j} - \omega_2\underline{k}) + \\ x_2(\omega_1\underline{k} - \omega_3\underline{i}) + x_3(\omega_2\underline{i} - \omega_1\underline{j}) \end{aligned} \qquad \textbf{(3.16)}$$

The velocity of P in our frame is given by $(\dot{x}_1\underline{i} + \dot{x}_2\underline{j} + \dot{x}_3\underline{k})$. If $\omega = 0$, that is, our frame is not moving, then this term would equal $\underline{v}$. We now denote this term using $\frac{d\underline{r}}{dt}$.

$$\underline{v} = \frac{d\underline{r}}{dt} = \frac{d\underline{r}}{dt} + \underline{i}(\omega_2 x_3 - \omega_3 x_2) + j(\omega_3 x_1 - \omega_1 x_3) + \underline{i}(\omega_1 x_2 - \omega_2 x_1) \quad \textbf{(3.17)}$$

Using our previous definitions for $\underline{\omega}$ and $\underline{r}$ we can show that

$$\underline{i}(\omega_2 x_3 - \omega_3 x_2) + j(\omega_3 x_1 - \omega_1 x_3) + \underline{i}(\omega_1 x_2 - \omega_2 x_1) = \underline{\omega} \wedge \underline{r} \quad \textbf{(3.18)}$$

Therefore

$$\frac{d\underline{r}}{dt} = \omega \wedge r \quad \textbf{(3.19)}$$

Therefore for any differentiable vector $\underline{F}(x_1, x_2, x_3)$

$$\frac{d\underline{F}}{dt} = \underline{\omega} \wedge \underline{F} \quad \textbf{(3.20)}$$

In the case of Euler's dynamical equations we need to consider the motion of a rigid body about some point that is fixed within that body. We can now substitute for $\underline{H}$ in equation 3.20 which gives us the rate of change of angular momentum about an origin 0,

$$\frac{d\underline{H}}{dt} = \underline{\omega} \wedge \underline{H} \quad \textbf{(3.21)}$$

If we now denote $\underline{L} = L_1\underline{i} + L_2\underline{j} + L_3\underline{k}$ to represent the vector moment of the external forces acting upon our rigid body, or the torque, we can write

$$\dot{\mathrm{H}} = L \quad \textbf{(3.22)}$$

Equation 3.22 describes the motion of a rigid body in an inertial frame X. It is more convenient to express forces, velocities and torques with respect to an Earth fixed terrestrial reference frame. Euler's dynamical equation is given in equation 3.23 and refers to the axes x_i $(i = 1,2,3)$ (Lambeck, 1980b; Munk and MacDonald, 1960).

$$\frac{d\underline{\mathrm{H}}}{dt} + \omega \wedge \underline{\mathrm{H}} = L \qquad \textbf{(3.23)}$$

As $\frac{d}{dt}$ describes motion relative to the frame we can define $\frac{d\underline{H}}{dt}$ using equation 3.12 as

$$\frac{d\underline{H}}{dt} = A\frac{d\omega_1}{dt} + A\frac{d\omega_2}{dt} + C\frac{d\omega_3}{dt} \qquad \textbf{(3.24)}$$

Also,

$$\underline{\omega} \wedge \underline{H} = (C - A)\omega_1\omega_2\,\underline{i} + (A - C)\omega_1\omega_3\,\underline{i} + 0\,\underline{k} \qquad \textbf{(3.25)}$$

Now if we substitute equation 3.25 and 3.24 into equation 3.23 we obtain

$$\begin{aligned}\underline{L} = \underline{i}\left\{A\frac{d\omega_1}{dt} + (C-A)\omega_2\omega_3\right\} + \underline{j}\left\{A\frac{d\omega_2}{dt} - (C-A)\omega_1\omega_3\right\} \\ + \underline{k}\left\{C\frac{d\omega_3}{dt}\right\}\end{aligned} \qquad \textbf{(3.26)}$$

Here L is a vector so equating components gives

$$\begin{aligned}
\frac{d\omega_1}{dt} + \frac{(C-A)}{A}\omega_2\omega_3 &= \frac{L_1}{A} \\
\frac{d\omega_2}{dt} - \frac{(C-A)}{A}\omega_1\omega_3 &= \frac{L_2}{A} \\
\frac{d\omega_3}{dt} &= \frac{L_3}{C}
\end{aligned} \qquad \textbf{(3.27)}$$

If no torques were present equation 3.27 becomes

$$\begin{aligned}
\frac{d\omega_1}{dt} + \frac{(C-A)}{A}\omega_2\omega_3 &= 0 \\
\frac{d\omega_2}{dt} - \frac{(C-A)}{A}\omega_1\omega_3 &= 0 \\
\frac{d\omega_3}{dt} &= 0
\end{aligned} \qquad \textbf{(3.28)}$$

When considering a rigid body rotating, as in this case, symmetrically about the x_3 axis we can say $\omega_3 = \text{constant} = \Omega$. If we now substitute this constant into equation 3.28 and let $\sigma_r = \frac{(C-A)}{A}\Omega$ (the frequency of motion) we now get

$$\begin{aligned}
\frac{d\omega_1}{dt} + \sigma_r\omega_2 &= 0 \\
\frac{d\omega_2}{dt} - \sigma_r\omega_1 &= 0
\end{aligned} \qquad \textbf{(3.29)}$$

The solutions of these equations are

$$\begin{aligned}
\omega_1 &= a_0 \cos\sigma_r t + b_0 \sin\sigma_r t \\
\omega_2 &= a_0 \sin\sigma_r t + b_0 \cos\sigma_r t \\
\omega_3 &= \text{constant} = \Omega
\end{aligned} \qquad \textbf{(3.30)}$$

where a_0, b_0, Ω are constants of integration (Lambeck, 1980b).

The equations 3.28, 3.29 and their solutions (equation 3.30) provide us with a good way of describing the rotation of a rigid body, if we approximate the Earth to be a rigid body. We have defined $\sigma_r = \frac{(C-A)}{A}\Omega$ where, for the Earth $\Omega = 7.292 \times 10^{-5} s^{-1}$ and, if we choose appropriate values for the Earth's principal moments of inertia, σ_r is approximately equal to 1/306 rev d^{-1} (revolutions per day). Hence, for small displacements of axis x_3 from the rotation axis ω , the latter rotates in a circular path according to equation 3.30. This motion is known as free Eulerian precession or free nutation see Lambeck (1980b).

Now substituting Euler's dynamical equations back into equation 3.10, we obtain in vector form

$$\frac{d(I \cdot \underline{\omega})}{dt} + \underline{\omega} \wedge (I \cdot \underline{\omega}) = \underline{L} \qquad \textbf{(3.31)}$$

Equation 3.31 is only valid when the inertial coordinate system X_i and the moving axes of the Earth x_i coincide. The equation will remain valid for any instant t as long as each different value of t a new inertial coordinate system is defined that coincides with the moving axes of the Earth. Thus, for a complete description of motion of a rotating rigid Earth, we need to define a relationship between the inertial system X_i at time t and inertial system X_i' at time t'. We can define this relationship using three Eulerian angles α_i (Woolard, 1953). Our inertial system X_i is defined by the mean X_1 X_2 plane and the mean equinox X_3 for the epoch T_0. The definition given by Woolard (1953) is

α_1 = inclination of the $x_1 x_2$ plane on the mean ecliptic

α_2 = angle in the X_1X_2 plane on the ecliptic. α_2 is measured positive from X_1.

α_3 = angle in the $x_1 x_2$ plane between descending node and the x_1 axis. $\alpha_3 = \omega_3 T \approx \Omega T$

Hence

$$\underline{X} = R_3(-\alpha_2)R_1(\alpha_1)R_3(-\alpha_3)\underline{x} \qquad \textbf{(3.32)}$$

where $R_i(\alpha_j)$ denotes an anti-clockwise rotation through an angle α_j about the axis x_i. The time derivatives of α_j represent the motion of the x_1 axis with respect to the inertial frame. Resolving these velocities along the x_1 axis and equating them to ω_i gives

$$\begin{pmatrix} \dot{\alpha}_1 \\ \dot{\alpha}_2 \sin\alpha_1 \\ \dot{\alpha}_3 + \dot{\alpha}_2 \cos\alpha_1 \end{pmatrix} = R(-\alpha_3)\begin{pmatrix} \omega_1 \\ \omega_2 \\ \omega_3 \end{pmatrix} \qquad \textbf{(3.33)}$$

where

$$R(-\alpha_3) = \begin{pmatrix} \cos\alpha_3 & -\sin\alpha_3 & 0 \\ \sin\alpha_3 & \cos\alpha_3 & 0 \\ 0 & 0 & 1 \end{pmatrix} \qquad \textbf{(3.34)}$$

We now have a complete description of the motion of a rigid rotating body both in inertial space and with respect to a fixed coordinate system, fixed to that particular body. These equations are known as Euler's kinematic equations of motion. Studies of polar motion and LOD use equation 3.31 and studies of precession and nutation use equation 3.33. Since $\alpha_3 \approx \Omega$ the Eulerian motion's nutation frequency in space is given by

$$\sigma^r + \Omega \qquad \textbf{(3.35)}$$

The free wobble is associated with an almost diurnal oscillation in space. For a more complete discussion see Woolard (1953), or Kinoshita (1977).

If no torques act on the body then $\underline{H}$, which is the axis of angular momentum of the body, is fixed in space. The instantaneous axis of rotation $\underline{\omega}$ moves around x_3 in a cone.

This is the free Eulerian motion or wobble with frequency σ^r. Also $\underline{\omega}$ traces out a smaller cone around $\underline{H}$. This is nutation described by Euler's kinematic equations of motion.

3.3.2 Non-rigid, body rotation

In the absence of external torques any rotating rigid body would have predictable motion once the initial conditions of that motion had been established. In section 3.3 we made the assumption that the Earth rotates rigidly, this is not the case for two reasons: the inertia tensor I of the Earth is time dependent, and motion occurs relative to the axes $\underline{x}$. We must therefore write the total angular momentum, compared with rigid body rotation equation 3.10, as

$$\underline{H}(t) = I(t)\underline{\omega}(t) + \underline{h}(t) \qquad \textbf{(3.36)}$$

where

$$h = \int_M (\underline{r} \wedge \underline{u})\mathrm{dM} \qquad \textbf{(3.37)}$$

is the angular momentum vector due to motion and $\underline{u}$ is velocity relative to $\underline{r}$. We now substitute equation 3.37 into equation 3.31 to obtain

$$L = \left(\frac{d}{dt}\right)\left[I(t)\underline{\omega} + \underline{h}(t)\right] + \underline{\omega} \wedge I(t)\underline{\omega} + \underline{h}(t) \qquad \textbf{(3.38)}$$

These are the Louville equations (Munk and MacDonald, 1960).

In most discussions on non rigid body rotation, and in the case of our Earth, the difference from uniform body rotation is small (Lambeck, 1980b). It is therefore convenient to write

$$\omega_1 = \Omega m_1, \quad \omega_2 = \Omega m_2, \quad \omega_3 = \Omega(1 + m_3), \tag{3.39}$$

where Ω is the angular momentum of the Earth and m_1, m_2, m_3, are small dimensionless quantities. The values $m_1, m_2, 1 + m_3$, represent direction cosines of $\underline{\omega}$ relative to the axis x_3.

Changes in the Earth's inertia tensor are also small, so we can write these changes as

$$I_{11} = A + \Delta I_{11}(t), \quad I_{22} = A + \Delta I_{22}(t), \quad I_{33} = C + \Delta I_{33}(t), \tag{3.40}$$

while for the other components in the inertia tensor we have the general formula

$$I_{ij} = \Delta_{ij}(t) \qquad i \neq j \tag{3.41}$$

In the previous section we defined $\underline{\omega} = \omega_{\underline{i}} + \omega_{\underline{j}} + \omega_{\underline{k}}$ so using equation 3.39 this becomes

$$\underline{\omega} = \begin{pmatrix} \Omega m_1 \\ \Omega m_2 \\ (1+m_3)\Omega \end{pmatrix} \tag{3.42}$$

Now using equations 3.41 and 3.42 and our definition of $\underline{H}$ from equation 3.36, and after neglecting squares and products of small terms, we obtain

$$L = I \cdot \underline{\omega} + \underline{h}(t) = \begin{pmatrix} A\Omega m_1 + \Omega \Delta I_{13} + h_1 \\ A\Omega m_2 + \Omega \Delta I_{23} + h_2 \\ C\Omega + C\Omega m_3 + \Omega \Delta I_{33} + h_3 \end{pmatrix} \tag{3.43}$$

Differentiation of L gives

$$\frac{d}{dt}[I\cdot\underline{\omega}+\underline{h}(t)]=\begin{pmatrix} A\Omega\dot{m}_1+\Omega\Delta\dot{I}_{13}+\dot{h}_1 \\ A\Omega\dot{m}_2+\Omega\Delta\dot{I}_{23}+\dot{h}_2 \\ C\Omega+C\Omega\dot{m}_3+\Omega\Delta\dot{I}_{33}+\dot{h}_3 \end{pmatrix} \qquad \textbf{(3.44)}$$

Now the vector product of $\underline{\omega}$ with L gives

$$\underline{\omega}\wedge[I\cdot\underline{\omega}+\underline{h}(t)]=\begin{pmatrix} C\Omega^2m_2-A\Omega^2m_2-\Omega^2\Delta I_{23}-\Omega h_2 \\ A\Omega^2m_1+\Omega^2\Delta I_{13}+\Omega h_1-C\Omega^2m_1 \\ 0 \end{pmatrix} \qquad \textbf{(3.45)}$$

Once again the squares and products of small terms have been neglected. Now substituting this into the Louville equation, equation 3.38, we get

$$L=\begin{pmatrix} A\Omega\dot{m}_1+\Omega\Delta\dot{I}_{13}+\dot{h}_1+C\Omega^2m_2-A\Omega^2m_2-\Omega^2\Delta I_{23}-\Omega h_2 \\ A\Omega\dot{m}_2+\Omega\Delta\dot{I}_{23}+\dot{h}_2+A\Omega^2m_1+\Omega^2\Delta I_{13}+\Omega h_1-C\Omega^2m_1 \\ C\Omega\dot{m}_3+\Omega\Delta\dot{I}_{33}+\dot{h}_3 \end{pmatrix} \qquad \textbf{(3.46)}$$

Since $\underline{L}=L_{\underline{i}}+L_{\underline{j}}+L_{\underline{k}}$, we are able to equate the terms in equation 3.46 for the three terms that make up the vector L. On equating the i term and rearranging we find

$$\frac{A\dot{m}_1}{\Omega(C-A)}+m_2=\left[\frac{\Omega^2\Delta I_{23}-\Omega\Delta I_{13}\cdot\Omega h_2-\dot{h}_1+L_1}{\Omega^2(C-A)}\right] \qquad \textbf{(3.47)}$$

In the previous section we defined $\sigma_r=\frac{(C-A)}{A}\Omega$, where this is the frequency for rigid body rotation, so equation 3.47 becomes (Lambeck, 1980b).

$$\frac{\dot{m}_1}{\sigma^r}+m_2=\psi_2 \qquad \textbf{(3.48)}$$

where

$$\psi_2 = \left(\frac{\Omega^2 \Delta I_{23} - \Omega \Delta \dot{I}_{13} + \Omega h_2 - \dot{h}_1 + L_1}{\Omega^2 (C - A)} \right) \quad \textbf{(3.49)}$$

Now if we similarly equate the j and k terms we obtain

$$\frac{\dot{m}_2}{\sigma^r} + m_1 = \psi_1 \quad \textbf{(3.50)}$$

where

$$\psi_1 = \left(\frac{\Omega^2 \Delta I_{13} - \Omega \Delta \dot{I}_{23} + \Omega h_1 - \dot{h}_2 + L_3}{\Omega^2 (C - A)} \right) \quad \textbf{(3.51)}$$

and

$$\dot{m}_3 = \psi_3 \quad \textbf{(3.52)}$$

where

$$\psi_3 = \left(\frac{-\Omega^2 \Delta I_{33} - \Omega h_3 + \Omega \int_0^t L_3}{C\Omega^2} \right) \quad \textbf{(3.53)}$$

The expressions ψ_1, ψ_2, ψ_3, are known as excitation functions and their units are dimensionless. These excitation functions contain all the geophysical processes that perturb the rotation of the Earth, or in other words, cause the Earth to rotate non-uniformly. These geophysical processes include the atmosphere and oceans, the coupling of the mantle and the core, the hydrological cycles on the land as well as some other factors that do not contribute (Dickey, 1992). These geophysical processes cause

small changes in the Earth's inertia tensor I which causes the rotation of the Earth to change.

We separate equations 3.49 and 3.51 from equation 3.53 because they perturb different elements of the inertia tensor, torques and angular momentum. The first two relate to the wobble of the Earth, or the position of the pole (XP, YP) with respect to a terrestrial reference, while the third equation is related to LOD. Complex number notation gives a more compact form of these equations (Lambeck, 1980b).

$$\begin{aligned} \underline{\mathrm{m}} &= m_1 + jm_2 \\ \underline{\psi} &= \Psi_1 + j\Psi_2 \\ \Delta\mathrm{I} &= \Delta I_{13} + j\Delta I_{13} \\ \underline{\mathrm{h}} &= h_1 + jh_2 \\ \underline{\mathrm{L}} &= L_1 + jL_2 \end{aligned} \qquad \textbf{(3.54)}$$

Now we can add equation 3.51 to equation 3.53 and multiplying by j we obtain

$$\frac{\dot{m}_1}{\sigma_r} + m_2 + j\frac{\dot{m}_2}{\sigma_r} - jm_1 = \psi_2 - j\psi_1 \qquad \textbf{(3.55)}$$

By rearranging equation 3.55 we obtain

$$\frac{1}{\sigma_r}(\dot{m}_1 + j\dot{m}_2) - j(m_1 + m_2) = -j(\psi_1 + j\psi_2) \qquad \textbf{(3.56)}$$

Now using the complex numbers notation that we introduced in equation 3.54

$$\frac{\dot{\underline{m}}}{\sigma_r} + j\underline{m} = j\underline{\psi} \qquad \textbf{(3.57)}$$

or

$$\frac{j\dot{\underline{m}}}{\sigma_r} + \underline{m} = \underline{\psi} \qquad \textbf{(3.58)}$$

where $\underline{\psi}$ is given by equations 3.51 and 3.53 multiplied by j, namely

$$\underline{\psi} = \frac{1}{\Omega^2 (C - A)} \left[\Omega^2 \Delta I - j\Omega \Delta \dot{I} + \Omega \underline{h} - j\underline{h} - j\underline{L} \right] \qquad \textbf{(3.59)}$$

Equation 3.58 is a simple first order linear equation whose solution is given by

$$\underline{\mathrm{m}} = e^{j\sigma_r t} \left[\underline{m}_0 - j\sigma_r \int_{-\infty}^{t} e^{j\sigma_r \tau} \underline{\psi}(\tau) d\tau \right] \qquad \textbf{(3.60)}$$

where m_0 is a constant of integration. The solution for the axial component m_3 is given in equation 3.52 and is simpler by comparison to equation 3.60. In the absence of external torques we can express the law of conservation of angular momentum as (Barnes et al., 1983).

$$\Omega C (1 + m_3) + \Omega \Delta I_{33} + h_3 \qquad \textbf{(3.61)}$$

where $m_3 = \left(\frac{\omega_3 - \Omega}{\Omega} \right)$ and $\Lambda = \frac{2\pi}{\omega_3}$ therefore

$$m_3 = \frac{-\Delta\Lambda}{\Lambda_0} \qquad \textbf{(3.62)}$$

where $\Delta\Lambda$ is the difference of LOD from its mean value $\Lambda_0 = \frac{2\pi}{\Omega}$ of 86400 seconds. In the next chapter we will discuss how we can then compare values of LOD to variations within the fluid Earth.

3.3.3 Rotational Deformation

The main difference between uniform and non-uniform rotation is caused by deformation due to centrifugal force. This section will look at the deformation of the Earth due to centrifugal force. It is convenient to describe other perturbations of the rotation of the Earth with reference to this deformation. We describe the potential U_C of the centrifugal force at a point P, and distance l from the instantaneous rotation axis as

$$U_C = \frac{1}{2}\omega^2 l^2 \qquad \textbf{(3.63)}$$

The direction cosines of ω are given by $m_i = \omega_i / \omega$ so that (Barnes et al., 1983).

$$l^2 = \sum_i x_i^{\,2} - \left(\sum_i \frac{\omega_i x_i}{\omega} \right)^2 \qquad \textbf{(3.64)}$$

Now if we substitute equation 3.64 into equation 3.63 we get

$$U_C = \frac{1}{2}\omega^2 r^2 - \frac{1}{2}\left(\sum_i \omega_i x_i \right)^2 \qquad \textbf{(3.65)}$$

with $r^2 = \sum_i x_i^{\,2}$ and $\omega^2 = \sum_i \omega_i^{\,2}$

The potential U_c can be written as

$$U_c = \frac{1}{3}\omega^2 r^2 + \Delta U_c \qquad \textbf{(3.66)}$$

where

$$\Delta U_C = \frac{1}{6}\omega^2 r^2 - \frac{1}{2}\left(\sum_1 \omega_i x_i\right)^2 \qquad \textbf{(3.67)}$$

The first term in equation 3.67 results in a small, purely radial deformation (about 0.004 cm at Earth's surface (Lambeck and Cazenave, 1973). The second term, however, is harmonic in degree-2 and can be written in terms of spherical harmonics as (Lambeck, 1980b).

$$\begin{aligned}\Delta U_C &= \left(\frac{R^2}{2}\right)\left(\omega_1^2 + \omega_2^2 - 2\omega_3^2\right)\left(\frac{r}{R}\right)^2 P_{20}(\sin\ \phi) - \left(\frac{R^2}{3}\right)\left(\frac{r}{R^2}\right) \\ &\times (\omega_1\omega_3 \cos\ \lambda + \omega_2\omega_3 \sin\ \lambda) P_{21}(\sin\ \phi) + \left(\frac{R^2}{12}\right)\left(\frac{r}{R}\right)^2 \\ &\times \left[\left(\omega_2^2 - \omega_1^2\right)\cos\ 2\lambda - 2\omega_1\omega_2 \sin\ 2\lambda\right] \times P_{22}(\sin\ \phi)\end{aligned} \qquad \textbf{(3.68)}$$

where $P_{nm}(\sin\ \phi)$ are the associated Legendre polynomials described in Chapter 2. The potential above causes the Earth to deform. For an elastic body, a further change can be described at the Earth's surface and outside the Earth's surface using Dirichlet's theorem (Lambeck, 1980b). On the Earth's surface, $r = R$, therefore

$$\Delta U_C'(R) = k_2 \Delta U_C(R) \qquad \textbf{(3.69)}$$

Outside the Earth, where $k_2 = 0.30$ (Lambeck, 1980b),

$$\Delta U_C'(r) = \left(\frac{R}{r}\right)^3 k_2 \Delta U_C(R) \qquad \textbf{(3.70)}$$

This equation can now be written in spherical harmonics in the form given by equation 2.12

$$\Delta U_C^{'}(R) = \frac{GM}{r}\left(\frac{R}{r}\right)^3 \sum_m \left(C_{2m}^* \cos m\lambda + S_{2m}^* \sin m\lambda\right) P_{nm}(\sin\phi) \qquad \textbf{(3.71)}$$

where

$$\begin{aligned}
C20^* &= \left(\frac{R^3}{6GM}\right)\left(\omega_1^2 + \omega_2^2 - 2\omega_3^2\right)k_2, \\
C21^* &= -\left(\frac{R^3}{3}\right)\left(\frac{\omega_1\omega_3}{GM}\right)k_2, \qquad S21^* = -\left(\frac{R^3}{3}\right)\left(\frac{\omega_2\omega_3}{GM}\right)k_2, \\
C22^* &= -\left(\frac{R^3}{12}\right)\left[\frac{\left(\omega_2^2 - \omega_1^2\right)}{GM}\right]k_2, \qquad S22^* = -\left(\frac{R^3}{6}\right)\left(\frac{\omega_1\omega_2}{GM}\right)k_2,
\end{aligned} \qquad \textbf{(3.72)}$$

Now equating $C2m^*$ and $S2m^*$ with the appropriate elements in the second degree inertia tensor (equation 2.10), then $\Delta I_{ij}(t)$ changes as follows (Lambeck, 1980b).

$$\begin{aligned}
\Delta I_{13} &= \frac{k_2 R^5 \omega_1 \omega_3}{3G} = \frac{k_2 R^5 \Omega^2 m_1 (1+m_3)}{3G} \cong \frac{k_2 R^5 \Omega^2 m_1}{3G} \\
\Delta I_{23} &= \frac{k_2 R^5 \omega_2 \omega_3}{3G} = \frac{k_2 R^5 \Omega^2 m_2 (1+m_3)}{3G} \cong \frac{k_2 R^5 \Omega^2 m_2}{3G}
\end{aligned} \qquad \textbf{(3.73)}$$

In the above equations small terms have been neglected for the final simplification step. This gives the deformation due to centrifugal force related to the appropriate parts of the Earth's inertia tensor. How rotational deformation is related to the excitation functions ψ_1 and ψ_2 found in equations 3.49 and 3.51 will now be described. In the case of rotational deformation, torque and angular momentum do not affect the excitation of rotation. Therefore, the terms in equations 3.49 and 3.51 involving torque $\underline{L}$ and angular momentum $\underline{h}$ are neglected. Now substituting equations 3.73 into 3.49 and 3.51 to obtain the excitation from rotational deformation (Lambeck, 1980b).

$$\psi_1 = \frac{\Omega^2}{C-A} k_2 \frac{R}{3G}\left(m_1 \frac{\dot{m}_2}{\Omega}\right) = \frac{k_2}{k_0}\left(m_1 + \frac{\dot{m}_2}{\Omega}\right),$$
$$\psi_2 = \frac{\Omega^2}{C-A} k_2 \frac{R}{3G}\left(m_2 \frac{\dot{m}_1}{\Omega}\right) = \frac{k_2}{k_0}\left(m_2 + \frac{\dot{m}_1}{\Omega}\right), \qquad \textbf{(3.74)}$$

where

$$k_0 = \frac{3(C-A)G}{\Omega^2 R^5} = \frac{3GMC_{20}}{\Omega^2 R^3} = 0.942 \qquad \textbf{(3.75)}$$

Here m_i are of the order 10^{-6} so that $\frac{\dot{m}_i}{\Omega} \approx 5\times 10^{-9} \langle\langle m_i$ (Lambeck, 1980b; Barnes et al., 1983). Hence 3.74 becomes

$$\psi_1 = \frac{k_2}{k_0} m_1, \qquad \psi_2 \frac{k_2}{k_0} m_2 \qquad \textbf{(3.76)}$$

σ_0 using σ_r which is the frequency for rigid body rotation defined in section 3.3.1 is defined as.

$$\sigma_0 = \sigma_r\left(1 - \frac{k_2}{k_0}\right) \qquad \textbf{(3.77)}$$

Now substituting the excitations ψ_1 and ψ_2 into equation 3.48 and 3.50 gives (in the absence of all other excitations)

$$\frac{\dot{m}_1}{\sigma_0} + m_2 = 0, \qquad \frac{\dot{m}_2}{\sigma_0} + m_1 = 0 \qquad \textbf{(3.78)}$$

The solution of these equations is (Lambeck, 1980b)

$$m_1 = m_0 \cos(\sigma_0 t + \theta),$$
$$m_2 = m_0 \sin(\sigma_0 t + \theta), \qquad \textbf{(3.79)}$$

where m_0 and θ are constants and σ_0 is given in equation 3.77. From the solution given in equation 3.79 we can see that the motion is once again circular, the same as given in rigid body rotation given in section 3.3.1. In the section on rigid body rotation the frequency of the Earth's wobble was given as $\sigma_0 = \frac{1}{306}\text{rev d}^{-1}$, whereas observations of this period give it as approximately $\sigma_0 = \frac{1}{435}\text{rev d}^{-1}$. Thus the elasticity of the Earth increases the period of the Earth's wobble from 306 days to approximately 435 days. The difference between a rigidly rotating Earth and an elastic Earth will now be shown.

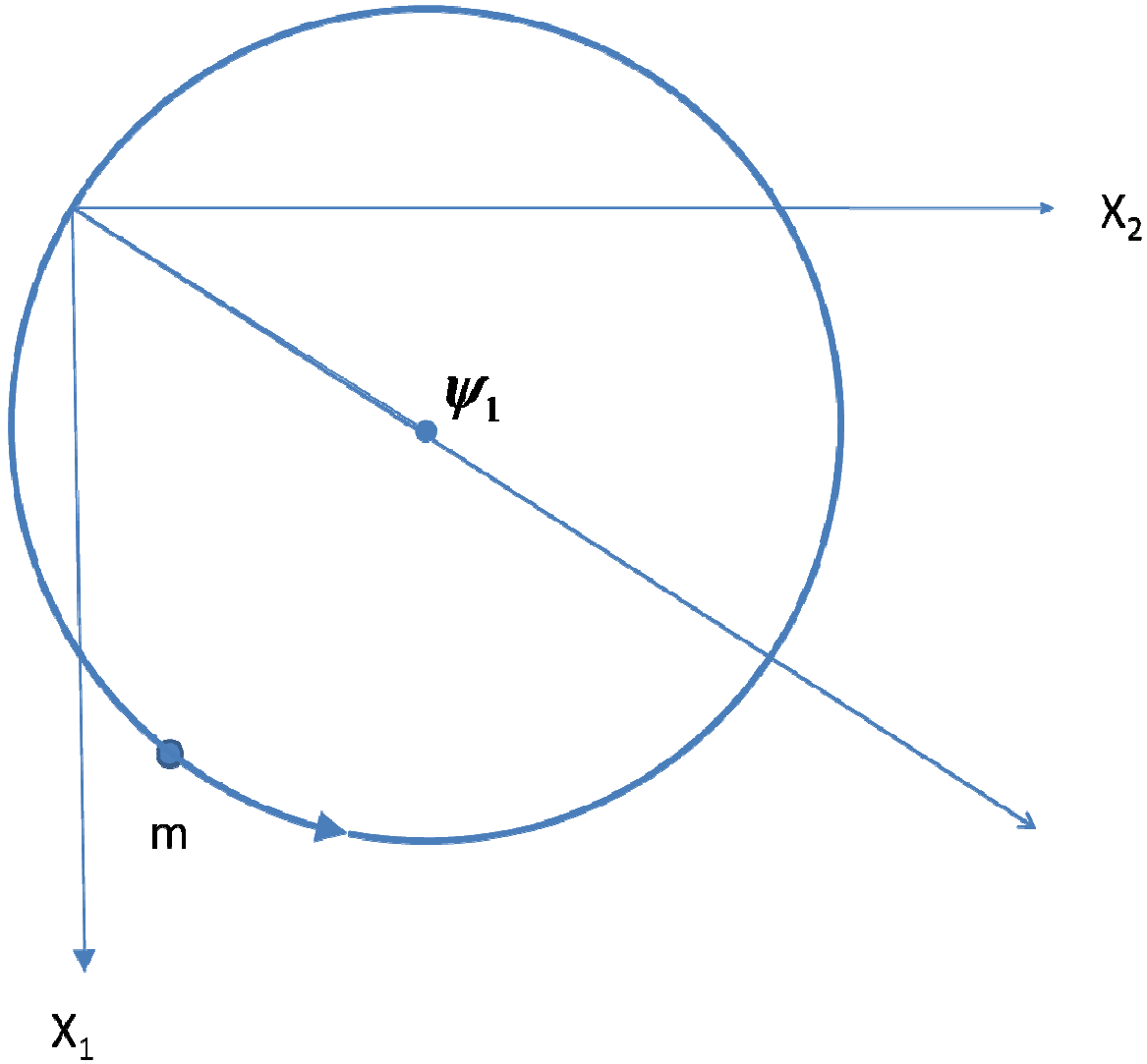

Figure 3.3 Motion of the rotation axis with respect to Earth fixed axes, Initial State for non rigid body rotation

Figure 3.3 illustrates rigid body rotation where m represents the motion around the rotation axis and the excitation axis $\underline{\psi}$ is relative to the body fixed axis $\underline{x}$. In its initial state $\underline{m}$ is aligned with the principle axis of rotation x_3, with $\underline{m}=0$ and $\psi=0$. If the body is perturbed then the excitation pole is shifted to $\underline{\psi}_r$ and $\underline{m}$ moves around the excitation pole with a frequency σ_r and amplitude $\underline{m}_0$.

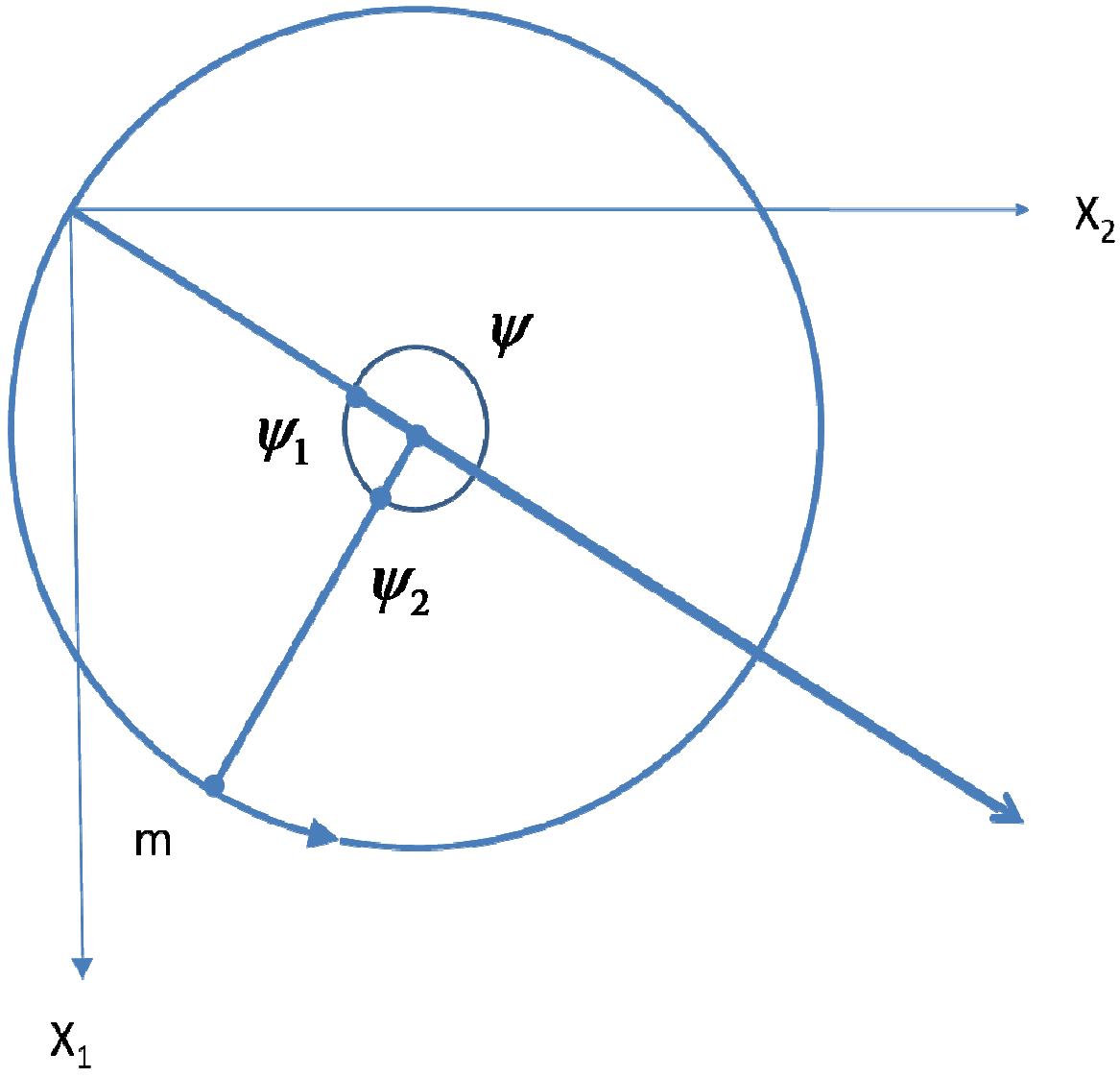

Figure 3.4 Motion of the rotation axis with respect to Earth fixed axes, initial state for rigid body rotation

Figure 3.4 represents the effects of perturbation on a non-rigid rotating body, i.e. the Earth responding elastically to a perturbation. In this case the rotating body has the same initial conditions as in Figure 3.3. This time, however, the rotation axis wobbles freely about a mean position. The excitation functions were given previously in

equation 3.74. These can also be written as $\psi_1 = \frac{k_2}{k_0} m_1$ and $\psi_2 = \frac{k_2}{k_0} m_2$ and in complex notation as $\underline{\psi}_D = \frac{k_2}{k_0} \underline{m}$. This excitation is due to the bulge adjusting itself to the constantly changing position of $\underline{m}$. The equations of motion from equation 3.57 can now be written as

$$j\frac{\dot{\underline{m}}}{\sigma_r} + \underline{m} = \underline{\psi}_D \quad \text{or} \quad j\frac{\dot{\underline{m}}}{\sigma_0} + \underline{m} = 0 \qquad \textbf{(3.80)}$$

Where $\sigma_0 = \sigma_r\left(\frac{1-k_2}{k_0}\right)$ is the frequency of the free oscillation of the elastic Earth (Lambeck, 1980b). Now, from our relationship between the Earth's inertia tensor and rotation given in equation 3.71, we have $\underline{\psi}_D$ as the orientation of the principal axes of the Earth with respect to $\underline{x}$.

In the above case $\underline{\psi} = \underline{\psi}_D$. Additionally, if the Earth is subjected to another excitation function, one of force, the total excitation $\underline{\psi}$ acting on the Earth, is made up of the new excitation of force $\underline{\psi}_r$ being considered and $\underline{\psi}_D$, which has already been defined. The equations of motion now become (remembering that $\underline{\psi} = \underline{\psi}_D + \underline{\psi}_r$)

$$j\frac{\dot{\underline{m}}}{\sigma_r} + \underline{m} = \underline{\psi}_D + \underline{\psi}_r \qquad \textbf{(3.81)}$$

Now substitute σ_r and $\underline{\psi}_D$.

$$j\frac{\dot{\underline{m}}}{\sigma_0}\left(\frac{1-k_2}{k_0}\right) + \underline{m} = \frac{k_2}{k_0}\underline{m} + \underline{\psi}_r$$

This reduces to

$$j\frac{\dot{\underline{m}}}{\sigma_0} + \underline{m} = \frac{k_0}{(k_0 - k_2)}\underline{\psi}_r \qquad \textbf{(3.82)}$$

showing that an elastic Earth changes the amplitude of the excitation function by $\frac{k_0}{k_0 - k_2}$. It can now be said that the amplitude of the wobble of the Earth increases as a result of the Earth, giving an elastic response rather than the response of a rigid Earth.

An anelastic response of the Earth to a disturbing potential will now be briefly considered. Using complex Love numbers (Lambeck, 1980b) we have

$$\underline{k}_2 = k_2 + j\kappa \qquad \textbf{(3.83)}$$

Now substituting this into the complex form of equation 3.74 gives

$$\underline{\psi} = \left[\frac{k_2 + j\kappa}{k_0}\right]\underline{m}$$

Now substituting for $\underline{\psi}$ gives

$$j\frac{\dot{\underline{m}}}{\underline{\sigma}_r} + \underline{m} = \left[\frac{k_2 + j\kappa}{k_0}\right]\underline{m} \quad \text{or} \quad j\frac{\dot{\underline{m}}}{\underline{\sigma}_0} + \underline{m} = 0 \qquad \textbf{(3.84)}$$

where, $\sigma_0 = \sigma_r\left(\frac{1-k_2}{k_0}\right) - j\sigma_r\frac{k}{k_0}$ is the frequency of the aneleastic response to excitation. So to allow for the anelastic response of the Earth we can introduce the complex frequency $\underline{\sigma}_0 = \sigma_0 + j\alpha$. Therefore, the solution to these equations using this new frequency is given by

$$\underline{m} = \underline{m}_0 e^{-\alpha t} e^{j\sigma_0 t} \qquad \textbf{(3.85)}$$

The amplitude of the free wobble is dampened by the factor $e^{-\alpha t}$ as a result of an anelastic response. This response is known as “damped linear motion” (Lambeck, 1980b).

3.4 Conclusion

Earth rotation theory has been discussed in some detail, deriving the fundamental equations needed to understand how the rotation of the Earth and how the processes that act on can be described mathematically. The final set of equations derived here describes how the rotation of the Earth can be “excited” by certain processes acting upon it. These equations are referred to as the excitation functions and can be linked to the movement of mass within the Earth system. In the subsequent chapters these equations will be used to investigate these mass redistributions within the Earth and their links with the gravity field of the Earth.

Chapter 4

4 Mass Redistribution and Angular Momentum

4.1 Introduction

This chapter will look at the different ways in which mass is redistributed throughout the Earth system including the atmosphere, oceans and continental hydrological effects as well as the effects of the Earth's core. The method of calculating the effects of each of these different processes on the redistribution of mass within the Earth system will be derived and examples of these excitation functions will be analysed. Finally, a comparison of Atmospheric Angular Momentum Function (AAMF) estimates from various organisations will be compared to assess which dataset might be the most appropriate to use in the orbit determination process.

4.2 Redistribution of Mass

Mass and angular momentum are, according to physics, conserved in a closed system. The Earth interacts very little with components outside of itself. The Earth therefore can be thought of as a closed system, and therefore mass components in one reservoir of the Earth system are exchanged with others (Salstein, 1993). Mass redistribution within the Earth system is caused by geophysical processes. This movement of geophysical fluid (mass) causes variations in the Earth's rotation, gravity field and geocentre. The improvement of geodetic techniques over the last few decades allows us to measure the effects of these processes on the Earth to an unprecedented accuracy. The continuous collection of this kind of data allows scientists the opportunity to investigate these processes over varying timescales.

As stated previously the changes in the rotation of the Earth are caused by the movement of mass in the Earth system, this has two effects. Firstly, the movement of geophysical fluids cause surface torques, which directly affect the rotation of the Earth and secondly, the associated redistribution of mass from this movement causes the Earth's inertia tensor to be modified, thus instigating rotational change. From this

knowledge it can be said that the Earth obeys the law of "conservation of angular momentum" (Chao et al., 2000).

The gravity field of the Earth is also closely associated with the geophysical processes within the Earth system. These processes cause changes in the Earth's gravity field through Newton's gravitational law (equation 2.1). This law states that a body creates its own gravity field according to the distribution of mass within that particular body.

Finally, changes in the Earth's geocentre obey the law of "conservation of linear momentum". This law states that the centre of mass of the solid Earth plus the geophysical fluids such as the atmosphere and oceans obeys the law of celestial mechanics in its translational motion around the solar system. This geocentre motion manifests itself, for example, as a translation of the ground based network of SLR stations with respect to the centre of mass of the whole Earth system that is defined by the orbits of the satellites (Chao et al., 2000).

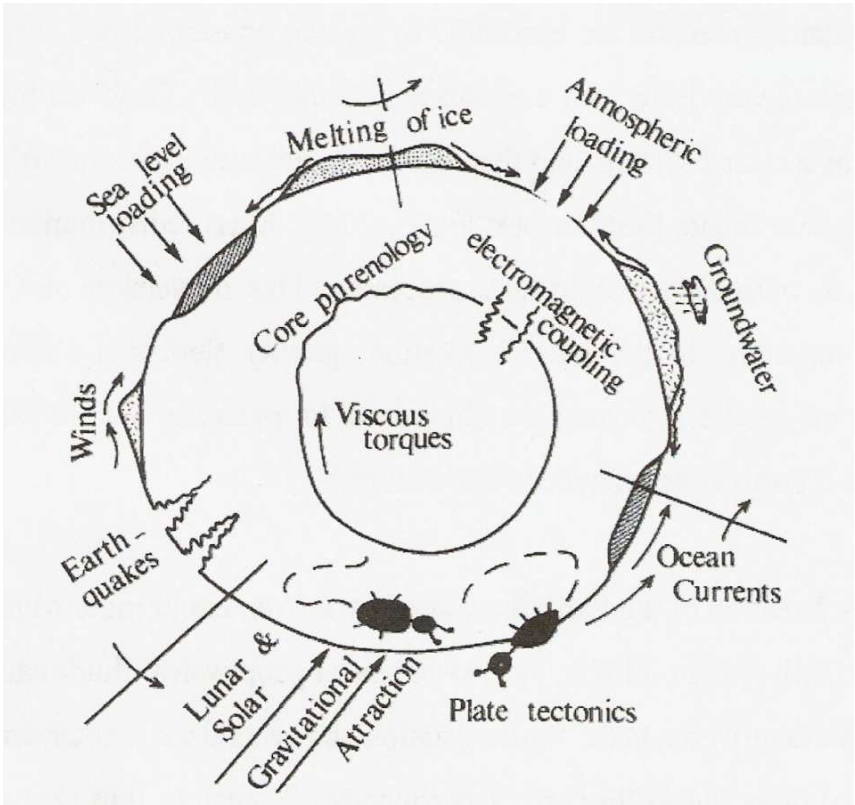

Figure 4.1 Forces that perturb the Earth's rotation (Lambeck, 1980a)

There are many processes (Figure 4.1) within the Earth system that cause mass to be redistributed. These include the atmosphere, oceans, hydrology (ground water), the Earth's core and mantle, Earthquakes, volcanoes, post glacial rebound, tides and the melting of ice.

The size of the effects on the geodynamics of the Earth by the mass transport of geophysical fluids is approximately proportional to (net transported mass)/(Earth mass) and (net transported distance)/(Earth radius). These processes cause variations in orientation, gravity and geocentre on all observable timescales (Gross et al., 2005).

4.2.1 Atmosphere

Variations in the Earth's rate of rotation or LOD and polar motion can be attributed to a variety of sources. These can be split into three categories: an overall increase from tidal dissipation, the long term variations (i.e. decadal variations) and finally higher frequency variations on annual and seasonal timescales (Dickey, 1993). Numerous studies have examined the effects of mass redistribution on the rotation and gravity field of the Earth. These studies have shown that the movement of the atmosphere is the most variable of the geophysical processes that affect the Earth system. Excitation is significant in all three components. Studies show good agreement between changes in the angular momentum of the Earth's atmosphere and that of the Earth's rotation and gravity field. At periods longer than approximately 10 days, signals for excitation by the atmosphere are well established (Eubanks, 1993).

The exchange of angular momentum between the atmosphere and the Earth is the major cause of variations in LOD for periods of approximately 5 years or less (Dickey, 1993; Lambeck and Cazenave, 1977). At periods greater than 5 years the atmosphere may contribute to the excitation of the Earth's rotation significantly (Lambeck, 1980a; Lambeck and Cazenave, 1977). The annual excitation of LOD is almost entirely dominated by the atmosphere after excluding the effects of the ocean and solid Earth; it has been shown that variations in the atmosphere contribute to the excitation of the Earth's rotation (Eubanks et al., 1985; Rosen and Salstein, 1985; Hide et al., 1980).

Polar motion is dominated by two almost circular oscillations, one at a period of 1 year, known as the annual oscillation, and the second at a period of approximately 436 days, known as the Chandler wobble. The amplitudes of both these signals are approximately 100-200 mas. There is also a long term drift of a few mas per year. The Chandler wobble is a free oscillation of the Earth and has not been fully accounted for, although the atmosphere is one of the major candidates for its excitation (Gross, 2000). A large part of the annual and semi-annual oscillation is driven by variations with the Earth's atmosphere (Kuehne and Wilson, 1991; Chao and Au, 1991). The evidence for the atmospheric pressure being the main source of variations on an inter-seasonal timescale is strong (Eubanks et al., 1988), as well as evidence that atmospheric winds may play a role in this excitation (Gross and Lindqwister, 1992). Decadal scale fluctuations in polar motion are less likely to be caused by the atmosphere but this cannot be entirely ruled out (Khrgian, 1985). High frequency variations show statistically significant coherences between atmospheric excitation and polar motion for as little as 10 days (Salstein and Rosen, 1989). It is thought that the atmosphere also contributes highly to shorter period excitations but this is less well established (Nastula et al., 2002).

4.2.2 Ocean

The oceanic excitation of polar motion does not have as good observational evidence as that of the atmosphere. Ocean tidal fluctuations have been found to have the greatest effect on sub daily timescales (Chao and Ray, 1997; Gipson, 1996). Ocean tides have also been found to have an effect at fortnightly and monthly timescales (Gross, 1996; Gross et al., 1997). The effects of the tides on Earth rotation parameters have been well modelled (Yoder et al., 1981) and are usually removed when investigating the effects of the oceans on Earth rotation. Oceanic excitation is driven to a great extent by atmospheric forcing and the thermohaline processes caused by heat and freshwater fluxes (Brzezinski, 2002). Modelling this is complicated, as it requires three-dimensional modelling of global ocean dynamics, This type of data has been produced by Ponte et al. (1998), and Johnson (1999) .

The seasonal effects of the ocean on polar motion have been studied (Ponte and Stammer, 1999; Gross, 2000). These studies agree that adding the effects of the oceans to the effects of the atmosphere bring the modelled excitation closer to the observed

excitation. Gross (2000) also finds that oceanic excitations explain some of the discrepancies in inter-seasonal and inter-annual periods, although discrepancies still remain. The possible forcing of the Chandler wobble by oceanic processes has also been investigated (Ponte and Stammer, 1999; Gross, 2000; Brzezinski and Nastula, 2002; Brzezinski et al., 2002). These studies have shown the ocean to be important in exciting the Chandler wobble with ocean bottom pressure having the greatest effect. Oceanic excitation has been found not to have enough power to seriously affect low frequency variations in polar motion (Gross, 2000).

The oceans also effect changes in the Earth's rate of rotation. Studies have shown that the ocean could be responsible for some of the remaining LOD variation that cannot be accounted for by the atmosphere (Johnson, 1999; Marcus et al., 1998; Chen et al., 2000).

4.2.3 Hydrology

Although advances in technology, such as the GRACE satellite mission and Aqua satellite (Barnes et al., 2003), have improved the availability of data used to estimate the effect of hydrology on the rotation of the Earth, several components of the effects of hydrology are known with large uncertainties (Rummel et al., 2009). Due to this the effect of hydrology on the rotation of the Earth is also difficult to estimate and remains one of the more interesting research areas with respect to mass redistribution within the Earth system. Traditionally, hydrological angular momentum functions have been derived from precipitation, evapotranspiration and surface runoff based on sparse climatological models (Chen et al., 2000).

Hydrology is thought to contribute to the secular change in polar motion by up to 20% of the total excitation. Melting of continental glaciers and other changes in continental water storage are the processes by which the mass is redistributed on the land (Gasperini et al., 1986; Trupin and Wahr, 1990; Kuehne and Wilson, 1991; Wilson, 1993). Hydrology is thought to be more important than the atmosphere in decadal scale variations of polar motion, as water can be stored over these timescales as glaciers, snow and lakes etc whereas the atmosphere cannot (Kuehne and Wilson, 1991; Wilson, 1993), especially in variations longer than 10 years. Chao et al. (1987), Chao and O'Connor (1988), and Trupin and Wahr (1990) studied the effects of long period

excitation from snow loads, reservoirs and glaciers and found that all of these processes only create 10% or less of the total excitation required. Studies have given contradictory results with regard to the importance of hydrological angular momentum (Kuehne and Wilson, 1991). Hydrology is thought to also contribute on a small scale to LOD variations on all timescales. More recent studies (Jin et al., 2010; Chen and Wilson, 2005) have shown that hydrology does not close the gap between observed polar motion and LOD variations and the excitation computed from available models.

4.2.4 Core

Decadal variations in the rotation of the Earth are thought to be caused by the angular momentum of the Earth's liquid core (Jault and Le Mouel, 1991; Lambeck, 1980b). This conclusion comes about by the process of exclusion as these variations are so large that it would take double the mean atmospheric zonal wind velocity or enough melting of the polar ice to increase the sea level by 20 cm to cause rotational variations on this scale. Neither of these phenomena has ever been observed. Since no theoretical process has been discovered that could generate enough excitation to produce this long term variation, it is assumed that this variation is caused by the torques between the Earth's core and mantle (Eubanks, 1993).

4.2.5 Other Effects

A secular variation has been detected in polar motion (Gross and Chao, 1990; Ming and Danan, 1987) although studies do not agree on the size of this variation, showing how difficult it is to determine secular motion of the Earth poles. This secular variation has been generally attributed to post glacial rebound (Wu and Peltier, 1984; Peltier, 1998) and is thought to be responsible for the secular change found in J2 and other gravitational harmonics. This secular change in J2 changed in 1998, the cause of which is not yet known for certain (Cox and Chao, 2002). The linear increase in LOD, attributed to tidal dissipation and glacial isostatic adjustment has been estimated to be about 1-2 milliseconds per century (Stephenson et al., 1984; Rummel et al., 2009).

The possibility of earthquakes exciting the Earth's rotation enough to account for discrepancies between the excitation needed to cause polar motion and LOD and that

excitation that can be modelled from the atmosphere, oceans and hydrology, as well as the possibility of earthquakes exciting the Chandler wobble, have been investigated. This, however, has been shown to be unlikely as all earthquakes between 1977 and 1990 only account for excitation equivalent to a few tenths of a millisecond (Gross, 1986, Chao and Gross, 1987)

For a more comprehensive review of the processes that cause the excitation of the Earth's rotation, see Eubanks (1993).

4.2.6 The Southern and Quasi-Biennial Oscillations

Measurements of LOD have shown interannual fluctuations (i.e. variations of between one and 10 years). Studies have shown correlations between these fluctuations and two quasi-periodic global oscillations in the oceans and atmosphere. These are known as the Southern Oscillation or SO (Stepanick, 1982; Chao, 1984; Eubanks et al., 1986; Hide and Dickey, 1991) and the Quasi-Biennial Oscillation (Chao, 1989).

El Nino and La Nina events are important temperature fluctuations in the eastern Pacific Ocean, the cause of which is still not totally understood. El Nino and La Nina events are now recognised as being part of the SO and are referred to together as ENSO cycles. An El Nino phenomenon occurs as a body of water in the eastern Pacific Ocean, which is as much as 2^{o} higher in temperature than the surrounding waters, moves across the Pacific in just a matter of months (Eubanks, 1993). It has been suggested that the cause may be the result of non-linear air-sea interactions, which cause changes in the temperature at the sea surface and therefore cause change in the wind stress on the ocean, which are also modified by the new atmospheric conditions (Philander, 1990; Barnett et al., 1991).

The Quasi Biennial Oscillation is a quasi-periodic oscillation of the equatorial zonal winds (Baldwin et al., 2001). The mean period of the oscillation is 28 months.

Studies, starting with Stepanick (1982) have connected these events with fluctuations in the Earth's rotation rates. During the very strong 1982-1983 El Nino event, Rosen et al. (1984) observed some unusually large and rapid rotational variations in LOD. These effects were later confirmed by subsequent studies (Chao, 1984; Eubanks et al., 1986)

showing that most LOD variations on inter-annual timescales were linked to these ENSO events and the Quasi Biennial Oscillation.

4.3 Excitation and Angular Momentum Function

In Chapter 3 we described the rotation of the Earth and introduced some excitation functions due to changes in the inertia tensor and angular momentum of the Earth. The excitation equations shown in equations 3.48 through 3.53 are well suited for calculating excitation functions when changes in relative angular momentum are well separated from changes in the Earths inertia tensor I or when one of these quantities is zero. These equations are, however, inadequate for computing excitation functions when looking at changes occurring due to redistribution of matter and relative angular momentum separately. The reason is that both angular momentum and the inertia tensor involving relative motion are both second order.

It should be noted that there are two different methods for calculating the effect of the atmosphere and oceans etc on the rotation of the Earth (Munk and MacDonald, 1960; Wilson and Haubrich, 1976; Lambeck, 1980b). In the torque approach, the torques that act upon the surface of the Earth, due to the movement of fluids within, above and on the Earth are related to the rate of change of angular momentum of the Earth. Alternatively, in the angular momentum approach, the angular momentum of the Earth and of the atmosphere and oceans are considered equal and opposite (Barnes et al., 1983). In this thesis we use the angular momentum approach due to the fact that wind data is readily available. Therefore, we must separate the excitation functions to look at each effect independently. Recall equations 3.53 and 3.59.

$$\Omega^2(C-A)\underline{\psi} = \left[\Omega^2\Delta I - j\Omega\Delta\dot{I} + \Omega\underline{h} - j\underline{h} - j\underline{L}\right] \qquad \textbf{(4.1)}$$

$$C\Omega^2\psi_3 = -\Omega^2\Delta I_{33} - \Omega h_3 + \Omega\int_0^t L_3 \qquad \textbf{(4.2)}$$

The excitation functions contain contributions from:

i. Redistribution of mass (matter),

ii. Relative motion of mass (motion),

iii. Torques.

This can be written as

$$\psi_i = \psi_i(matter) + \psi_i(motion) + \psi_i(torques) \qquad \textbf{(4.3)}$$

where from equation 4.1

$$\begin{aligned} \Omega^2(C-A)\underline{\psi}(matter) &= \Omega^2\Delta I \\ \Omega^2(C-A)\underline{\psi}(motion) &= -j\Omega\Delta I + \Omega\underline{h} - j\underline{h} \\ \Omega^2(C-A)\underline{\psi}(torques) &= j\underline{L} \end{aligned} \qquad \textbf{(4.4)}$$

and from equation 4.2.

$$\begin{aligned} C\,\Omega^2\psi_3(matter) &= -\Omega^2\Delta I_{33} \\ C\,\Omega^2\psi_3(motion) &= -\Omega\, h_3 \\ C\,\Omega^2\psi_3(torque) &= -\Omega\int_0^t L_3\,dt \end{aligned} \qquad \textbf{(4.5)}$$

Equations 4.1 and 4.2 can now be written as (Munk and MacDonald, 1960)

$$\Omega^2(C-A)\underline{\psi} = \int_V \Delta\rho\,\underline{F}(matter)dV + \int_V \rho\,\underline{F}(motion)dV + \underline{F}(torque) \qquad \textbf{(4.6)}$$

$$\Omega^2 C\psi = \int_V \Delta\rho F_3(matter)dV + \int_V pF_3(motion)dV + F_3(torque) \quad \textbf{(4.7)}$$

where $\underline{F} = F_1 + jF_2$

Now, to obtain equations for F_1, F_2 and F_3 in Cartesian coordinates, recall equation 3.1, namely the general form of I in Cartesian coordinates.

$$I_{ij} = -\int_m x_i x_j dM \qquad (i \neq j) \quad \textbf{(4.8)}$$

Since $dM = \rho dV$ where ρ is the density, then

$$I_{ij} = -\int_V \rho x_i x_j dV \qquad (i \neq j) \quad \textbf{(4.9)}$$

Now consider

$$\Delta I_{ij} = -\int_V \Delta\rho x_i x_j dV - \int_V \rho \frac{d}{dt}(x_i x_j)dV \qquad (i \neq j) \quad \textbf{(4.10)}$$

From Chapter 3 recall $\Delta I_{ij} = I_{ij}$ where $i \neq j$, therefore equation 4.10 becomes

$$I_{ij} = \Delta I_{ij} = -\int_V \Delta\rho x_i x_j dV - \int_V \rho \frac{d}{dt}(x_i x_j)dV \qquad (i \neq j) \quad \textbf{(4.11)}$$

The above equation can now be separated to obtain expressions for both matter and motion.

$$
\begin{aligned}
&matter: \qquad \Delta I_{ij} = \int_V \Delta\rho x_i x_j dV \\
&motion: \qquad \Delta I_{ij} = \int_V \rho \frac{d}{dt} x_i x_j dV
\end{aligned}
\tag{4.12}
$$

Now on setting the torque to zero ($L_i = 0$), we can write the excitation functions in CCartesian coordinates as

$$
\begin{aligned}
\Omega^2 (C - A)\psi_1 &= -\Omega^2 \int_V \rho x_1 x_2 dV + \int_V \rho (x_3 \dot{u}_1 - x_1 \dot{u}_3 - 2\Omega x_3 u_2) dV \\
\Omega^2 (C - A)\psi_2 &= -\Omega^2 \int_V \rho x_2 x_3 dV + \int_V \rho (x_3 \dot{u}_2 - x_2 \dot{u}_3 - 2\Omega x_3 u_1) dV
\end{aligned}
\tag{4.13}
$$

In equation 4.13 the first integrals on the right hand side are the matter terms while the second integrals are the motion terms as they involve velocities u_i as well as density ρ.

The expressions for F_1, F_2 and F_3 are obtained from equations 4.6 and 4.7 in terms of Cartesian coordinates using equations 4.4, 4.5 and 4.12. This gives:

$$
\begin{aligned}
&matter \ : \ F_1 = -\Omega x_1 x_3, \ F_2 = -\Omega x_2 x_3, \ F_3 = -\Omega (x_1^2 + x_2^2) \\
&motion \ : \begin{Bmatrix} F_1 = -2\Omega x_3 u_2 + x_3 \dot{u}_1 - x_1 \dot{u}_3 \\ F_2 = 2\Omega x_3 u_1 + x_3 \dot{u}_2 - x_2 \dot{u}_3 \\ F_3 = \Omega (-x_1 u_2 + x_2 u_1) \end{Bmatrix} \\
&torque \ : \ F_1 = -L_2, \ F_2 = L_1, \ F_3 = \Omega \int_0^t L_3 dt
\end{aligned}
\tag{4.14}
$$

Similarly these functions can be written in terms of spherical harmonics by letting u_λ, u_θ and u_r designate the East, South and Up components of velocity respectively and $dV = r^2 \sin\theta \, dr d\theta \, d\lambda$ as the differential volume. We then have (Munk and MacDonald, 1960)

$$
\begin{aligned}
&\textit{matter}:\left\{\begin{array}{c} F_1=-r^2\Omega^2\sin\theta\cos\theta\cos\lambda \\ F_2=-r^2\Omega^2\sin\theta\cos\theta\sin\lambda \\ F_3=-r^2\Omega^2\sin^2\theta \end{array}\right\} \\
&\textit{motion}:\left\{\begin{array}{c} F_1=-2\Omega r\cos\theta\left(u_\lambda\cos\lambda+u_\theta\sin\theta\sin\lambda+u_r\sin\theta\sin\lambda\right) \\ +r\left(-\dot{u}_\lambda\cos\theta\sin\lambda+\dot{u}_\theta\cos\lambda\right) \\ F_2=-2\Omega r\cos\theta\left(-u_\lambda\sin\lambda+u_\theta\cos\theta\cos\lambda+u_r\sin\theta\cos\lambda\right) \\ +r\left(-\dot{u}_\lambda\cos\theta\sin\lambda+\dot{u}_\theta\sin\lambda\right) \\ F_3=-\Omega r\sin\theta u_\lambda \end{array}\right\}
\end{aligned}
\qquad \textbf{(4.15)}
$$

The torque is more complicated and is written as the sum of two terms.

$$
L_i = \int_V \rho\varepsilon_{ijk}\, x_j\, f_k\, dV + \int_S \varepsilon_{ijk}\, x_j\, p_{km}\, n_m\, dS \qquad \textbf{(4.16)}
$$

where

$$
\begin{aligned}
&\varepsilon_{ijk}=0 \text{ if} && i=j,\ \ j=k,\ \ i=k \\
&\varepsilon_{ijk}=1 \text{ if} && i,j,k \textit{ is an even permutation of } 1,2,3 \\
&\varepsilon_{ijk}=-1 \text{ if} && i,j,k \textit{ is an odd permutation of } 1,2,3
\end{aligned}
$$

The excitation χ caused by the atmosphere can be concisely written in terms of complex numbers.

$$
\chi=\chi_1(t)+j\chi_2(t)
$$

$$
\chi_1(t)+i\chi_2(t)=\frac{1.61}{\Omega(C-A)}\left[h_x(t)+ih_y(t)+\frac{\Omega}{1.44}\left(\Delta I_{13}(t)+i\Delta I_{23}(t)\right)\right] \qquad \textbf{(4.17)}
$$

$$
\Delta\Lambda(t)=\frac{\Lambda_0}{C_m\Omega}\left[h_z(t)+0.756\,\Omega\Delta I_{33}(t)\right] \qquad \textbf{(4.18)}
$$

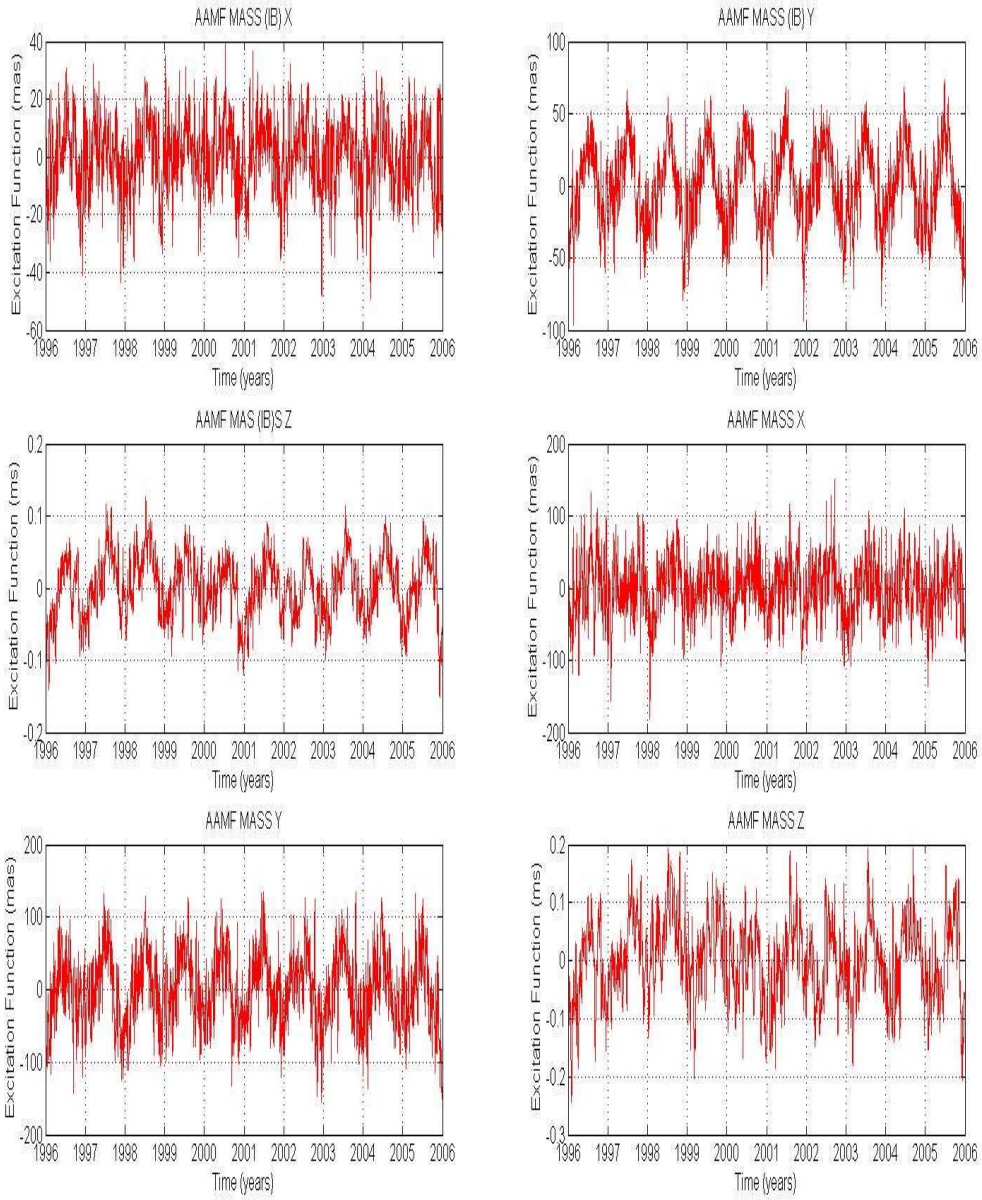

Figure 4.2 Atmospheric Angular Momentum Functions mass terms using an Inverted Barometer (IB) and non Inverted Barometer derived by NCEP

where the terms 1.61 and 1.44 in equation 4.17 account for the effect of core decoupling and the yielding of the solid Earth to the loading respectively. The term 0.756 in equation 4.18 again accounts for the yielding of the solid Earth to the load.

Using equations 4.17 and 4.18 we can compute excitation functions from geophysical data. Figure 4.2 and Figure 4.3 show the excitation functions calculated from the NCEP

reanalysis atmospheric angular momentum values (Kalnay et al., 1996) from 1996 to 2006 inclusive.

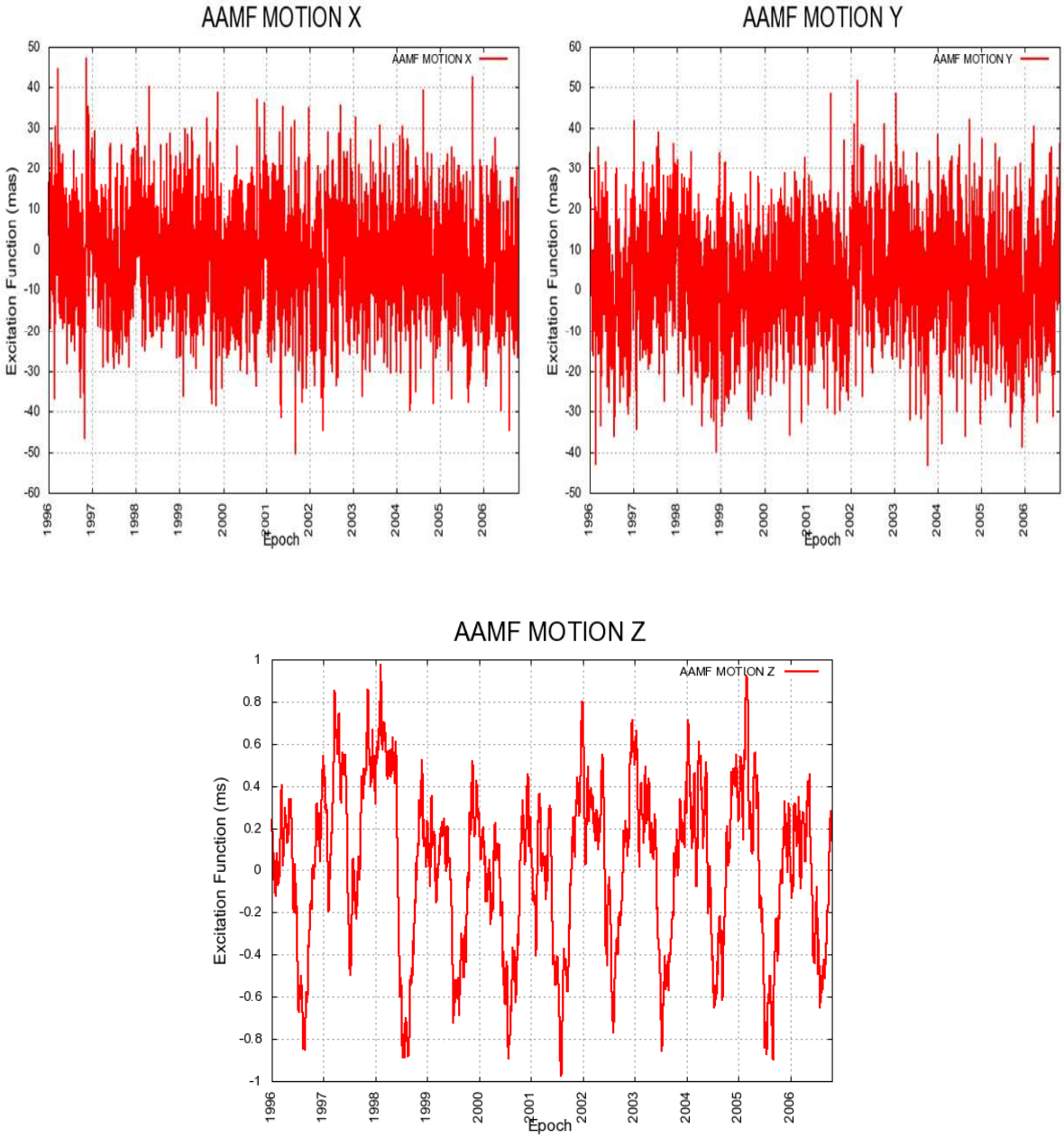

Figure 4.3 Atmospheric Angular Momentum Functions motion terms derived by NCEP

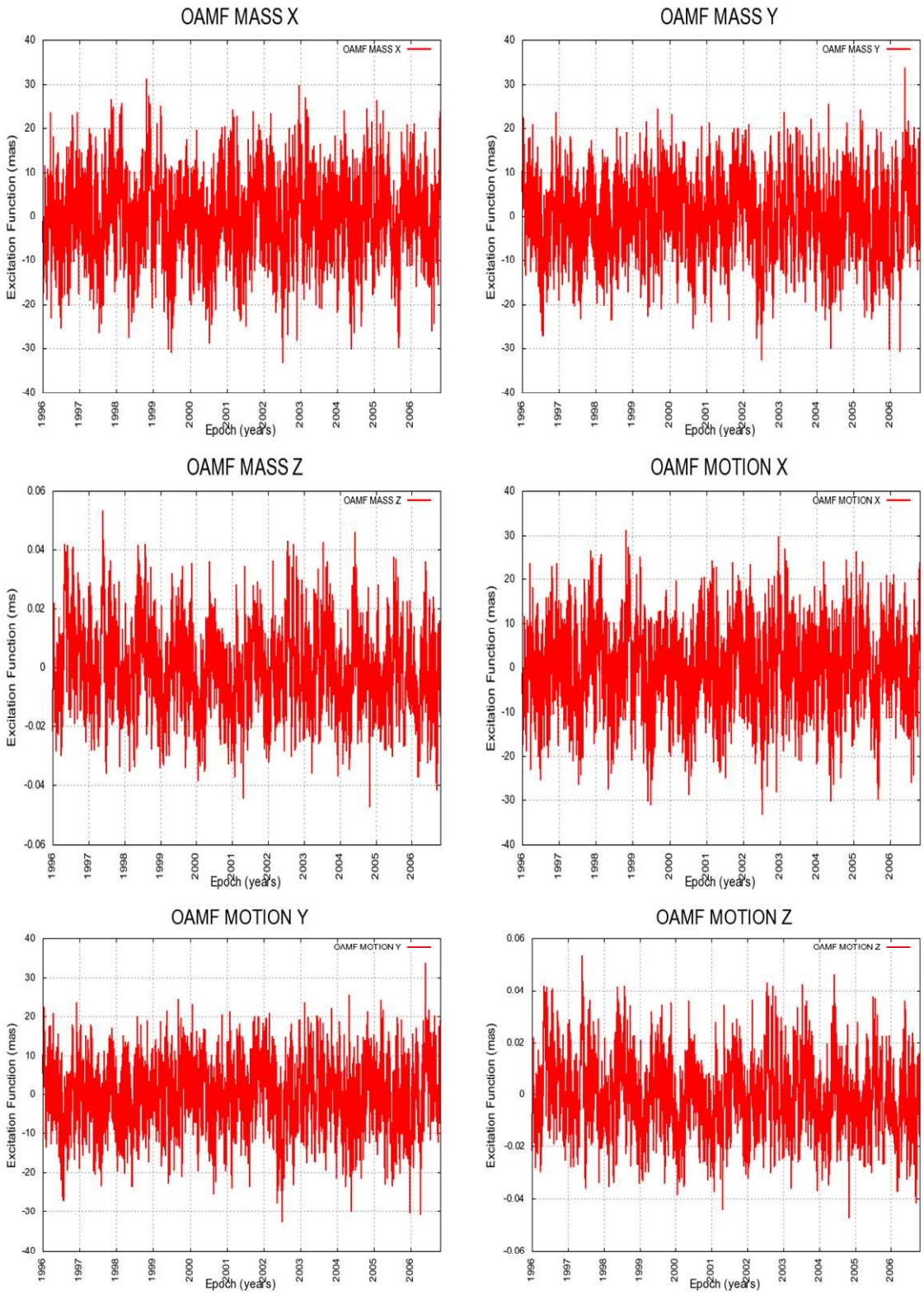

Figure 4.4 Oceanic Angular Momentum Functions motion and mass terms using the JPL ECCO circulation model kf049f

It should be noted at this point that the variance of the mass terms X, Y and Z derived using the Inverted Barometer (IB) correction are smaller than those when not utilizing this correction. This is due to the fact that in areas where the atmospheric pressure is far different from the mean atmospheric pressure over the Earth, using the correction gives a better approximation of the effects of atmospheric loading.
The IB correction effect is given by (Wunsch and Stammer, 1997):

$$IBC= -1/\rho G(\rho-P_{ref}) \quad \textbf{(4.19)}$$

where P_{ref} is the global mean pressure over the ocean, ρ is the density of the sea water and G is gravity. This correction takes into account the variability of the atmospheric pressure over the oceans. The correction involves substituting the mean atmospheric pressure with the atmospheric surface pressure over the oceans at every point (Salstein, 1993).

It should also be noted that the annual signal on the X component is less well defined than the annual signal on the other components. The reason for this may be that the major driver for the annual signal of polar motion is the build up of high pressure over Siberia every winter which is much closer to the Y axis than the X axis.

In Figure 4.4 the corresponding excitation functions from the movements and mass distribution of the oceans are plotted using the JPL ECCO circulation model kf049f as this was the most recent version at the time the work in this thesis was carried out. ECCO is based on an earlier MIT global ocean circulation model (Marotzke et al., 1999), details of which are given by Chen and Wilson (2003b). It can be noticed that excitation caused by the mass and motion of the oceans to the movement of the Earth is much smaller in the Y and Z terms compared with the effect of the mass and motion of the Earth's atmosphere. This effect is still significant within the Earth system. The effects on the X terms are similar when using the IB corrected mass term from the atmospheric data.

It can also be noticed that the motion Z term from the oceans is considerably smaller than that of the Z motion term from the atmosphere. The Z term is 10 times smaller in

the oceans than in the atmosphere. This is due to the much larger movements of the atmosphere (the zonal winds) around the rotation axis of the Earth when compared to the transport of the oceans. On the other hand the motion terms from X and Y are of similar size when compared with atmospheric terms and therefore must be considered as significant in how they affect the inertia of the Earth's rotation.

In Figure 4.5 the corresponding excitation functions from the distribution of the hydrology from the NCEP reanalysis model are plotted. Hydrology does not contribute to the motion part of the excitation so only mass terms are plotted. There is a very clear annual signal on all three components of the hydrological angular momentum functions. The sizes of the mass terms are similar to the mass terms computed from the ocean.

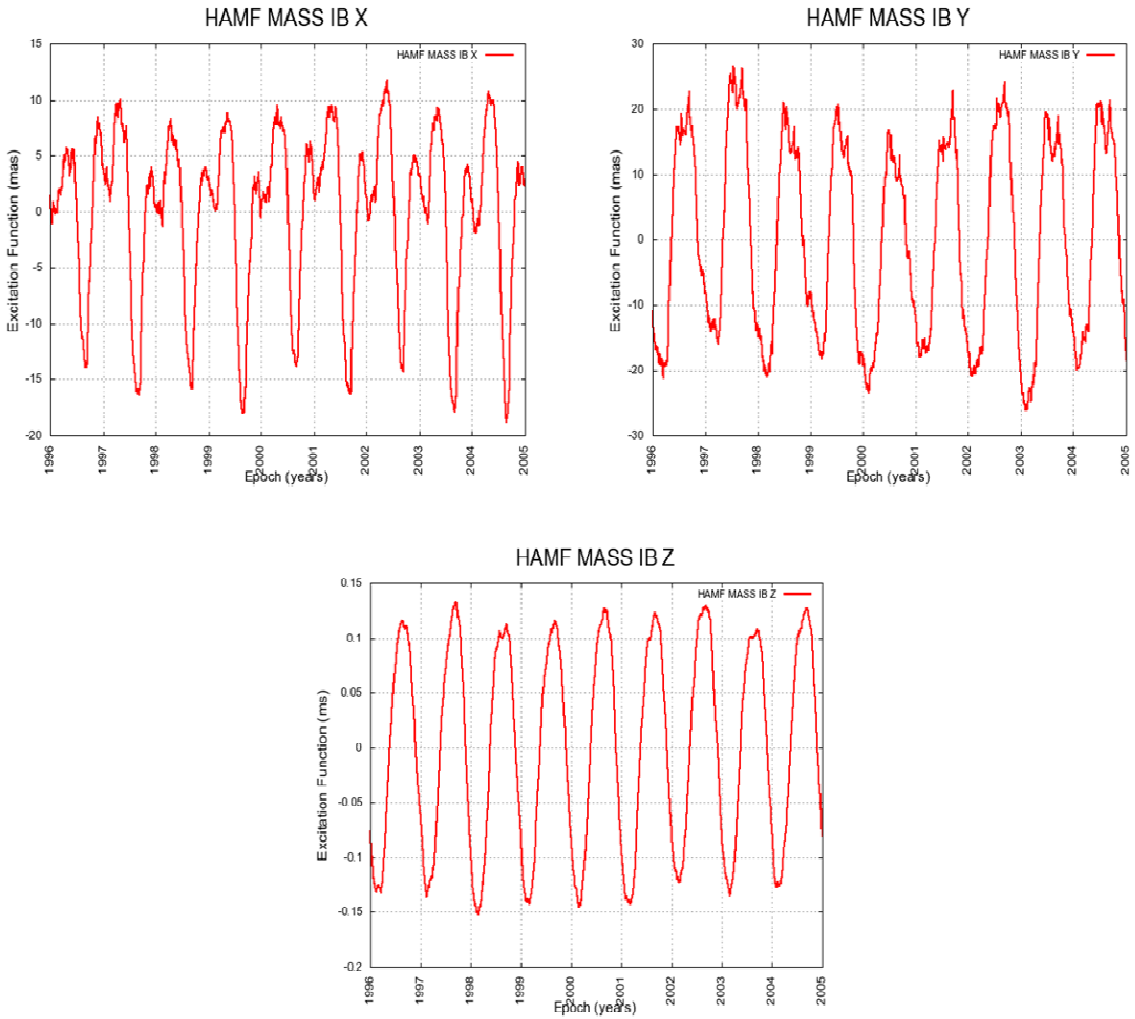

Figure 4.5 Hydrological Angular Momentum Functions mass terms from NCEP reanalysis

4.4 Angular Momentum Models

Geophysical data from which angular momentum values are derived, and thus excitation functions as shown above, come from a variety of sources. To assess how the values derived from these sources vary when compared to each other, an analysis of the difference between the models has been undertaken. This analysis of the different models will aid in choosing which model is the best suited in the new orbit determination procedure being developed in this thesis. As the atmosphere is the greatest contributing factor to the effect on the rotation of the Earth the values of AAMF from different organisations have been compared below.

Figure 4.6 - 4.11 show the comparison from four different organisations that produce values of AAMF; The four organisations are the European Centre for Medium Range Weather Forecasts (ECMWF), the Japan Meteorological Agency (JMA), the National Centre for Environmental Prediction (NCEP) and the United Kingdom Met Office (UKMO). Each of these centres computes the data at a different sampling rate. To make all the data the same sampling rate of 1 value every 15 days, to match the output from *FAUST*, weighted daily averages were taken for organisations whose sampling rates were greater than one day.

There were two possibilities for this. First, some data was given every 6 hours. In this case a weighted average at midday was computed using weights of $^1/_8$, $^1/_4$, $^1/_4$, $^1/_4$, $^1/_8$ for the 6 hour data starting at 0 hour.

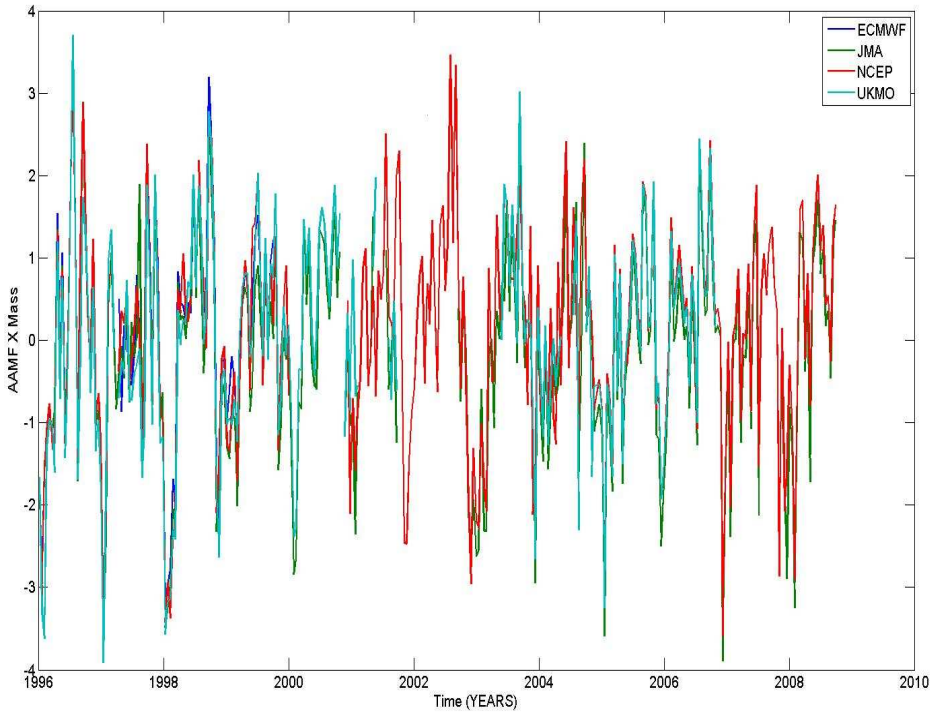

Figure 4.6 Comparison of AAMF X mass term from 4 different organisations

The second scenario was data given at midnight and at midday. In this case a weighted average of three values using weights of $^1/_4$, $^1/_2$, $^1/_4$, was derived from the data values spanning midnight, midday and next midnight respectively. Other data was already daily and this data was interpolated to give a daily value at midday. Once all the data had been converted into daily values a weighted 15 day average was computed to give a value at the middle of the 15 day period.

Figure 4.6 shows that there is very good agreement between all four organisations; estimates of the X mass term. It can also be seen that the data from ECMWF only spans the first few years of the compared data set and that there are large periods of data missing in the JMA and the UKMO time series. The only data series that is complete is the data series from NCEP.

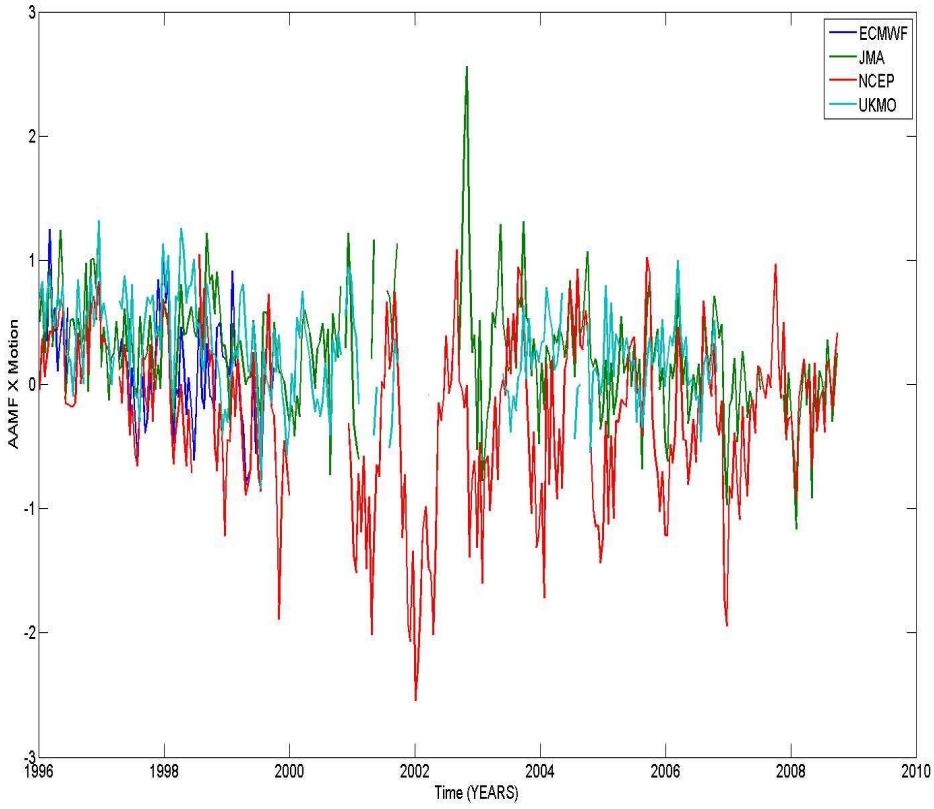

Figure 4.7 Comparison of AAMF X motion term from 4 different organisations

In contrast, when comparing the X motion term of AAMF from the same four organisations (Figure 4.7) it is immediately clear that the agreement is much less well defined. In the mass term shown in Figure 4.6 the annual signal, that would be expected to be present, caused by the semi annual and annual tides is very clear on all sets of data, whereas in Figure 4.7 although there is some resemblance of an annual signal, especially from NCEP data, the agreement of this seasonality between data sets is sketchy. This suggests that defining the motion term in the X axis from the collected data is much more difficult than defining the mass term.

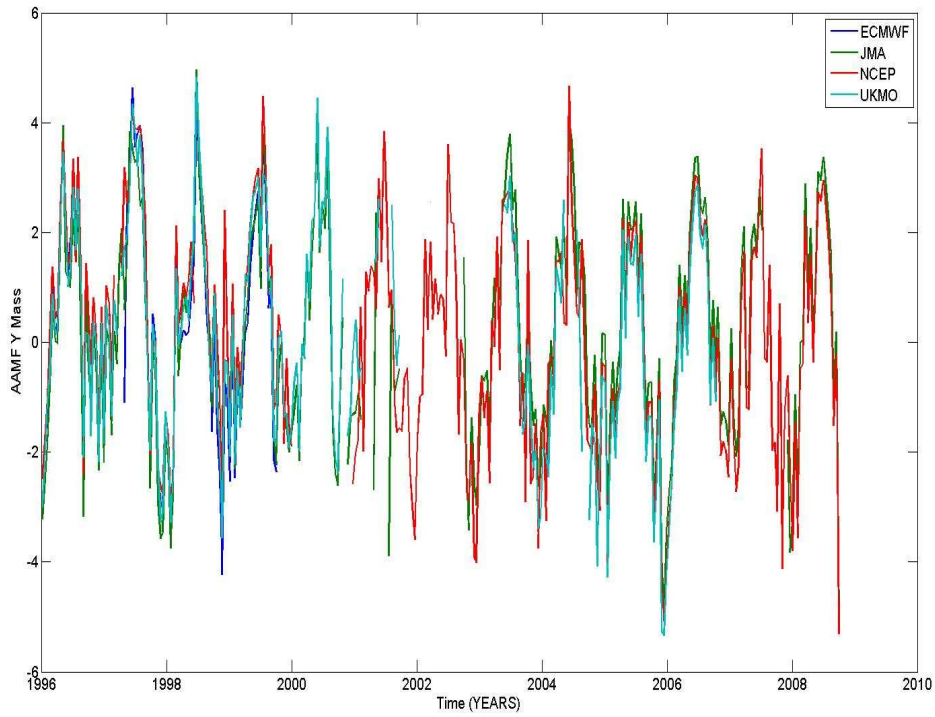

Figure 4.8 Comparison of AAMF Y mass term from 4 different organisations

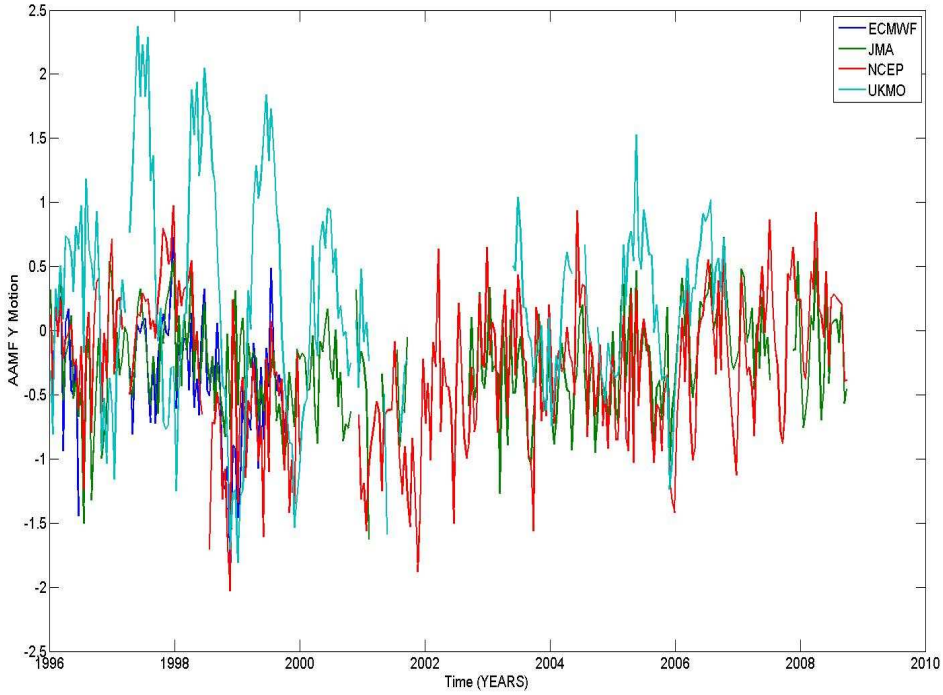

Figure 4.9 Comparison of AAMF Y motion term from 4 different organisations

Figure 4.8 shows the Y component of the AAMF, once again compared against each other. The comparison of the mass and motion Y components demonstrates very similar attributes to the X term, these being a very well defined annual signal in the mass term and a less well defined annual signal in the motion term (Figure 4.9).

In addition, the X motion and the Y motion terms do not agree well. Again this confirms that it is more difficult to define the motion term of the excitation functions. Once again the data with the best defined annual signal is that of the NCEP (Figure 4.9).

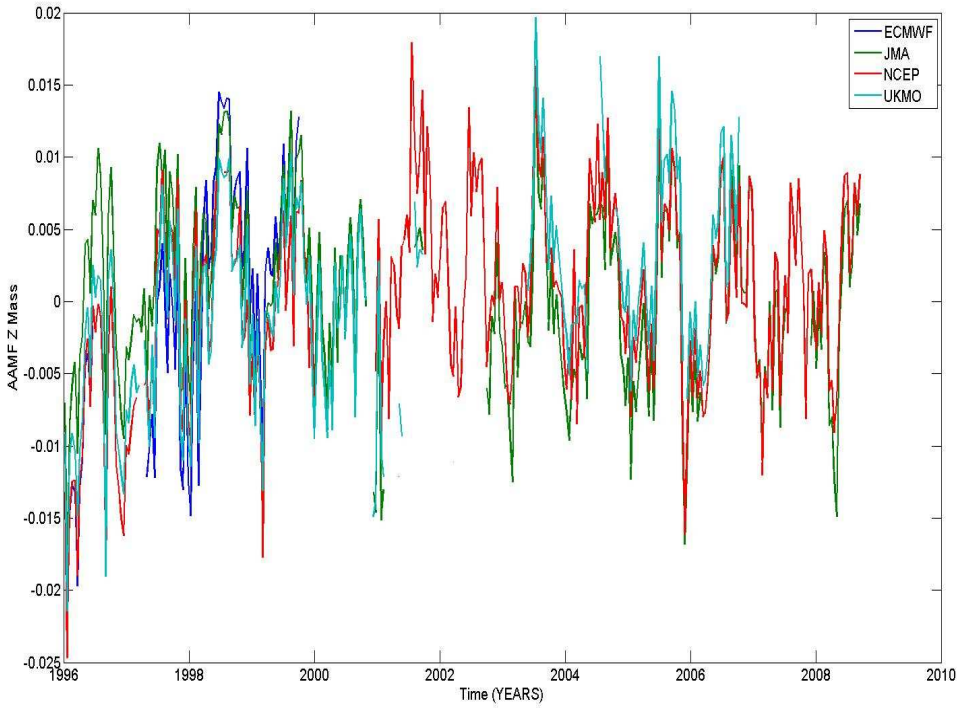

Figure 4.10 Comparison of AAMF Z mass term from 4 different organisations

Finally Figure 4.10 and Figure 4.11 show the comparisons of the data of the Z component of the AAMF. This time both the mass and motion terms from the Z component of AAMF from all centres have a clearly defined annual signal that corresponds to the changes in the seasons and weather patterns. There is also good agreement between all data sets for both the mass and the motion, although the agreement, in contrast to the X and Y components, seems to be better on the motion component. This suggests that evaluating the excitation on the Z axis is easier than

defining the excitation in the X and Y axes, especially when considering the motion part of the signal.

This data comparison has shown the AAMF data that is available and how complete the data sets are. The comparison has also shown how well these data sets agree with one another, which may give an insight into how AAMF data might compare with excitation computed from gravity and from ERP values as described in Chapter 3 and the beginning of this chapter.

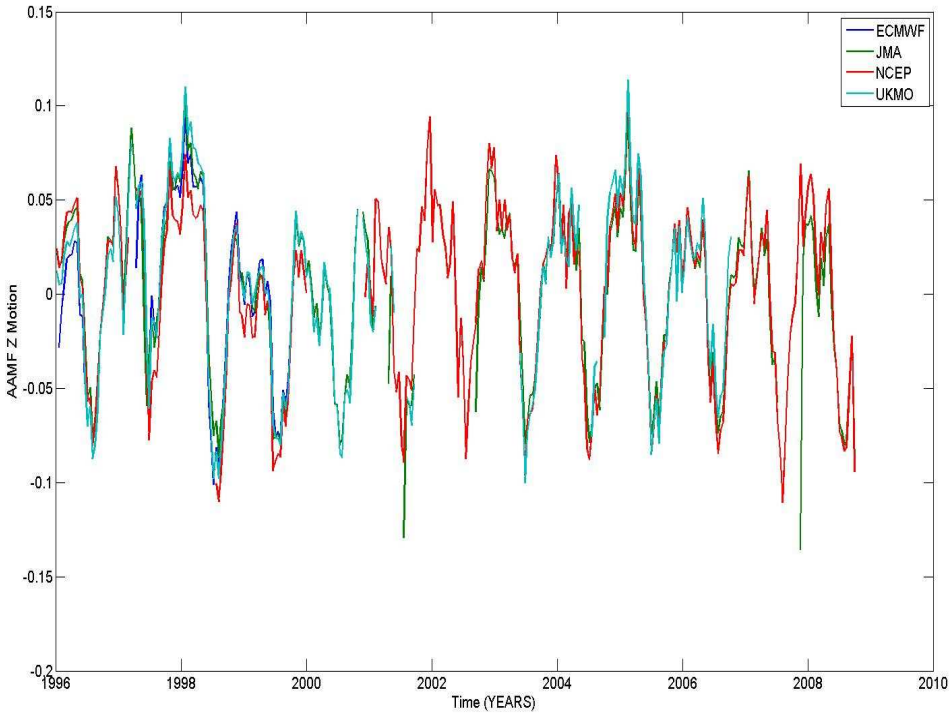

Figure 4.11 Comparison of AAMF Z motion term from 4 different organisations

Due to the fact NCEP data is the most complete data set, as well as being the data set that displays the most consistent annual signals in all the components of the excitation functions, the NCEP data will be chosen for use in the orbit determination process.

4.5 Conclusion

This chapter has discussed those excitation functions which are currently estimated by different organisations and discussed briefly how these terms are derived, what each excitation function includes and by whom the excitation functions have been derived. It has been shown that the major excitations with regard to the rotation of the Earth are driven by the atmosphere, which causes the largest excitation on an annual timescale. In addition, the ocean excitation is similar in size to the atmospheric excitation in the mass terms but less important in the motion terms, while the hydrological cycle which has a similar effect to that of the oceans in terms of mass load is not considered in terms of motion as this data is not available.

Finally values of AAMF computed by different meteorological organisations have been compared for consistency of signal, as well as how well-defined these signals are, as this may be important in an orbit determination process. It was noticed that the data from the NCEP was the most complete and best defined data set.

Chapter 5

5 Recovery of Gravity and Earth Rotation Parameters from SLR observations to LAGEOS

5.1 Introduction

In this chapter we will focus on the process of computing precise orbits for the LAGEOS satellites using Newcastle University's (POD) software *FAUST* (Moore et al., 1999; Boomkamp, 1998). Approximately 10 years of SLR data have been processed in 15 day arcs using the methods and models summarised in this chapter. All available SLR station data in the MERIT II format (ILRS, 2012) has been utilised in this research. The results from this processing will then be analysed.

5.2 Geodetic Satellites for Satellite Laser Ranging

In this study the satellites that have been used to calculate gravity field coefficients, station coordinates and ERPs are LAGEOS I and LAGEOS II where LAGEOS is an acronym for LAser GEOdynamics Satellite (Figure 5.1).

Both satellites are passive dense spheres with the surface covered by retro reflectors, allowing them to be tracked using SLR. LAGEOS I was developed by NASA and orbits the Earth in a high inclination (109º) orbit so that ground stations all over the world can track its orbit. LAGEOS II was developed jointly by NASA and the Italian Space Agency (ASI) and has been placed in an orbit (56º inclination) to complement LAGEOS I and more specifically to enable scientists to understand irregularities noticed in LAGEOS I's orbit as well as to provide more coverage of seismic activity particularly in the Mediterranean and in California (NASA, 2010). Both LAGEOS satellites orbit at an altitude of 5,900 km and have an orbital period of approximately 225 minutes. Due to their highly stable orbits the LAGEOS satellites orbits will not degrade significantly for millions of years. It is possible however that the degradation of the retro reflectors may shorten this lifespan.

Figure 5.1 LAGEOS I

The LAGEOS satellites have been specifically designed for very precise orbit determination. They have a high mass to limit the effects of non-gravitational forces as well as being light enough to be placed in a highly inclined orbit to improve coverage. They have a relatively small surface area to minimise the effects of solar radiation pressure. The material that they are made out of has been chosen to reduce the effect of the Earth's magnetic field (NASA, 2010). Overall these considerations make the orbits of the LAGEOS satellites very stable and therefore one of the most precise positioning references available. For these reasons LAGEOS has been chosen for this particular thesis.

5.3 Orbital Motion

In this section we will give a brief overview of the principles used in the *FAUST* software (Boomkamp, 1998; Moore et al., 1999). Most principles are consistent with the IERS2003 Conventions (McCarthy and Petit, 2003).

The orbital motion of a satellite can be described, in a coordinate system and under a force F by the equations of motion as

$$\ddot{\bar{r}} = \bar{F}(\bar{r}, \dot{\bar{r}}, t)/m \qquad \textbf{(5.1)}$$

where m is the mass of the satellite, t is time, $\bar{r}$ is the position, $\dot{\bar{r}}$ the velocity and $\ddot{\bar{r}}$ the acceleration.

FAUST uses a least squares estimation process to determine the orbit of the satellite. The basic idea of a least squares minimisation is to determine the orbital parameters of the satellite to minimise the squared difference between the mathematical model and the observed measurements. The problem that arises is that each measurement may have different units; therefore each measurement is weighted and what is actually used is the square of the weighted residuals (Montenbruck and Gill, 2000). Let the state vector be given by

$$\bar{x}(t) = \begin{pmatrix} \bar{r}(t) \\ \dot{\bar{r}}(t) \\ \bar{p} \\ \bar{q} \end{pmatrix} \qquad \textbf{(5.2)}$$

We can describe $\dot{\bar{x}}$ as

$$\dot{\bar{x}} = f(t, \bar{x}) \qquad \textbf{(5.3)}$$

with an initial value of

$$\bar{x}_0 = \bar{x}(t_0) \qquad \textbf{(5.4)}$$

i.e. $\bar{x}_0$ is the initial value of $\bar{x}$ at epoch t_0 .

Let z be defined by

$$\bar{z} = \begin{pmatrix} z_1 \\ \vdots \\ z_n \end{pmatrix} \tag{5.5}$$

This is the n-dimensional vector of measurements taken at epochs t_n, where the observations are described by (Montenbruck and Gill, 2000):

$$z_i = g_i(t_i, \bar{x}(t_i)) + \varepsilon_i = h_i(t_i \bar{x}_0) + \varepsilon_i \tag{5.6}$$

where $\bar{z}$ is the observation, in this case the range to the satellite, and g_i is the model value of the *ith* observation as a function of time t_i. On the other hand h_i is the same but as a function of the state $\bar{x}_0$ at the reference epoch t_0. The values ε_i give the difference between the actual and the modelled observations due to measurement errors and modelling deficiencies. This can be written briefly as

$$\bar{z} = \bar{h}(x_0) + \varepsilon \tag{5.7}$$

The least squares orbit determination problem can now be defined as finding the state that minimises the loss function (i.e. the squared sum of the residuals p_i)

$$\bar{J}(\bar{x}_0) = \bar{\rho}^T \bar{\rho} = \left(\bar{z} - \bar{h}(\bar{x}_0)\right)^T \left(\bar{z} - \bar{h}(\bar{x}_0)\right) \tag{5.8}$$

for some given set of measurements $\bar{z}$(Montenbruck and Gill, 2000).

5.3.1 Time

There are many different systems that are used in geodesy to describe time. All of these systems use units of days and seconds. As *FAUST* uses data that have time tags recorded using different time systems it is necessary to understand the difference

between these systems. The satellite equations of motion are defined in *FAUST* with reference to Terrestrial Time (TT). The observations are defined with reference to Universal Coordinated Time (UTC) and UT1 is used to perform the transformation between the terrestrial and celestial reference frames. A brief description of the time systems used in *FAUST* is now given (Montenbruck and Gill, 2000).

- TT, a conceptually uniform time scale that would be measured by an ideal clock on the surface of the geoid.
- International Atomic Time (TAI), which provides the practical realization of a uniform time scale based on atomic clocks and agrees with TT except for a constant offset and the imperfections of the clocks.
- GPS Time, which is a common time reference for GPS. Apart from management error (less than 100ns) GPS time differs from TAI by a constant offset:
  GPS time = TAI - number of leap seconds
- UT1, today's realization of a mean solar time, which is derived from Greenwich Mean Sidereal Time (GMST) by a conventional relation.

$$\begin{aligned} &GMST\,(0^h UT1) = 24110^s.54841 \\ &+ 8640184^s.812866 \cdot T_0 + 0^s.093104 \cdot T_0^{\,2} - 6^s.2 \times 10^{-6} \cdot T_0^{\,3} \end{aligned} \qquad \textbf{(5.9)}$$

where

$$T_0 = \frac{\mathrm{JD}(0^{\,\mathrm{h}}\,\mathrm{UT1})\ \text{-}\ 2451545}{36525} \qquad \textbf{(5.10)}$$

- UTC differs from TAI by an integer number of leap seconds to follow UT1 within 0.9s
- GMST, also known as Greenwich Hour Angle, denotes the angle between the mean vernal equinox of date and the Greenwich meridian.

$$\begin{aligned} &GMST = 24110^s.54841 \\ &+ 8640184^s.812866 T_0 + 1.00273790935079\,5\, UT1 \\ &+ 0^s.093104 T^2 - 6^s.2 \times 10^{-6} T^3 \end{aligned} \qquad \textbf{(5.11)}$$

where the time argument is

$$T = \frac{\text{JD(UT1)} - 2451545}{36525} \qquad \textbf{(5.12)}$$

which specifies the time in Julian centuries of Universal Time elapsed since 1st Jan 2000.

- Greenwich Apparent Sidereal Time (GAST), which represents the hour angle of the true equinox.
- TDB (barycentric dynamical time) is designated as the coordinate time in the barycentric frame of the solar system for a description of planetary and lunar motion. It differs from TT due to general relativistic effects. TDB is used to determine the positions of the solar system bodies, nutation and precession angles.

5.3.2 Reference Systems

The motion of a satellite is described within a reference frame that has its origin at the centre of the Earth but is free from rotation, known as a celestial reference frame (Montenbruck and Gill, 2000). SLR ranging of orbiting satellites is observed from stations that are fixed to the surface of the Earth which rotate with respect to the celestial reference frame. The coordinates of these ground stations are defined within a terrestrial reference frame. It is therefore essential to define the relationship between these two reference frames.

The J2000 reference system: In *FAUST* the satellite orbits are defined within the J2000 reference frame. The origin is defined as the Earth's centre of mass and the Z and X axes are defined as the mean rotation axis of the Earth and the mean equinox at 12 hour on 1st January 2000. The origin of this frame undergoes a small acceleration due to the annual rotation around the Sun and is therefore referred to as quasi-inertial.

Earth Centred Fixed (ECF) reference system: The origin of this reference frame is defined as the centre of mass of the Earth. The Z axis points toward the conventional

North Pole, while X is defined by the IERS zero meridian. This is realised by the ITRF2000 station coordinates.

True of Date reference system: The origin is defined as the Earth's centre of mass but the X axis is defined by the true equinox of date and Z is perpendicular to the true equator of date.

The relationship between these systems is given as

$$\begin{aligned} r(J2000) &= \underline{R}_2(-x)\underline{R}_1(-y)\underline{R}_3(GAST)\underline{N}\underline{P}\underline{r}(ECF) \\ r(TOD) &= \underline{N}\underline{P}\underline{r}(ECF) \end{aligned} \qquad \textbf{(5.13)}$$

where $\underline{N}$ and $\underline{P}$, the nutation and precession matrices (Montenbruck and Gill, 2000) and x and y are the angles that define polar motion and $R_i(\alpha)$ denotes the rotation matrix for an anti-clockwise rotation α about the i^{th} axis.

5.4 Equations of Motion

The equations of motion can be expanded from (Montenbruck and Gill, 2000)

$$\ddot{\underline{r}} = -\frac{GM}{r^3}\underline{r} \qquad \textbf{(5.14)}$$

to give

$$r = a_0 + a_\varepsilon \qquad \textbf{(5.15)}$$

$$a_0 = \frac{GM_e}{r^3}\mathbf{r} \qquad \textbf{(5.16)}$$

$$\mathbf{a}_{\varepsilon} = \sum_{i=1}^{8} \mathbf{a}_{\mathbf{i}} \qquad \textbf{(5.17)}$$

5.5 Force Model

Precise orbit determination requires us to model the forces that act on a satellite and perturb its motion. The main cause of orbital perturbation is the acceleration caused by non-spherical mass redistribution within the Earth described by equation 2.12. Gravity field theory has been described in more detail in Chapter 2. There are other effects that perturb the orbit of a satellite to a lesser degree; these are tidal effects, third body attraction, atmospheric drag, solar radiation pressure, Earth reflected radiation due to the Earth albedo and infrared radiation and relativistic effects. This therefore gives the equation of motion as:

$$a_{\mathbf{0}} = \frac{GM_e}{r^3}\mathbf{r} + \underline{a}_{\varepsilon} \qquad \textbf{(5.18)}$$

where

$$\underline{a}_{\varepsilon} = \underline{a}_1 + \underline{a}_2 + \underline{a}_3 + \underline{a}_4 + \underline{a}_5 + \underline{a}_6$$

Each element of $\underline{a}_{\varepsilon}$ as seen in equation 5.17, taken into consideration within *FAUST* will now be briefly described.

$a_1 =$ Perturbation caused by third body attraction

$a_2 =$ Perturbation caused by atmospheric drag

$a_3 =$ Perturbation caused by solar radiation pressure

$a_4 =$ Perturbation caused by albedo

$a_5 =$ Perturbation caused by tidal effects

$a_6 =$ Perturbation caused by relativistic effects

5.5.1 Third Body Attraction ($\underline{a}_1$)

As well as the Sun and Moon the planets cause a gravitational attraction that is large enough to consider in precise orbit determination. These planets are large distances from the Earth and can therefore be thought of as point masses. This gives Newtonian attraction of the form of equation 2.4. The equations of motion are described in the J2000 reference frame, this is a semi-inertial geocentric frame and therefore the effect of the gravitational attractions of the other planets is given as the difference between those attractions and that of the Earth as described by

$$\frac{\delta U_d}{\delta x_s} = -GM_d\left(\frac{x_d - x_d}{\left\|r_d - r_s\right\|^3} - \frac{x_d}{\left\|\underline{r}_d\right\|^3}\right) \qquad \textbf{(5.19)}$$

with similar expressions for x and y (Boomkamp, 1998). According to (Melbourne, 1983) the only bodies in the solar system for which equation 5.18 is non-negligible are, in order of importance, Sun, Moon, Venus, Jupiter, Mars and Mercury.

5.5.2 Atmospheric Drag ($\underline{a}_2$)

Atmospheric drag is the largest non-gravitational force acting on low orbiting satellites but has near negligible effect at higher altitude at which the LAGEOS satellites orbit. The effect of the atmosphere on the satellite depends on (Seeber, 2003):

- The geometry of the satellite
- The velocity of the satellite
- The orientation of the satellite, with respect to the flow
- The density, temperature and composition of atmospheric gas.

The mathematical representation of this is therefore quite complicated; here the acceleration of the satellite is given in the opposite direction to the flow.

$$\ddot{\underline{r}}_D = -\frac{1}{2}C_D\rho(\underline{r},t)\frac{A}{m_s}(\dot{\underline{r}} - \dot{\underline{r}}_a)\left|\dot{\underline{r}} - \dot{\underline{r}}_a\right| \qquad \textbf{(5.20)}$$

where m_s is the mass of the satellite, A the cross sectional area of the satellite, C_D the drag coefficient of the satellite, $\rho(\underline{r},t)$ the density of the atmosphere and $\underline{\dot{r}}_a$ is the velocity of the satellite relative to the ambient atmosphere.

5.5.3 Solar Radiation Pressure ($\underline{a}_3$)

Solar radiation pressure is the force exerted on a satellite by radiation from the Sun. The magnitude of its effect on a satellite's orbit depends upon the satellite mass and surface area. The acceleration of a satellite caused by solar radiation pressure is given by (Montenbruck and Gill, 2000).

$$\ddot{r} = -P_\Theta \frac{AU^2}{r_\Theta^2}\frac{A}{m}\nu\cos(\theta)\left[(1-C_r)e_\Theta + 2\varepsilon\cos(\theta)n\right] \qquad \textbf{(5.21)}$$

where m is the mass of the satellite, n is the normal vector that gives the orientation of the surface area A. ε is the reflectivity, n is inclined at an angle θ and the vector e_Θ points with respect to the direction of the Sun. P_Θ is the solar radiation pressure multiplicative coefficient, AU is the astronomical unit defined as $1.5\times10^8\,km$, r_Θ the satellite-sun distance in astronomical units, and C_r is the reflectivity of the satellite and $\cos(\theta)$ is defined as

$$\cos(\theta) = n^T e_\Theta$$

where n and e_Θ are unit vectors.

In equation 5.17 ν is the shadow function:

ν = 0, satellite is in the Earth's shadow,
ν = 1, satellite is in sunlight, and
0 < ν < 1, satellite is in the penumbra.

5.5.4 Albedo ($\underline{a}_4$)

Albedo is solar radiation pressure that has been reflected back onto the satellite by the Earth as well as the infra red radiation produced by the Earth's black body temperature (Wang, 2004). Once again the effect on the satellite is proportional to the surface area of the satellite and also to the reflectivity of the satellite. The perturbing acceleration is written as (Montenbruck and Gill, 2000).

$$\underline{\ddot{r}}_{SP} = \nu P_S \frac{C_r A}{m} (AU)^2 \frac{(\underline{r} - \underline{r}_S)}{(|\underline{r} - \underline{r}_S|^3)} \qquad \textbf{(5.22)}$$

where P_S is the Sun constant (quotient of solar flux and velocity of light in the Astronomical Unit), $\frac{A}{m}$ is the cross section area of the satellite as seen from the Sun divided by its mass, and C_r is the reflectivity of the satellite.

5.5.5 Tidal Effects ($\underline{a}_5$)

The tidal effects caused by the Moon and the Sun cause changes in the geopotential of the Earth. The effect caused by the solid Earth tides is expressed as

$$\underline{\ddot{r}}_e = \frac{k_2}{2} \frac{Gm_d}{r_d^3} \frac{a_e^5}{r^4} \left(3 - 15\cos^2\theta\right) \frac{\underline{r}}{r} + 6\cos\theta \frac{\underline{r}_d}{r_d} \qquad \textbf{(5.23)}$$

where m_d is the mass of the disturbing body, r_d is the geocentric position vector of the disturbing body, θ is the angle between the geocentric position vector $\underline{r}$ of the satellite and r_d and k_2 is the degree-2 Love number.

The effect of ocean tides on the Earth's geopotential is more difficult to model because of irregular coastlines. It is possible to use a global tide model e.g. (Eanes, 1994) to

compute for each point P on the ocean's surface the tidal heights and thus the total induced mass variations (Seeber, 2003):

$$dm_p = \rho_0 h(P,t) d\sigma \qquad \textbf{(5.24)}$$

where P_0 is the average density of water, t is the time and $d\sigma$ is a surface element. The variation of the potential is given by

$$\Delta U = \frac{G dm_p}{a_e} \sum_n (1 + k_n^{'}) P_{n0}(\cos\psi) \qquad \textbf{(5.25)}$$

where P_{n0} are the Legendre polynomials, $k_n^{'}$ are the deformation coefficients and ψ is the angle between the initial point A and the surface point P.

5.5.6 Relativistic Effects ($\underline{a}_6$)

According to McCarthy and Petit (2003) the correction to the satellite equations of motion for relativistic effects is given by

$$\mathbf{a} = \frac{GM_e}{c^2 r^3}\left[\left(4\frac{GM_e}{r} - \dot{r}^2\right)\mathbf{r} + 4(\mathbf{r}\cdot\dot{\mathbf{r}})\dot{\mathbf{r}}\right] \qquad \textbf{(5.26)}$$

5.5.7 Tropospheric Correction

The tropospheric model used within the *FAUST* software is the method described by Marini and Murray (1973)

$$\Delta R = \frac{f(\lambda)}{f(\phi, H)} \cdot \frac{A + B}{\sin E + \dfrac{B/(A+B)}{\sin E + 0.01}} \qquad \textbf{(5.27)}$$

where

$$A = 0.002357 P_0 + 0.000141_{E0}$$
$$B = \left(1.084 \times 10^{-8}\right) P_0 T_0 K + \left(4.734 \times 10^{-8}\right) \frac{p_0^2}{T_0} \frac{2}{(3 - 1/K)}$$
$$K = 1.163 - 0.00968 \cos 2\phi - 0.00104 T_0 + 0.00001435 P_0$$

where,

$\Delta R =$ range correction in metres

E = true elevation of satellite

P_0 = atmospheric pressure at the laser site

T_0 = atmospheric temperature at the laser site

e_0 = water vapour pressure at the laser site

$f(\lambda)$ = laser frequency parameter

$f(\phi, H)$ = laser site function, and

ϕ = geodetic latitude

5.5.8 Magnitude of Perturbations

Table 5.1 shows the relative magnitude of the accelerations caused by the aforementioned perturbations. It presents the accelerations acting on the Earth sensing satellite ENVISAT at an altitude of near 800 km given as an example of how the effects of the processes described above can affect satellite motion only. The effects on the LAGEOS satellites will be different, particularly in respect of atmospheric drag which is negligible due to the altitude of the LAGEOS satellites.

i	Cause	Magnitude of accelerations
1	Earth's oblateness C_{20}	10^{-3}
1	High-order geopotential harmonics: e.g. l=18, $_m$ =18	10^{-8}
2	Perturbation due to the Moon	10^{-7}
2	Perturbation due to the Sun	10^{-8}
2	Perturbation due to other planets (e.g. Venus)	10^{-11}
2	Indirect oblateness of the Earth	10^{-12}
2	Indirect oblateness of the Moon	10^{-15}
3	Atmospheric drag	10^{-8}
4	Solar radiation pressure	10^{-8}
5	Earth radiation pressure	10^{-9}
6	Solid Earth tides	10^{-8}
6	Ocean tides	10^{-9}
7	General relativistic correction	10^{-10}

Table 5.1 The orders of magnitude for various perturbing forces on ENVISAT (Montenbruck and Gill, 2000)

5.6 Integration of Equations of Motion

There are two methods of integrating the equations of motion of an Earth satellite (Seeber, 2003). These are analytical integration and numerical integration.

In analytical integration we attempt to find algebraic expressions for the forces acting on the satellite and integrate them in closed form. In this case we would define the Keplerian elements of the satellite's orbit and use Lagrange's equation of motion

$$\dot{a} = \sqrt{\frac{p}{GM_e}} \frac{2a}{1-e^2} \left\{ e \sin f \cdot R + \frac{p}{r} \cdot S \right\} \qquad \textbf{(5.28)}$$

$$\dot{e} = \sqrt{\frac{p}{GM_e}}\{\sin f \cdot R + (\cos f + \cos E) \cdot S\} \quad \textbf{(5.29)}$$

$$\dot{i} = \frac{r\cos(\omega + f)}{na^2(1-e^2)^{1/2}} W \quad \textbf{(5.30)}$$

$$\dot{\Omega} = \frac{r\sin(\omega + f)}{na^2(1-e^2)^{1/2}\sin i} W \quad \textbf{(5.31)}$$

$$\dot{\omega} = \frac{1}{e}\sqrt{\frac{p}{GM_e}}\left\{-\cos f \cdot R + \left(1 + \frac{r}{p}\right)\sin f \cdot S\right\} - \cos i \cdot \dot{\Omega} \quad \textbf{(5.32)}$$

$$\dot{M} = n + \frac{1-e^2}{nae}\left\{\left(\cos f - 2e\frac{r}{p}\right) \cdot R - \left(1 + \frac{r}{p}\right)\sin f \cdot S\right\} \quad \textbf{(5.33)}$$

where

a = axis of the oscillating ellipse

e = eccentricity,

i = inclination of the orbit with respect to the reference plane

Ω = right ascension of the ascending node

ω = argument of perigee

M, f and E are mean anomaly, true anomaly and eccentric anomaly respectively.

n = is the mean angular velocity of the satellite

p = $= a \cdot \left(1 - e^2\right)$

R, S and W are three components decomposed from $\mathbf{a}_\varepsilon$ i.e., radial, perpendicular to radius in the instantaneous orbital plane and normal to the orbital plane.

Numerical integration is the more widely used of the two methods, due to the increased complexity of the force modelling and the need for high accuracy (Seeber, 2003). It differs from the analytical method as all forces acting on a satellite at a particular

position are explicitly calculated and then used as starting conditions for a step wise integration, therefore the accelerations are integrated directly (Seeber, 2003).

5.7 Precise Orbit Determination Using *FAUST*

Newcastle University's POD software *FAUST* (Boomkamp, 1998) is a multi satellite, multi arc satellite orbit determination software. It uses a least squares process to minimise the sum of the residuals to obtain the best position of the satellite at a specific epoch. *FAUST* can process data from DORIS, PRARE and SLR as well as satellite altimetry (raw heights and crossovers), GRACE intersatellite range-rate data and Cartesian positioning derived independently from say GNSS tracking.

5.7.1 Modifications to *FAUST*

In the initial stages of this project several modifications were made to the *FAUST* software for the purposes of this thesis. It was essential that *FAUST* was able to calculate ERPs so that these could be used later to investigate the relationships between gravity, angular momentum and Earth rotation. Other corrections were also added to bring *FAUST* in line with IERS conventions. The major changes and corrections are discussed below.

5.7.1.1 Earth Rotation Parameters

Determining ERPs over a long period of time was an essential part of this project. The *FAUST* software therefore needed to be modified to allow it to solve for XP, YP, LOD and UT1. The basic concept of SLR is shown here.

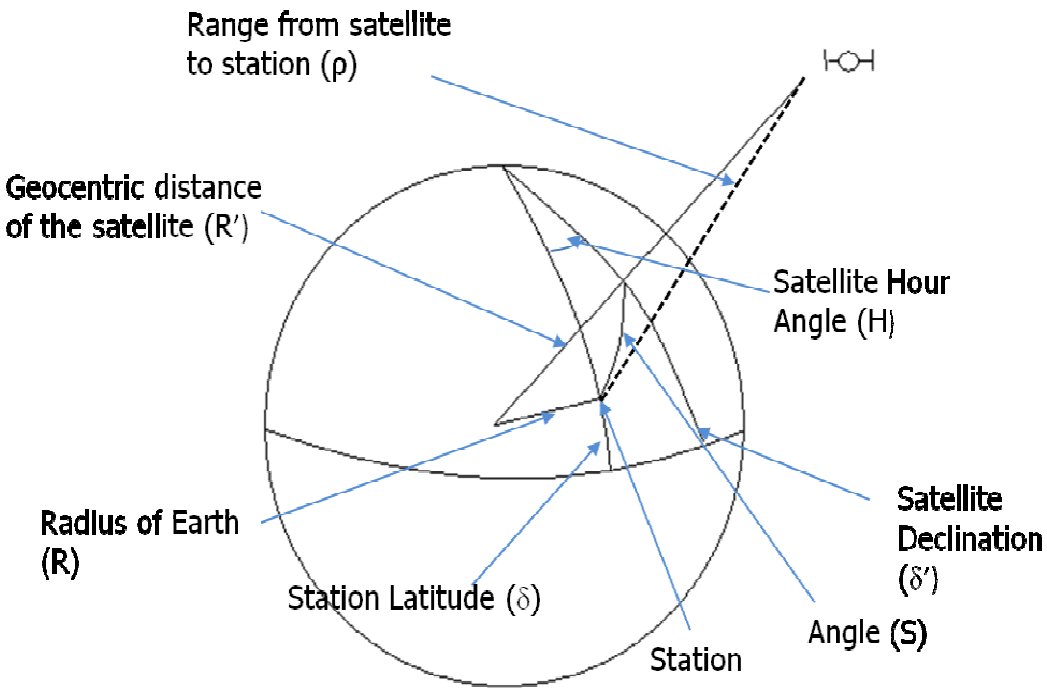

Figure 5.2 Principle of Satellite Laser Ranging (SLR) (I)

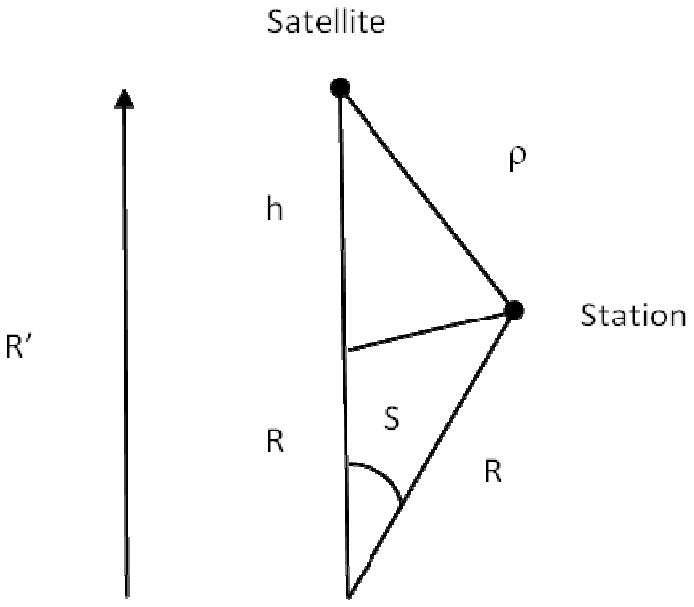

Figure 5.3 Principle of Satellite Laser Ranging (SLR) 2 (II)

where

R = radius of Earth

h = altitude

ρ = range of satellite from station

R’ = distance from centre of Earth to satellite

H = hour angle

δ’ = satellite declination

δ = station Latitude

and

$$\cos S = \sin\delta'\cos\delta + \cos\delta'\cos\delta\cos H$$

The software was modified so that satellites could be used to solve for ERPs. The observation equation for satellites being tracked by SLR for example is given by

$$\rho^2 = R^2 + R'^2 - 2RR'(\sin\delta'\cos\delta + \cos\delta'\cos\delta\cos H) \quad \textbf{(5.34)}$$

Partial differentiation of this equation yields the equations 5.34 and 5.35 below, which have been used within the least squares process in *FAUST* to solve for ERPs.

If there is a small change in UT1-UTC, then the effect is equivalent to increasing UT1 by this amount, with UTC fixed. This yields:

$$\frac{\partial\rho}{\partial(UT1-UTC)} = \frac{\partial\rho}{\partial H}\frac{\partial H}{\partial(UT1-UTC)} = \frac{\partial\rho}{\partial H}1.0027379 \qquad \textbf{(5.35)}$$

where the factor 1.0027379 is the ratio of the rate of change of sidereal time in a solar day.

From the partial differential for UT1-UTC we can obtain the partial differential for LOD at the midpoint of the arc as given below.

$$\frac{\partial \rho}{\partial LOD} = \frac{\partial \rho}{\partial (UT1 - UTC)} t \qquad \textbf{(5.36)}$$

We will now look at the coordinates of the pole. Let XP and YP be the coordinates of the pole and θ and λ the latitude and longitude of the station relative to the equator of date (i.e. the Earth's equator at a particular epoch is used as the fundamental plane of the reference system). Finally let θm and λm be the latitude and longitude of the station relative to BIH or CIO in an Earth fixed frame. The latitude and longitude of the station relative to the equator of date are given by Heiskanen and Moritz, 1967:

$$\begin{aligned} \theta &= \theta m + Xp \cos \lambda m - Yp \sin \lambda m \\ \lambda &= \lambda m + \tan \theta m \left(Xp \sin \lambda m + Yp \cos \lambda m \right) \end{aligned} \qquad \textbf{(5.37)}$$

This in turn gives the partial derivatives with respect to the range from SLR to be

$$\frac{\partial \rho}{\partial Xp} = \frac{\partial \rho}{\partial \theta}\frac{\partial \theta}{\partial Xp} + \frac{\partial \rho}{\partial H}\frac{\partial H}{\partial Xp} = \frac{\partial \rho}{\partial \theta}\cos \lambda m + \frac{\partial \rho}{\partial H}\tan \theta m \sin \lambda m \qquad \textbf{(5.38)}$$

$$\frac{\partial \rho}{\partial Yp} = \frac{\partial \rho}{\partial \theta}\frac{\partial \theta}{\partial Yp} + \frac{\partial \rho}{\partial H}\frac{\partial H}{\partial Yp} = -\frac{\partial \rho}{\partial \theta}\sin \lambda m + \frac{\partial \rho}{\partial H}\tan \theta m \cos \lambda m \qquad \textbf{(5.39)}$$

All equations are referenced to the true equator and equinox of date.

5.7.1.2 Ocean Tide Loading

Prior to this study *FAUST* did not account for deformations of the Earth caused by Ocean Tide Loading (OTL). Corrections to the a-priori station coordinates to account for this have been added and tested within the *FAUST* software. The mathematical models used for this came from IERS Conventions 2003 (McCarthy and Petit, 2003) with help from Dr Nigel Penna at Newcastle University whose own OTL software was

modified and implemented within *FAUST*. Corrections for 3 dimensional ocean tide loading are computed by

$$\Delta c = \sum_j a_{cj} \cos\left(\omega_j t + \chi_j - \phi_{cj}\right) \qquad \textbf{(5.40)}$$

with

$$\begin{aligned} a_{cj}\cos\phi_{cj} &= K_j\left[\frac{A_{ck}\cos\Phi_{ck}}{\overline{K}_k}(1-p)+\frac{A_{c,k+1}\cos\Phi_{c,k+1}}{\overline{K}_{c,k+1}}p\right] \\ a_{cj}\sin\phi_{cj} &= K_j\left[\frac{A_{ck}\sin\Phi_{ck}}{\overline{K}_k}(1-p)+\frac{A_{c,k+1}\sin\Phi_{c,k+1}}{\overline{K}_{c,k+1}}p\right] \end{aligned} \qquad \textbf{(5.41)}$$

where

$\Delta c =$ displacement component (radial, west, south)

K_j = amplitude

ω_j = velocity

$\chi_j =$ astronomical argument at $t = 0^h$

$A_{ck} =$ amplitudes of ocean tides

$\Phi_{ck} =$ phase of ocean tides

The phase and amplitudes are taken from the relevant model and input in equation 5.40 (McCarthy and Petit, 2003). OTL has been tested and is now being successfully used to process satellite data within *FAUST*.

5.7.1.3 Relativistic effects

The relativistic propagation correction for laser ranging is due to space-time curvature near the Earth. It amounts to about 1cm. The correction is given in seconds Δt . The

equations are given below and are taken from the IERS Conventions 2003 (McCarthy and Petit, 2003).

$$R_1 = \sqrt{x_{Sta}^2 + y_{Sta}^2 + z_{Sta}^2}$$
$$R_2 = \sqrt{x_{Sat}^2 + y_{Sat}^2 + z_{Sat}^2} \quad \textbf{(5.42)}$$

$$\Delta t = \frac{(1+\gamma)GM}{c^3} \ln\left(\frac{R_1 + R_1 + \rho}{R_1 + R_1 - \rho}\right) \quad \textbf{(5.43)}$$

where

x_{Sta} = x position of the station

x_{Sat} = x position of the satellite

R_1 = distance from the body's centre (of the Earth) to the beginning of the light path

R_2 = distance from the body's centre (of the Earth) to the end of the light path

c = speed of light

GM = gravitational parameter of the deflecting body

γ = PPN parameter equal to 1 in general relativity

5.7.1.4 SINEX

Data submitted to and used by the ILRS are required to be in SINEX format. The SINEX format has been used since 1995 by the International GNSS Service (IGS) and was developed as a tool for storing GPS products. SINEX was further developed to handle other geodetic techniques and the ILRS and International VLBI Service (IVS) use it for their projects which meant that additions were made to the then SINEX 1.00 to become SINEX 2.00. The format of output from *FAUST* at the start of this project was an in house format only used in *FAUST*. *FAUST* now outputs results in both the original format and in SINEX version 2.00.

5.7.2 Orbit Determination Strategy

Precise orbit determination of LAGEOS I and LAGEOS II for the period July 1996 – March 2007 from satellite laser tracking has been processed for this study. The SLR data (normal points) utilised in this study were obtained from the ILRS data archive hosted by the Crustal Dynamics Data Information System (CDDIS) in the MERIT-II data format. All available data in this data set was used in this study, although some data was rejected based on rejection criteria that will be explained later in this thesis.

Although all the available data in the MERIT-II data set has been used the number and distribution of SLR stations is far from ideal. Figure 5.4 shows the locations of all the SLR stations and their current status.

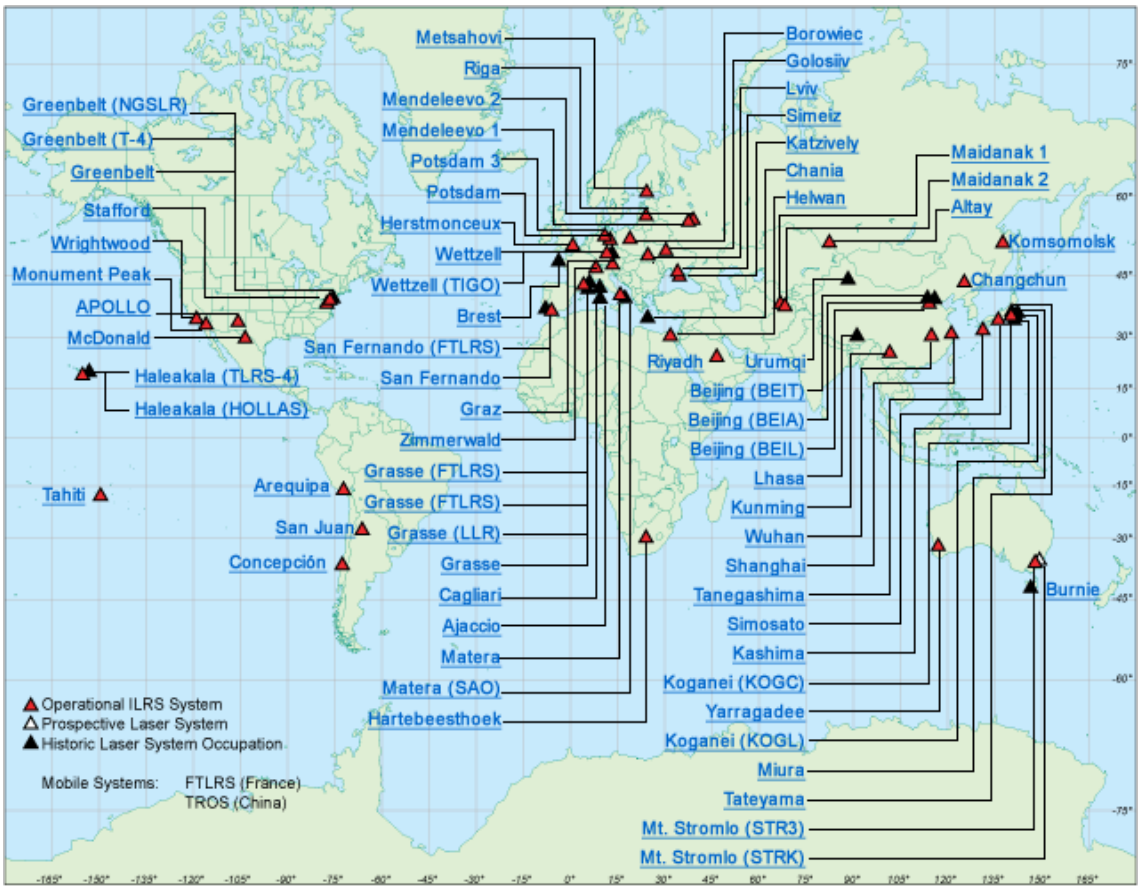

Figure 5.4 Map showing the distribution of SLR stations (ILRS, 2011)

Figure 5.5 shows the relative average single shot RMS in mm for LAGEOS (column 14), from different ILRS stations, for the last quarter in 2007, with RMS values ranging from 5.8 mm to 70 mm. The ILRS produce a report similar to this each quarter. Below is a description of what is contained in each column of the report card. By reference to these report cards the data used in the study can be identified.

Column 1 *is the station location name.*
Column 2 *is the monument marker number.*
Column 3 *is the LEO pass total during the past 12 months.*
Column 4 *is the LAGEOS pass total during the past 12 months.*
Column 5 *is the high satellite pass total during the past 12 months.*
Column 6 *is the pass total (i.e., all satellites) during the past 12 months.*
Column 7 *is the LEO NP total during the past 12 months.*
Column 8 *is the LAGEOS NP total during the past 12 months.*
Column 9 *is the high satellite NP total during the past 12 months.*
Column 10 *is the NP total (i.e., all satellites) during the past 12 months.*
Column 11 *is the total tracking minutes (i.e., all satellites) during the past 12 months.*
Column 12 *is the average single-shot calibration RMS (mm), during the last quarter.*
Column 13 *is the average single-shot Starlette RMS (mm), during the last quarter.*
Column 14 *is the average single-shot LAGEOS RMS (mm), during the last quarter.*

Station dependant weights of between 10 cm and 30 cm have been chosen according to the quality of the data from a particular station. These weights have been chosen by analysing data from the ILRS (ILRS, 2007). Any station with a LAGEOS RMS greater than 20 mm has been weighted using 30 cm in the solution. All other stations are weighted using 10 cm.

Site Information		Data Volume									Data Quality		
Column 1	2	3	4	5	6	7	8	9	10	11	12	13	14
Location	Station Number	LEO pass Tot	LAGEOS pass Tot	High pass Tot	Total passes	LEO NP Total	LAGEOS NP Total	High NP Total	Total NP	Minutes of Data	Cal. RMS	Star RMS	LAG RMS
Baseline		1000	400	100	1500								
Yarragadee	7090	9157	1799	1333	12289	185376	23606	12582	221564	159023	4.8	8.8	9.5
Zimmerwald_423	7810	5812	1192	686	7690	91464	14378	4363	110205	75943	11.5	14.3	17.6
Zimmerwald_846		5736	1199	625	7560	90428	16171	3563	110162	75403	24.9	21.6	24.7
San_Juan	7406	5022	892	1173	7087	79811	11156	7721	98688	83366	8.5	24.9	14.2
Mount_Stromlo_2	7825	4882	1193	502	6577	61919	11713	3325	76957	61113	3.2	4.7	6.5
Graz	7839	4811	825	529	6165	96207	9263	4380	109850	64786	2.3	4.0	8.0
Wettzell	8834	4152	1041	518	5711	43944	8055	2288	54287	42329	5.8	12.9	18.5
Changchun	7237	4361	772	541	5674	48822	6321	2810	57753	40822	14.1	14.4	17.5
Riyadh	7832	3773	970	658	5401	48095	8135	3881	60111	51027	11.2	14.2	17.2
Herstmonceux	7840	3858	932	413	5203	60840	11396	1843	74079	47268	6.1	10.1	12.9
Concepcion_847	7405	2188	1078	238	3504	30884	14860	1897	47641	50858	5.4	10.1	12.0
Concepcion_423		21	4		25	185	19		204	120	4.1	8.3	10.4
Matera_MLRO	7941	2261	753	232	3246	31590	8142	2076	41808	37355	2.1	5.0	5.9
San_Fernando	7824	2587	523	52	3162	38147	4072	286	42505	21414	5.2	11.5	15.1
Monument_Peak	7110	2482	484	192	3158	48238	5188	1664	55090	31832	5.3	13.2	15.9
Arequipa	7403	2065	218		2283	24398	1481		25879	10793	5.5	7.9	6.9
Greenbelt	7105	1830	321	69	2220	41050	3412	400	44862	19619	5.6	8.7	9.5
Beijing	7249	1702	339	154	2195	23782	3287	1213	28282	20292	7.3	16.9	16.6
Potsdam_3	7841	1724	304		2028	32666	3532		36198	15563	12.2	14.7	19.2
McDonald	7080	1378	412	236	2026	15249	3735	925	19909	16535	15.8	13.1	12.5
Hartebeesthoek	7501	1535	304	35	1874	19676	2708	214	22598	12756	6.0	7.8	10.4
Haleakala	7119	1488	350		1838	23479	4056		27535	15518	4.8	9.9	9.9
Katzively	1893	1192	287	36	1515	19542	2453	227	22222	12395	31.1	42.8	40.2
Koganei	7308	703	248	164	1115	10638	2529	1509	14676	16316	9.7	13.1	15.5
Shanghai_2	7821	957	53	3	1013	11459	486	22	11967	4865	14.6	22.1	24.8
Simosato	7838	717	266	1	984	13349	3914	11	17274	12255			
Maidanak_1	1864	509	216	141	866	6086	1672	600	8358	7849		51.1	69.5
Riga	1884	557	111		668	9965	1134		11099	4912	7.4	9.0	12.0
Simeiz	1873	450	151	11	612	5375	1348	166	6889	4944		54.8	58.7
Borowiec	7811	360	99	4	463	5910	1039	14	6963	3961	13.8	19.8	
Tanegashim	7358	240	70	54	364	4071	683	464	5218	4896	3.3	4.5	5.8
Lviv	1831	127	18		145	2344	166		2510	1055	14.3	47.6	70.0
Burnie_Tafe	7370	100	2		102	1957	12		1969	686	5.9	11.7	17.7
Helwan	7831	54			54	379			379	113	6.0	8.4	
Kunming	7820	18	2		20	262	15		277	118	18.5	16.9	37.4
Papeete	7124	19			19	254			254	83			
NRL	7865	9			9	131			131	10			
Kiev	1824	1			1	12			12	6			

Figure 5.5 Table showing the relative quality of SLR stations 4th quarter 2007 (ILRS, 2007)

Pre-processing of the normal point MERIT-II data was carried out to extract the one way ranges, time tags and meteorological data. Also the data is sorted chronologically: duplicates are removed and ranging and timing biases corrected using data provided by the ILRS. Finally the data is converted into a format readable by *FAUST*.

In the first instance a base solution was calculated within the *FAUST* software. This base solution will be used firstly to validate the implementation of the new processing methods within *FAUST* and then as a means of testing orbit determination processes using a new method for calculating the low degree harmonics of the Earth's gravity field. It also defines the processing strategy that will be used throughout this thesis, the models and constraints described below will be utilised throughout the work carried out in this thesis unless otherwise stated.

To produce the base solution and to reduce errors in modelling, a satellite state vector (positions and velocities) was estimated over a 5 day arc, along with two empirical along track accelerations and one solar radiation pressure parameter. As the LAGEOS satellites are effectively above the Earth's atmosphere air-drag is negligible. However, there are some drag-like effects which are modelled as constant terms over 2.5 days and estimated within the solution. The individual 5 day arcs were grouped together into 15 day arcs over which global parameters (e.g. station coordinates, ERPs, gravity field harmonics) were to be estimated. This is because the global parameters give more reliable results when solved for over longer periods of time and the satellite dependant parameters are better solved over shorter arcs. These sets of three 5 day arcs were first processed with no global parameters and iterated until convergence. After convergence any stations with less than 20 measurements and/or with a post fit RMS of over 5 cm were removed from the orbits. These orbits were then re-processed again until convergence was obtained.

To create the base solution the global parameters were now introduced. In the base solution the ERPs XP, YP and LOD were estimated at midday on a daily basis using the a-priori values taken from the IERS C04 file that have been linearly interpolated to give parameters at midday. The IERS C04 data was used as a-priori for the ERPs as at the time of writing it was the most up to date long term data set for ERPs. The C04 daily values for UT1-UTC were held fixed to place a constraint on the LOD values. In

addition to Earth rotation parameters the station coordinates for each of the stations used in any particular 15 day arc were also estimated.

The a-priori estimates for station coordinates were taken from ITRF2000. The computations were obtained by placing weak constraints of 1m on station coordinates and the equivalent of 1m surface displacement on polar coordinates while holding UT1-UTC fixed. The estimation of UT1-UTC and LOD are not independent as Earth rotation cannot be separated from satellite motion. In particular, errors in the satellite force model ascending node cannot be separated from LOD. However, by assuming that the mis-modelling gives rise to long –term errors in the node, the seasonal and shorter term signatures in the LOD can be attributed to mass and motion excitations. Orbital modelling included the GGM01C gravity field model (Tapley et al., 2003) to degree and order 20 and the CSR4.0 (Eanes, 1994) ocean tidal model.

The same constraints have been used in all solutions in this thesis unless otherwise stated. The same models have been used as input to *FAUST* in all solutions mentioned in this thesis unless otherwise stated.

To begin with *FAUST* was utilised as described above to determine orbits and estimates of ERPs and station coordinates over the specified period. No estimates for gravity field coefficients have been calculated in the base solution.

Using the base solution as the starting point, orbits were then estimated by solving for low degree harmonics of the Earth's gravity field up to degree three. By solving for gravity field harmonics it is only possible to compute one estimate for each harmonic over the 15 day arc as 5 days is too short.

5.7.2.1 Determination of the Satellite Orbits

The first solution estimated using *FAUST* was a solution estimating only the state vector, the two along track empirical accelerations over each 5 day arc and a single solar radiation pressure coefficient per 5 day arc. This was undertaken to have an initial validation of the addition of ERPs to the *FAUST* software. The results in Figure 5.6

show that all post fit residual RMS values for the estimation procedure without solving for any global parameters are at the 4 cm level; all post fit residual RMS values are below 5 cm with the mean for the combined solution being 3.89 cm and the median 3.93 cm.

As specified earlier the daily ERPs and the coordinates of the station used in the solution are now solved for. This solution is subsequently called the base solution. A brief analysis of the base solution orbit will now be undertaken. Figure 5.7 shows the post fit residual RMS of the base solution over the 15 day time periods. This will be used as a comparison for all other data sets to be analysed.

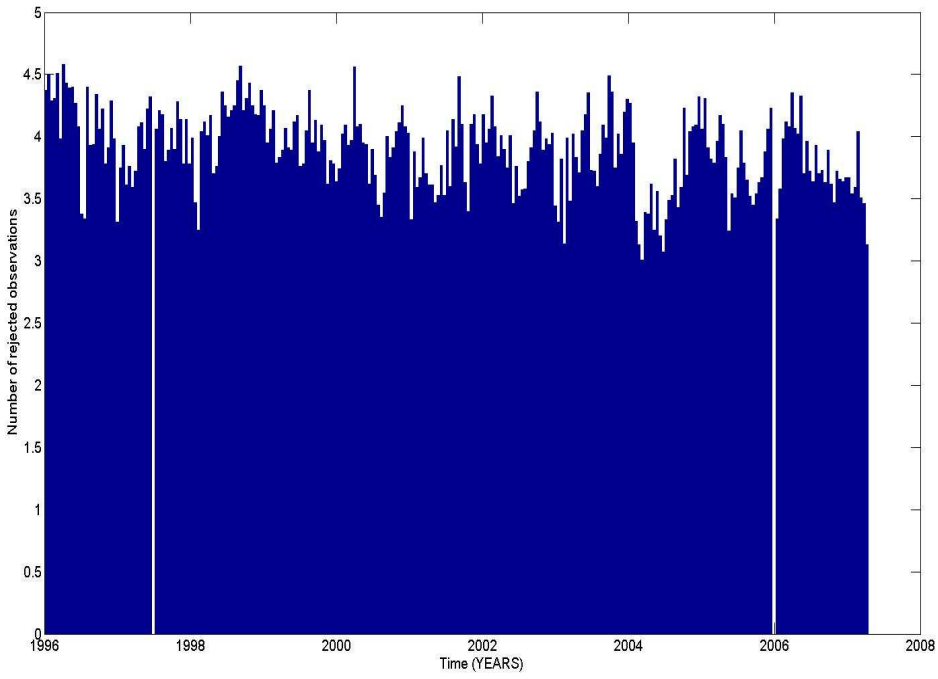

Figure 5.6 RMS fit of orbit solution solving only for state vectors, 2 along track accelerations and 1 solar radiation pressure every 5 days

It is expected that the estimation of the additional parameters XP, YP and LOD on a daily basis would improve the fit to the overall solution shown in Figure 5.6. It can be seen that the corresponding 15 day data fit in Figure 5.7 is always less than 2.5 cm. The mean fit of the data is 1.35 cm and the median is 1.31 cm. When Figure 5.7 is compared

with Figure 5.6 there is a large improvement in the fit of the orbits with the mean value of the combined orbits lowered by 65% and the median lowered by 66%. This gives strong supporting evidence to the fact that the ERP procedure has been successfully introduced into *FAUST*.

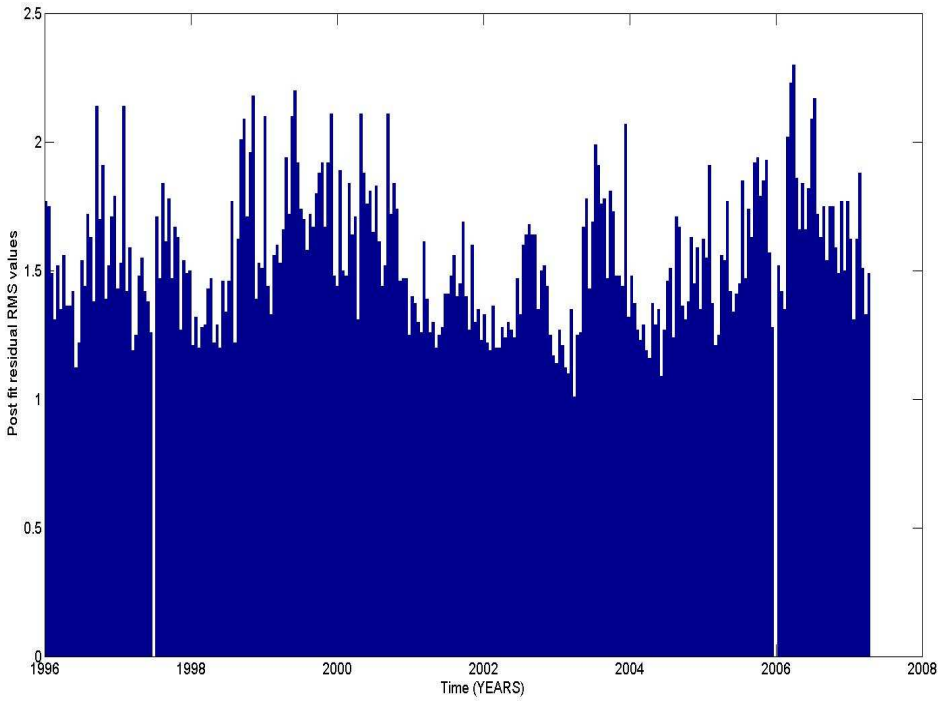

Figure 5.7 RMS fit of base solution; i.e. (solving for state vectors, 2 along track accelerations and 1 solar radiation pressure every 5 days and station coordinates and ERPs estimated over 15days)

Figure 5.8 shows the number of rejected observations per 15 day arc. The number of rejected observations decreases with time over the course of the data analysis. This is likely to be due to the improvements made in laser technology over the period of the data utilised in this study.

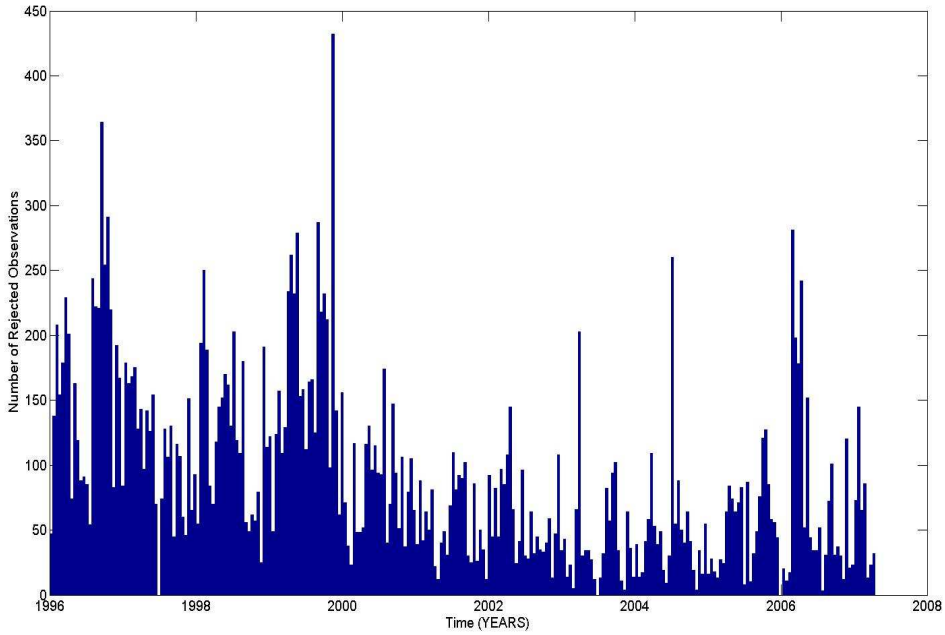

Figure 5.8 Number of rejected observations for base solution

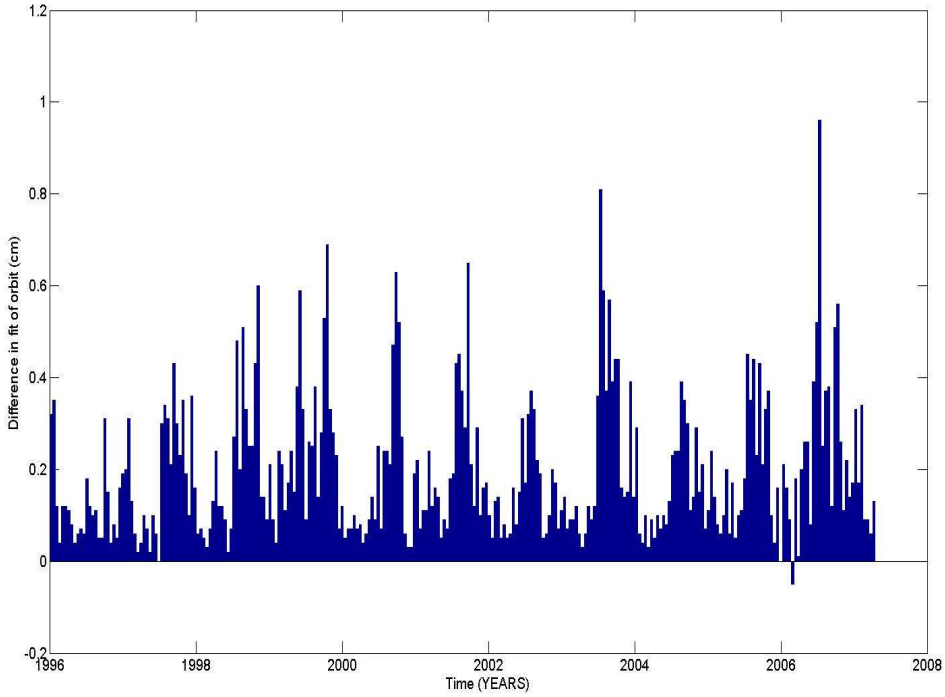

Figure 5.9 The difference of RMS fit from the base solution to the RMS fit of the base solution plus degree-3 gravity estimates (positive values show improvement with gravity estimates)

The base solution is now compared with the RMS fit to the tracking data when solving for gravity field harmonics up to degree and order 3. Figure 5.9 shows that by solving for degree-3 harmonics of the Earth's gravity field the overall fit of the orbits are improved on 99.6% of the processed arcs**.**

Figure 5.10 shows the difference in the number of rejected observations arc to arc over the processed data period between the base solution and the base solution plus estimates of the Earth's gravity field. The graph shows that the vast majority of arcs (221 out of 273 or 81%) have used either the same number or a larger number of measurements to estimate the orbits. This shows that solving for gravity over a 15 day arc results in a large improvement on the overall fit of the orbit compared with using a constant value for gravity.

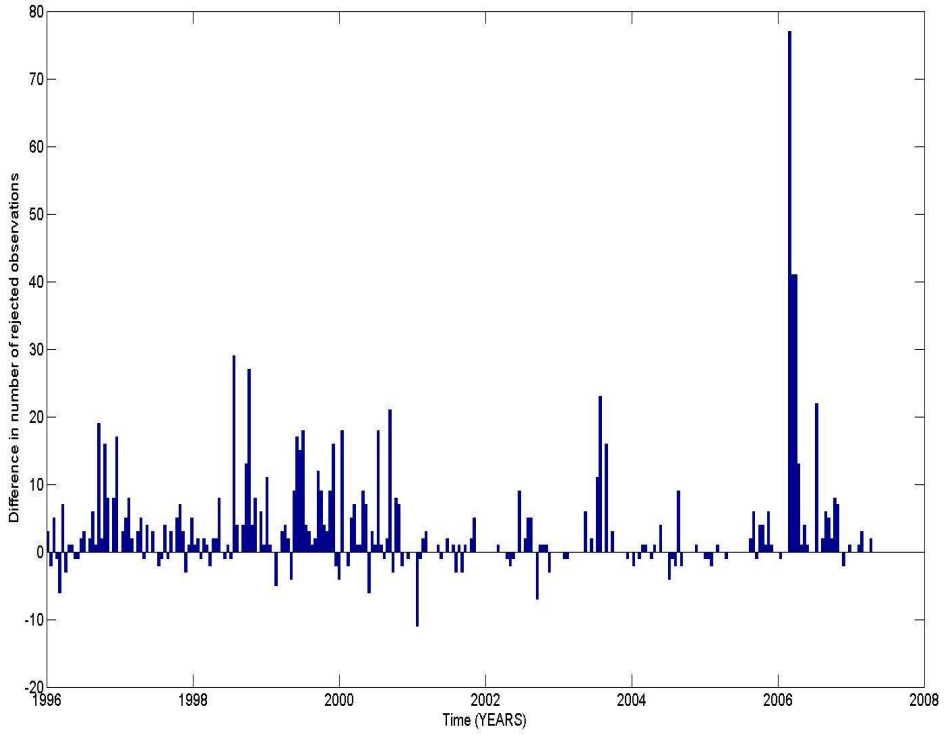

Figure 5.10 The difference in the number of rejected observations of the base solution plus degree-3 gravity estimates (positive values show improvement with gravity estimates)

In addition to this, *FAUST* was used to compute orbits that use estimates of the gravity field harmonics up to degree and order 4. The difference in the low degree gravity field harmonics J2, C21 and S21 from the degree-3 solutions and a degree-4 solution will be compared in section 5.7.2.3.

Figure 5.11 shows that by solving for higher degree and order terms of the Earth's gravity field there is a further improvement in the post fit residual RMS of the processed orbits. 270 (or 99%) out of the 273 arcs estimated obtained either the same or better post fit residual RMS than solving for only the degree-3 harmonics. The improvement after introducing degree-4 gravity field coefficients can be seen to be less than the improvement in fit when first introducing the degree-3 harmonics. The mean improvement in post fit residual RMS over the time period when adding the degree-4 harmonics is 0.07 cm.

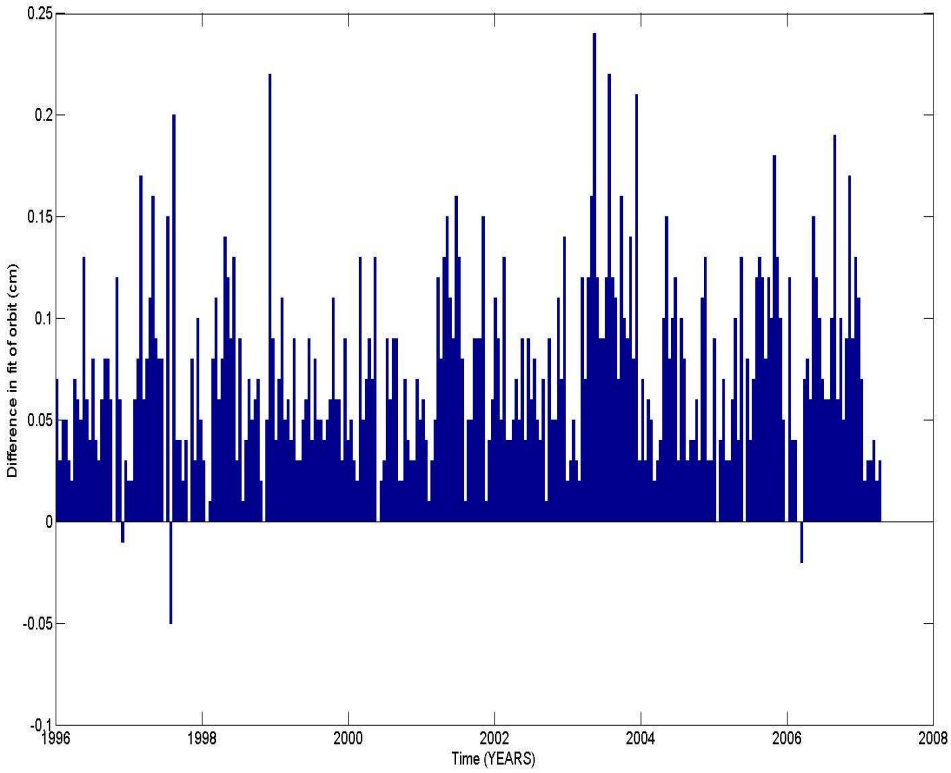

Figure 5.11 The difference of RMS fit between the degree-3 gravity estimates and the degree-4 gravity estimates (positive values show improvement with degree-4 gravity estimates)

Finally Figure 5.12 shows the difference in the number of rejected observations between the orbits solved with degree-3 gravity field harmonics and degree-4 gravity field harmonics. In this graph the improvement is less obvious but still shows an improvement on the number of observations used in the processing.

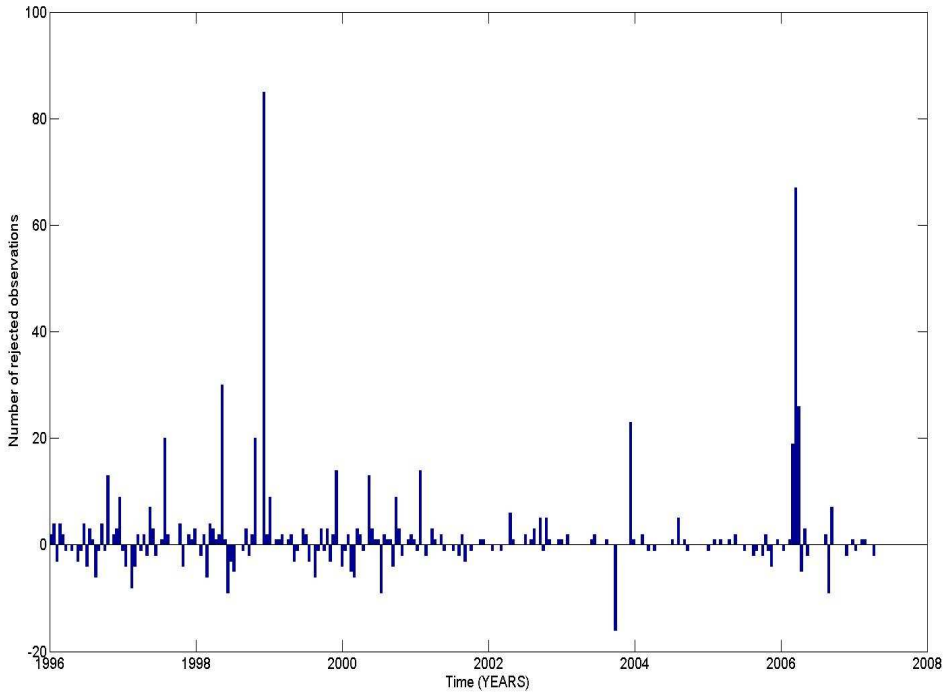

Figure 5.12 The difference in the number of rejected observations between the degree-3 gravity estimates and the degree-4 gravity estimates (positive values show improvement with degree-4 gravity estimates)

This section has analysed the post fit residual RMS of the orbits solved using the *FAUST* software for the same raw data set (although in each case different numbers of observations have been rejected) while solving for different parameters. These and the parameters estimated will be used throughout this thesis as a basis for comparing outputs from the edited versions of *FAUST* that are to be tested as the fundamental research topic of this thesis. The results show in the first instance the orbital fit of the processed data in what is to be called the 'base solution' that includes ERPs and then compared this solution with solutions that solve for the Earth's gravity field. This analysis has given some initial evidence that the base solution using ERPs is a good addition to the software and that the implementation has been successful. This hypothesis will be further investigated in the following section.

5.7.2.2 Earth Rotation Parameters

FAUST has been used to calculate the combined orbits of LAGEOS I and LAGEOS II in several different scenarios. In the base solution and the base solution plus degree-3 gravity field harmonics and degree-4 gravity field harmonics the ERPs have been solved for as described at the beginning of section 5.7.2. In this section a comparison will be made between the ERP estimates calculated in each of these scenarios compared with the IERS C04 ERP values used as a-priori values in the solution.

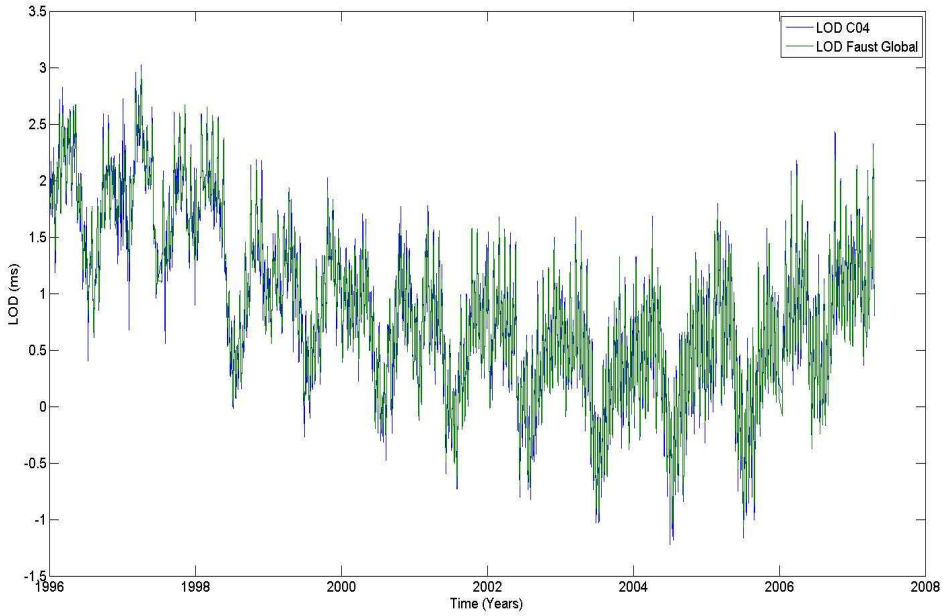

Figure 5.13 Comparison of LOD from IERS C04 and from *FAUST* (base solution)

Figure 5.13 shows a comparison of the LOD given by the IERS C04 time series, used as the a-priori input for this study, and the solution for ERPs from *FAUST*. A similar comparison between the coordinates of the pole is also shown in Figure 5.14. The two solutions are so close to each other on these scales that to compare them the difference of the two time series has been taken. These differences are shown in Figure 5.15

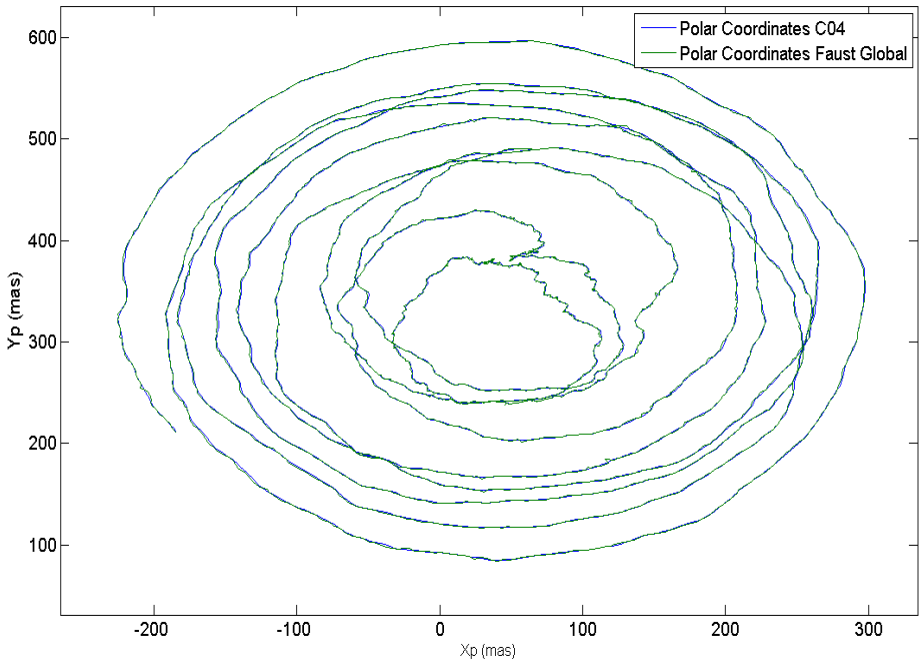

Figure 5.14 Comparison of XP plotted against YP from IERS C04 and from *FAUST* (base solution)

Figure 5.15 shows the difference between the IERS C04 Earth rotation time series and the estimates for the same parameters from *FAUST*. The IERS C04 time series has been derived from a combination of several space geodetic techniques including Lunar Laser Ranging (LLR), SLR, VLBI, and more recently GPS and DORIS. In terms of the values of XP, YP and LOD only SLR, VLBI, GPS and DORIS are used in their derivation. The combination of these parameters is not equally weighted, based more heavily on contributions from GPS, with DORIS being weighted the least. Measurement from VLBI and SLR are weighted approximately equally and their importance lies somewhere between that of GPS and DORIS (Bizouard and Gambis, 2009).

The values plotted in Figure 5.15 have been filtered by excluding any value that is larger than four times that of the standard deviation of the time series. This is to remove any outliers that are likely to be due to solutions that demonstrate a poor post residual RMS fit. In this thesis the C04 ERP time series is being taken as the standard. In this case it should be expected that by differencing *FAUST*'s solution with a solution that is assumed to be the truth that the estimated solution differences would oscillate around a zero mean. The means of both the XP and YP time series show a positive bias. This bias is most likely to be due to the fact that the C04 time series is a combination of Earth

rotation products while the *FAUST* solution is SLR only. The relatively poor distribution of SLR stations, when compared with the distribution of GPS stations, may also be a contributing factor in this effect.

The RMS values show that the precision of the *FAUST* time series is approximately 0.6 mas and 0.5 mas when the bias is present. If this bias is removed these values fall to 0.2 mas and 0.4 respectively. The mean of the LOD time series is zero at three significant figures and shows a precision of 0.1 ms.

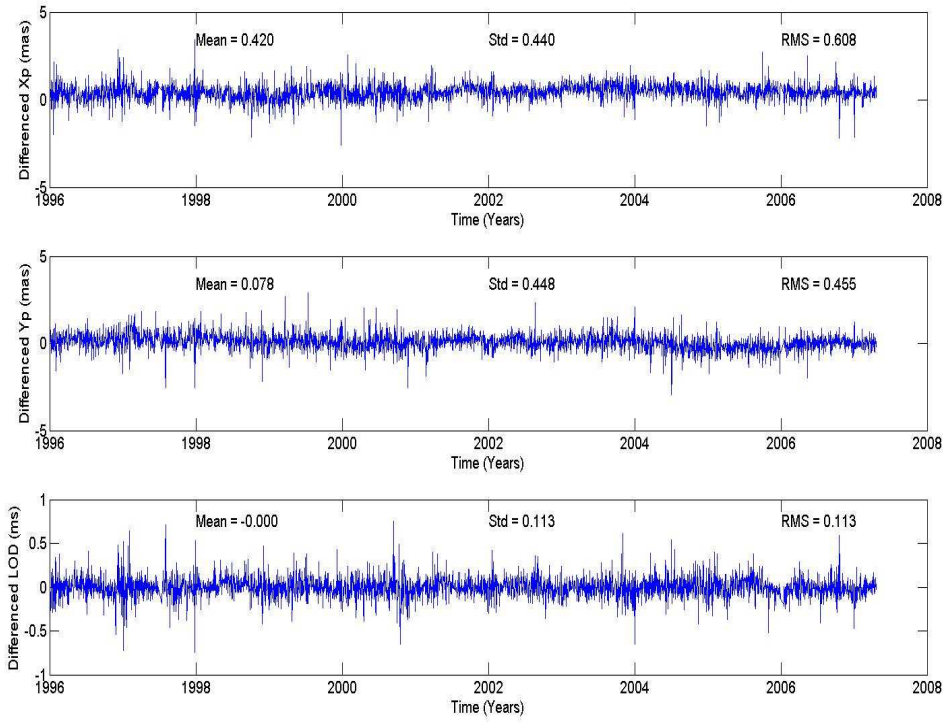

Figure 5.15 Difference between ERPs from IERS C04 and solutions from *FAUST* (base solution)

To analyse how the ERP values from *FAUST* have changed after introducing degree-3 gravity estimates into the estimation process the difference between *FAUST*'s degree-3 gravity solutions and the C04 ERP values are plotted in Figure 5.16.

The introduction of degree-3 gravity estimates to the process has improved both the mean values of XP, YP and LOD, the standard deviations of the time series and the RMS error when compared with the C04 time series.

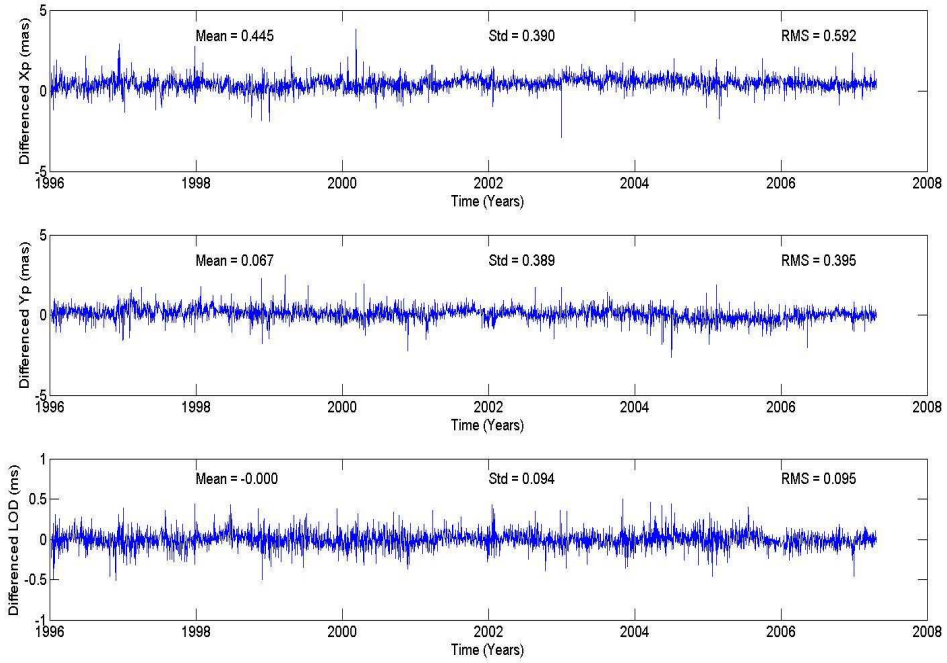

Figure 5.16 Difference between ERPs from IERS C04 and solutions from *FAUST* (degree-3 gravity solution)

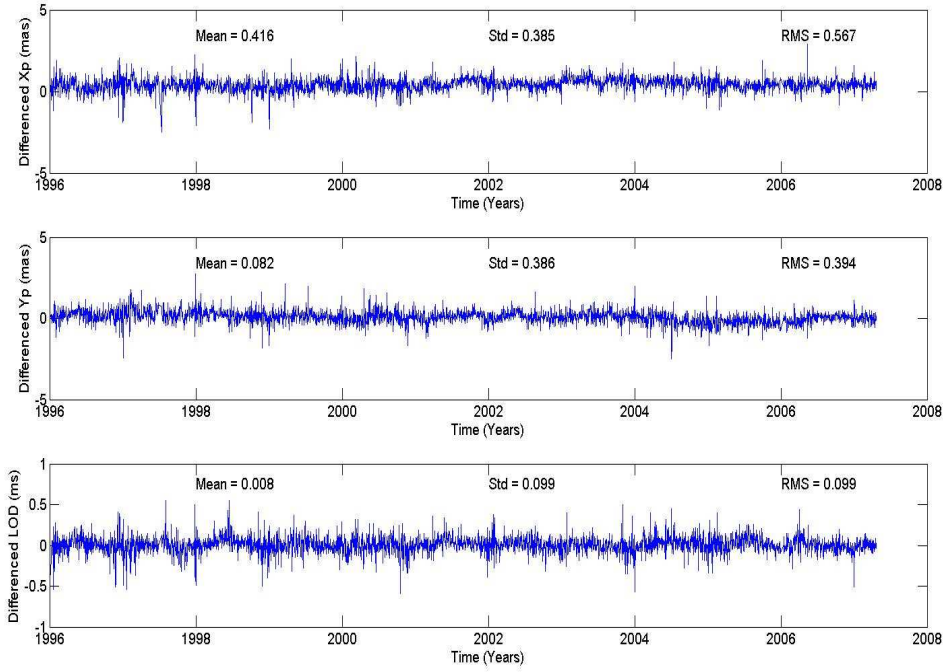

Figure 5.17 Difference between ERPs from IERS C04 and solutions from *FAUST* (degree-4 gravity solution)

Figure 5.17 shows the results of the *FAUST* solution using estimates of up to degree and order 4 of the Earth's gravity field. The results show that the differences between the degree-3 solution and the degree-4 solution are small, but slightly degraded in most cases. It should be noted that there is now a small positive bias in the LOD time series. The reason that this solution is worse when the fit of the orbit is the best indicates over parameterization. This is most likely a consequence of the high correlations that are experienced between the degree-2 and degree-4 spherical harmonics of the Earth's gravity field and their relationship with the ERPs (as described in Chapter 3).

The comparison with the C04 time series has shown that there are some differences between the data sets especially in the mean values of XP and YP. It is likely that these differences can be explained by the different geodetic data used to derive the combined C04 solution compared to an SLR only solution.

5.7.2.3 Gravity Field

As stated previously *FAUST* has been used to estimate orbits for LAGEOS I and II in several different scenarios.

Two of these scenarios have produced the low degree harmonics of the gravity field of which a large part of this thesis is primarily concerned. This section will compare the results from each of these scenarios with low degree harmonics of the Earth's gravity field calculated from other sources.

Figure 5.18 shows a comparison of the degree-2 spherical harmonics of the Earth's gravity field estimated from three different space geodetic techniques, namely SLR, GPS and GRACE. The SLR results are from *FAUST* using the base solution plus solving for up to degree and order 3 gravity harmonics. GPS data is taken from weekly GPS Solution INdependent EXchange (SINEX) files (re-analysed) from the International GNSS Service (IGS) analysis centre at the Scripps Institution of Oceanography (SIO) [ftp://garner.ucsd.edu/pub/combinations]. The data was downloaded in 2007, further details on the data set can be found in Nikolaidis, 2002. The SINEX was processed and the gravity field harmonics calculated from this process

were provided for this analysis by Dr David Lavellee. The GRACE data is taken from GSM and GAC geopotential products from the Center for Space Research (CSR) Release 4.

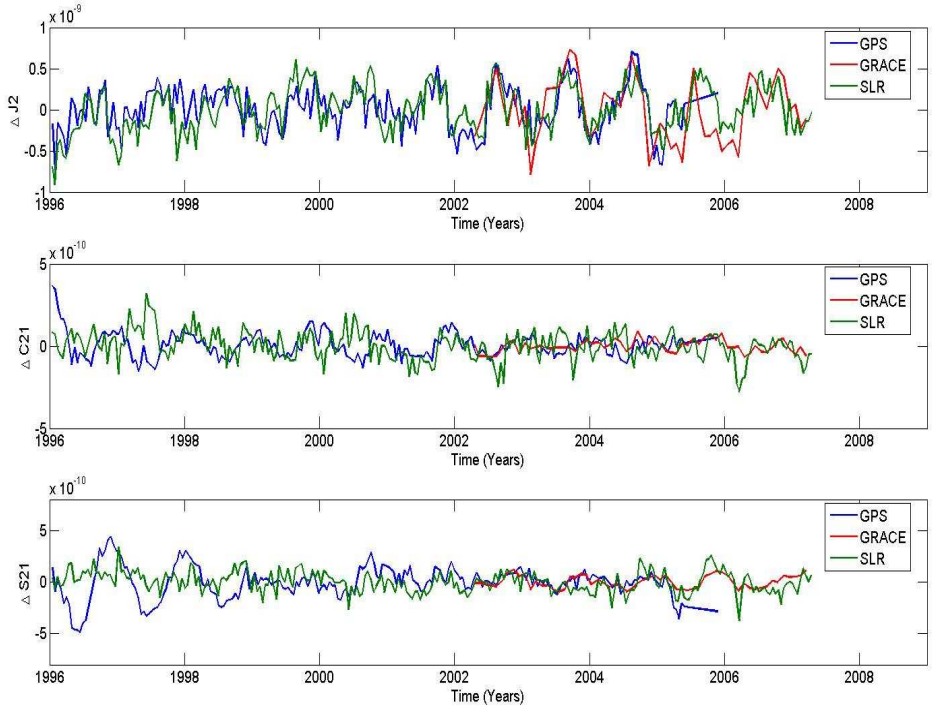

Figure 5.18 Comparison of degree-2 (with *FAUST* Solving for up to degree-3) spherical harmonics of the Earth's gravity field from GPS, GRACE and SLR.

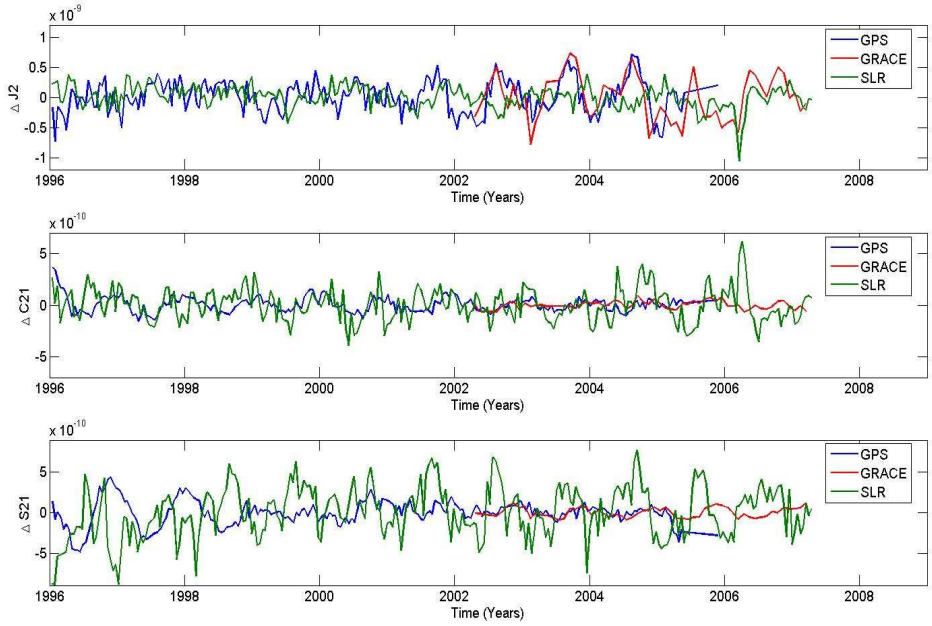

Figure 5.19 Comparison of degree-2 (with *FAUST* Solving for up to degree-4) spherical harmonics of the Earth's gravity field from GPS, GRACE and SLR.

From Figure 5.18 it can be seen that there is reasonable agreement between the results from the three different techniques although the SLR measurements are noisier than GPS and GRACE. This may be to do with the relatively sparse number of SLR stations and therefore a worse geometry and their varying quality. The agreement is best on the J2 harmonic and worst on the C21 harmonic.

Figure 5.19 again shows a comparison of the degree-2 spherical harmonics of the Earth's gravity field estimated from three different space geodetic techniques, namely SLR, GPS and GRACE. The SLR results this time are estimated using *FAUST* for the base solution plus solving for up to degree and order 4 gravity harmonics. When Figure 5.19 is compared with Figure 5.18 it can clearly be seen that the SLR low degree harmonics agree less with GPS and GRACE when introducing estimates for the degree-4 harmonics of the Earth's gravity field. This is most likely due to the high correlations between the degree-2 harmonics and the degree-4 harmonics within the least squares process.

5.8 Conclusion

This chapter has described the method used to estimate the orbits of LAGEOS I and LAGEOS II using the precise orbit determination software *FAUST*. The mathematical models used within *FAUST* to compute the orbit as well as the models used as input into the software have been explained to provide an understanding of how the calculations were carried out.

As part of this thesis the *FAUST* software was modified in several ways to bring it in line with the IERS conventions. These included adding the ability to solve for ERPs, the introduction of an ocean tide loading correction and a correction for relativistic effects on the satellites and the ability to output the results in SINEX format.

Finally, the method for producing the orbits has been described. Orbits have been processed over three 5 day arcs to give a single combined 15 day arc over which global parameters such as ERPs, station coordinates and gravity can be solved. A base orbit solution has been defined for comparison purposes as well as a short analysis of the

ERP estimates and the gravity field estimates with comparison against similar values computed from other geodetic techniques. These comparisons have shown the SLR results from *FAUST* compare reasonably well with results from other geodetic techniques. This is a fundamental issue that needed to be addressed before the next stage of the thesis can proceed.

Chapter 6

6 Excitation Functions

6.1 Introduction

Space geodetic techniques such as SLR, DORIS, GPS and VLBI are used to calculate regular time series of ERPs for rotational dynamics and station coordinates for estimating plate tectonics. Space geodetic techniques can also be used to investigate surface mass redistribution in the atmosphere, oceans and continental water storage as these variations cause changes in the Earth's gravity field harmonics (Wahr et al., 1998) that have a direct effect on the orbits of the satellites. Degree-2 gravitational variations can be estimated from accurately obtained Earth rotation variations (Chen and Wilson, 2003a). $\Delta J2$ (defined as $J2 = -\sqrt{5}\, C20$), $\Delta C21$ and $\Delta S21$ are estimated using Earth rotation variations calculated within *FAUST*, from the SLR estimated orbits of the LAGEOS satellites, and excitation functions calculated using angular momentum data derived from geophysical models.

6.2 Comparison of Excitation Functions from LAGEOS and Geophysical Data from Models

As has been established in the preceding chapters, variations in the Earth's rotation for periods of less than a few years are forced mainly by the mass redistribution of the atmosphere, oceans and hydrosphere/cryosphere via the conservation of angular momentum. The causes of Earth rotation variations can be divided into two categories. These are (1) surface mass load contributions from atmospheric surface pressure, continental water storage (including snow and ice), ocean bottom pressure, and (2) motion contributions caused by wind and ocean currents which cause an exchange of angular momentum between the atmosphere, oceans and the Earth.

Previous studies of surface mass redistribution from space geodetic techniques have utilised satellite laser ranging to passive geodetic satellites such as LAGEOS, Starlette, Stella or Ajisai (Dong et al., 1996, Cheng et al., 1997; Cazenave et al., 1999; Cheng and

Tapley, 1999; Nerem et al., 2000; Cox and Chao, 2002; Moore et al., 2005) to investigate secular variations in zonal harmonics and annual and semi-annual variability in lower degree and order harmonics. Several of these studies have shown good agreement between the geodetic results and the geophysical models.

Space geodetic techniques provide ERP parameters at daily intervals with the possibility of even shorter time scales using GPS. However, the typically low sensitivity of orbits to the gravity field variability or the high correlation between the harmonics means that there is little possibility of space geodetic techniques providing accurate measurements of mass change, even at low spatial resolutions, at intervals of less than a few days/weeks (e.g. SLR, GPS) or weeks/months (GRACE). However, the disparity in temporal resolutions raises the possibility of simultaneously recovering and using higher frequency degree-2 harmonics from the ERP data (on utilizing angular momentum data) within an orbital determination procedure.

Excitations of the Earth rotation due to mass variations are comparable with changes in the degree-2 spherical harmonics of the Earth's gravity field (Chen and Wilson, 2003b; Hancock and Moore, 2007; Wahr, 1982; Eubanks, 1993). The excitation in the Earth's rotation caused by mass variations cannot be separated from the variations caused by motion when using geodetic methods. Geophysical models are used to estimate the excitation caused by both the mass term and the motion term (see Chapter 4 of this thesis). The excitation caused by mass χ_i^{mass} can be calculated by using the observed excitation χ_i^{obs} calculated from the ERPs estimated simultaneously from LAGEOS I and II. By utilizing the relationship between the conservation of angular momentum and Earth rotation described in Chapter 3, the relationship between the observed excitation functions and polar motion is given in complex number notation as

$$\chi(t) = p(t) + \frac{i}{\sigma_r}\frac{dp}{dt}; \qquad \sigma_r = \Omega\frac{(C-A)}{A} \tag{6.1}$$

where

$\chi(t)$ = the observed excitation functions from polar motion *p* at time t

σ_r = the frequency of the Chandler wobble

Ω = the mean rotation rate of the Earth

C = Earth's Polar moment of inertia

A = Earth's Equatorial moment of inertia

Similarly the relationship between excitation functions and LOD is given as

$$\chi_3(t) = \frac{\Delta\Lambda(t)}{\Lambda_0} \qquad \textbf{(6.2)}$$

where

$\chi_3(t)$ = the observed excitation functions from LOD at time t

$\Delta\Lambda$ = the LOD measured from LAGEOS I and II

Λ_0 = the nominal value of LOD, given as 86400 seconds

The equations for the relationship between the angular momentum quantities taken from the geophysical models are given in Chapter 3. The estimated excitation caused by motion estimated from geophysical models is now removed from the total observed excitation to yield the excitation caused by mass variations.

$$\chi_i^{mass}(t) = \chi_i^{obs}(t) + \chi_i^{motion}(t) \qquad \textbf{(6.3)}$$

The period of study for this research covers 1996 – 2008 inclusive. Geophysical data has been obtained from several sources. Atmospheric Angular Momentum (AAM) terms for both mass and motion have been derived from the NCEP/NCAR reanalysis (Salstein and Rosen, 1997). The atmospheric data is provided every 6 hours. For the Oceanic Angular Momentum (OAM) both mass and motion terms have been taken from the JPL ECCO circulation model kf049f. ECCO is based on an earlier MIT global ocean

circulation model (Marotzke et al., 1999), details of which are given by Chen and Wilson (2003b). Hydrological Angular Momentum (HAM) mass values were derived from the NCEP hydrological mass dataset. At the time of writing the HAM data was only available until the end of 2004 and therefore any comparisons of excitation functions that include HAM are between 1996 and 2004. The NCEP data contains information regarding soil moisture and snow cover. Water storage is taken as the sum of soil wetness and snow water with the former consisting of two layers of thickness 10 cm and 190 cm. The soil and snow water were converted into daily equivalent water heights. It is noted that the data does not take into account any motion terms that are caused by rivers but such an omission will have negligible impact on the results. Both OAM and HAM are provided as daily values. The AAM data was therefore reduced to daily data compatible with both OAM and HAM. To do this simple weighting was used of $(1/8, 1/4, 1/4, 1/4, 1/8)$ over five values.

How well the excitation functions derived from ERP estimates derived within *FAUST* match with the excitation functions from geophysical models, should be a good indicator of the projected performance of using the said parameters within the orbit determination process. Prior to comparison of the excitation functions from geophysical data and from LAGEOS, it should be noted that the effects of long period solid earth and ocean tides have been removed from the LOD data and long period ocean tides from the polar motion data by reference to the IERS conventions (McCarthy and Petit, 2003). Also the ERP values have been de-trended to eliminate the long period core-mantle interaction which, although non-linear over geological time, can be taken as secular over the period of this study. A long term signature was also removed from the LOD to account for the accumulation of errors due to aliasing from satellite motion, core mantle interaction and the unmodelled 18.6 yr tide. This was done by fitting and removing a polynomial from the data.

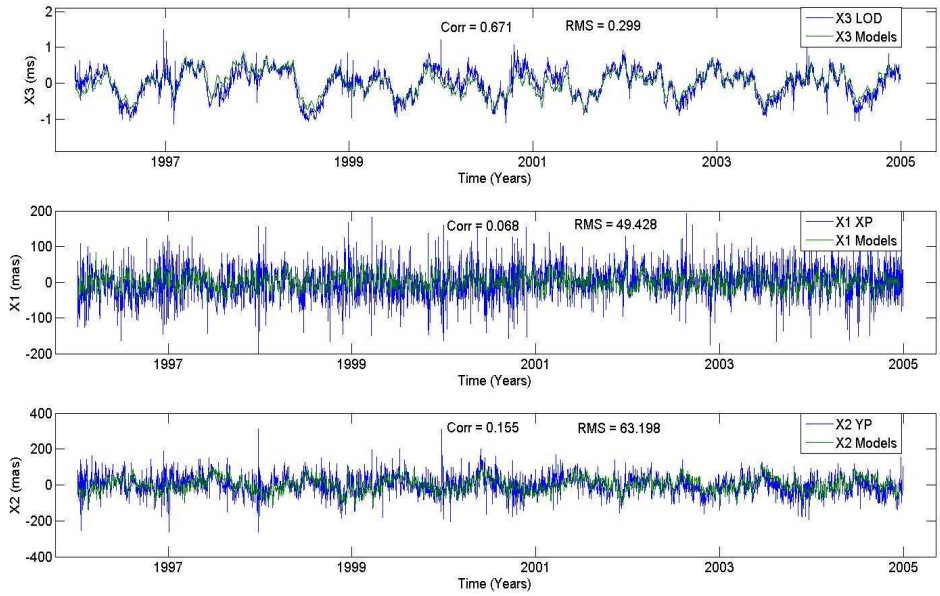

Figure 6.1 Comparison of χ_1, χ_2 **and** χ_3, combined mass and motion terms, daily values, derived from LAGEOS ERP estimates and geophysical models

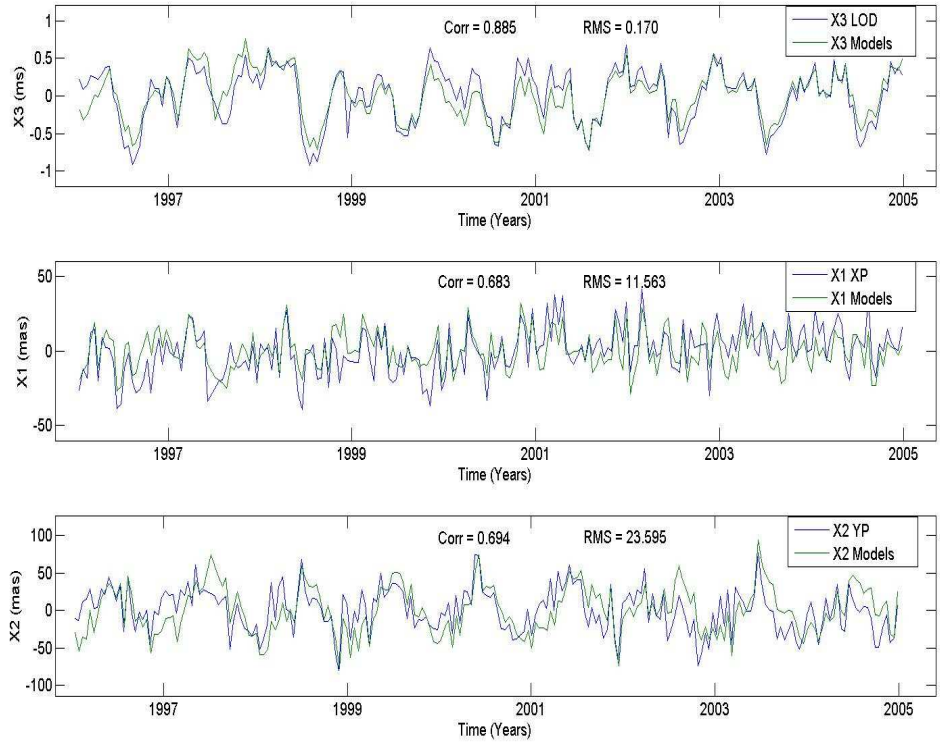

Figure 6.2 Comparison of χ_1, χ_2 **and** χ_3, combined mass and motion terms 15 day averages, derived from LAGEOS ERP estimates and geophysical models

Figure 6.1 shows the three excitation functions (daily values) as explained in Chapters 3 and 4 χ_1, χ_2 and χ_3, containing both mass and motion terms, in mas for χ_1, χ_2 and ms for χ_3 from LAGEOS derived Earth rotation values plotted against the equivalent values computed from the combination of atmosphere, ocean and hydrological angular momentum models (NCEP data used). The means have been removed from all the data.

Figure 6.2 shows the three excitation functions (weighted 15 day averages) of χ_1, χ_2 and χ_3 containing both mass and motion terms, in mas for χ_1, χ_2 and ms for χ_3 from LAGEOS Earth rotation values plotted against the equivalent values computed from the combination of atmosphere, ocean and hydrological angular momentum models.

From Figure 6.1 it can clearly be seen that χ_3 from both sources are in very good agreement with each other at least when looking at the annual/semi annual signals that appear in the data. The correlation function gives a value of just 0.671 and this is most likely due to the variations on small time scales not matching well. Figure 6.2 adds weight to this theory as it shows that the match between the data is very good when the high frequency data is removed with the correlation value increasing to 0.885.

The computed excitations from χ_1 and χ_2 are much noisier when computed from the LAGEOS ERP estimates than from the geophysical models on a daily basis. There is not a very good match between the data over short periods and thus the correlation values are very small for both χ_1 and χ_2. Taking a closer look at the data there is much better agreement between the data over longer periods. Again this is confirmed by comparing the excitation functions that have been averaged over 15 days shown in Figure 6.2. The correlation values have also increased (0.680 from 0.068 for χ_1 and 0.69 from 0.150 for χ_2 showing that again the agreement is better over the longer terms. The residual RMS fit of the data is also much better after the data has been averaged over 15 days showing that the agreement is better over the longer terms than over the high frequency periods.

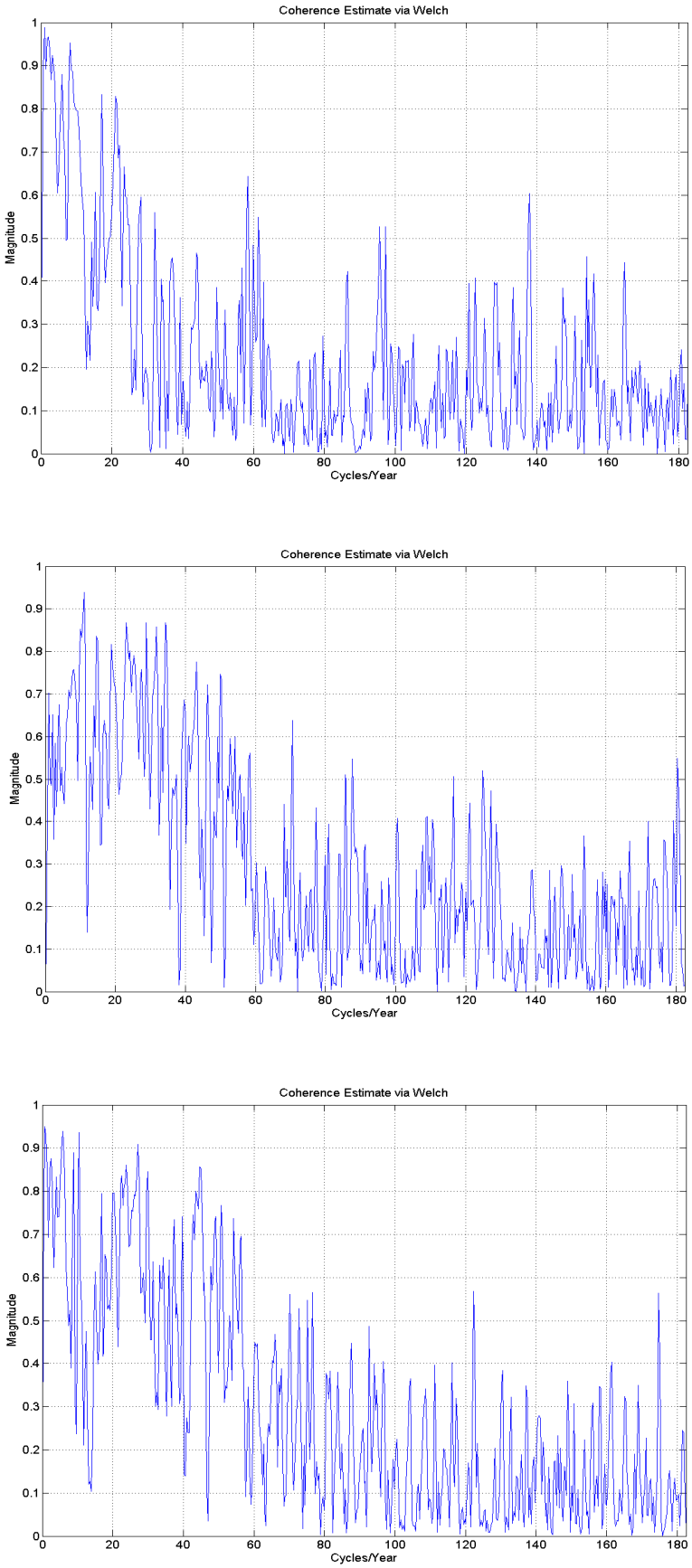

Figure 6.3 Coherence estimates of χ_3 (top), χ_1 (middle) and χ_2 (bottom) using daily values

To investigate the correlation between the excitation functions in more detail a coherence estimate has been calculated. Figure 6.3 shows the coherence estimates between χ_1, χ_2 and χ_3 using daily estimates given by:

$$C_{xy}(f) = \frac{\left|P_{xy}(f)\right|^2}{P_{xx}(f)P_{yy}(f)} \qquad \textbf{(6.4)}$$

where $P_{xx}(f)$ and $P_{yy}(f)$ are the power spectral densities of x and y and $P_{xy}(f)$ is the cross power spectral density of x and y (Kay, 1988). The coherence is displayed as cycles/year against the magnitude of the coherence, where a value of 1 would show perfect coherence between the two signals and a value of 0 shows no coherence between the two signals at that particular frequency.

Firstly, for χ_3, there is very high, 95% significant coherence between the two signals at the dominant annual and semi annual periods as well as other lower temporal frequencies. This significance although not shown in Figure 6.3 is shown in (Hancock and Moore, 2007). The good agreement between the models and LAGEOS at longer periods must give optimism for the observed mass from LAGEOS being in good agreement with the geophysical data at these periods. This high coherence may be due solely to the dominance of the AAM motion term and how well it matches with estimates of LOD. The coherence values after 20 cycles/year show much less agreement, suggesting that higher frequency terms may not be as well defined. At the lower temporal frequencies coherence is once again clearly evident in χ_2 but less so for χ_1, particularly at the dominant annual and semi annual period. The weaker agreement in χ_1 is attributed to the greater contribution of meridional motion terms. However, and surprisingly, both χ_1 and χ_2 exhibit relatively high coherence on the higher frequency terms up to approximately 50 cycles/year, with χ_1 showing the better agreement on the higher frequencies than χ_2.

These results stimulate further research into the investigation of the residual components of the excitation functions to analyse if the errors can be seen in one

particular part of the excitation terms. To do this the excitation functions from the geophysical models AAM, OAM and HAM, are estimated in both mass and motion terms. The separated mass and motion terms can be used to estimate the contribution of that specific term to the excitation of polar motion and LOD on a daily basis. Therefore, the mass terms from the models can be used to recover the residual values from the LAGEOS ERP derived excitation functions (that contain both the excitation contributions from mass and motion) which should then equate to the contribution of the motion terms and vice versa (see equation 6.3).

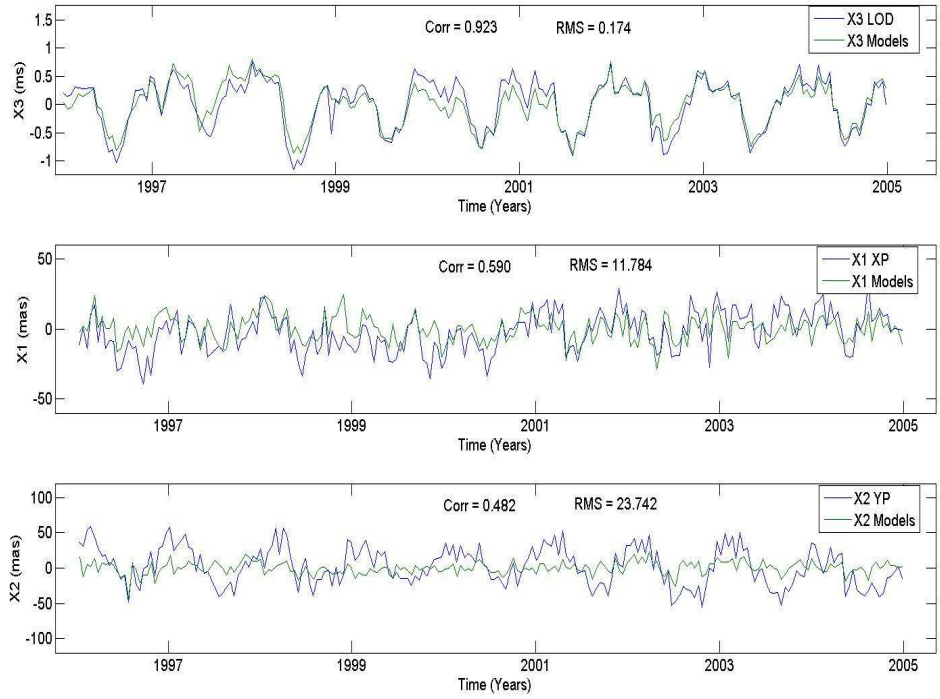

Figure 6.4 χ_3 (top), χ_1 (middle) and χ_2 (bottom) estimates of the contribution of the motion term to excitation

Using this strategy Figure 6.4 shows the contribution of motion from χ_1, χ_2 and χ_3 from 15 day averaged values of excitation functions in mas and ms respectively. **Error! Reference source not found.** shows the contributions of mass from χ_1, χ_2 and χ_3 from 15 day averaged values of excitation functions in mas and ms. It is immediately evident that the motion term for χ_3 Figure 6.4has a much better agreement than the mass term Figure 6.5 **χ_3 (top), χ_1 (middle) and χ_2 (bottom) estimates of the contribution of the mass term to excitation**Figure 6.5 In the case of χ_3 this might have been expected due to the dominance of the motion term in the signal meaning any small errors in the

definition of the motion term or LOD from LAGEOS will demonstrate itself as a large residual when removing the motion term from the LOD derived excitation function. This effect can be seen clearly during orbits that are poorly defined as a large spike in the time series. If these large errors are removed the agreement between the longer term temporal variations such as the annual and semi annual terms still seem to be in fairly good agreement with each other.

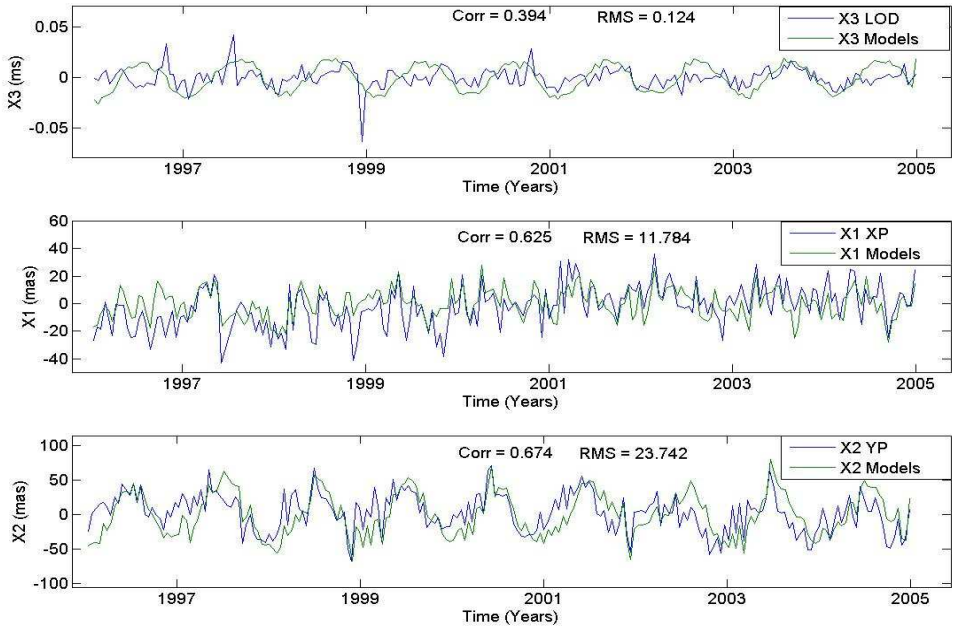

Figure 6.5 χ_3 (top), χ_1 (middle) and χ_2 (bottom) estimates of the contribution of the mass term to excitation

In the case of χ_1 the agreement seen between the mass terms and the motion terms is comparable and agreement is good for both on the longer term variations seen in the averaged results. The agreement on χ_1 for these longer terms is less for the reasons previously stated. In the case of χ_2 agreement is good on the mass term but not good when comparing the motion terms; at this scale the annual and semi annual signals are not well defined in the motion term. This is probably due to the fact that the χ_2 mass term is dominant when compared to the χ_2 motion term on both the atmospheric data and ocean data. χ_1 does not have the same problem as χ_3 and χ_2 in that the contributions of mass and motion terms to the total excitation contribution are much more comparable as discussed in Chapter 4. To investigate the fit of these parameters further the coherence of the mass terms and the motion terms has also been computed.

Figure 6.6, Figure 6.7 and Figure 6.8 show the coherence estimates of χ_3 and χ_1, χ_2 mass (top) and motion (bottom) terms respectively.

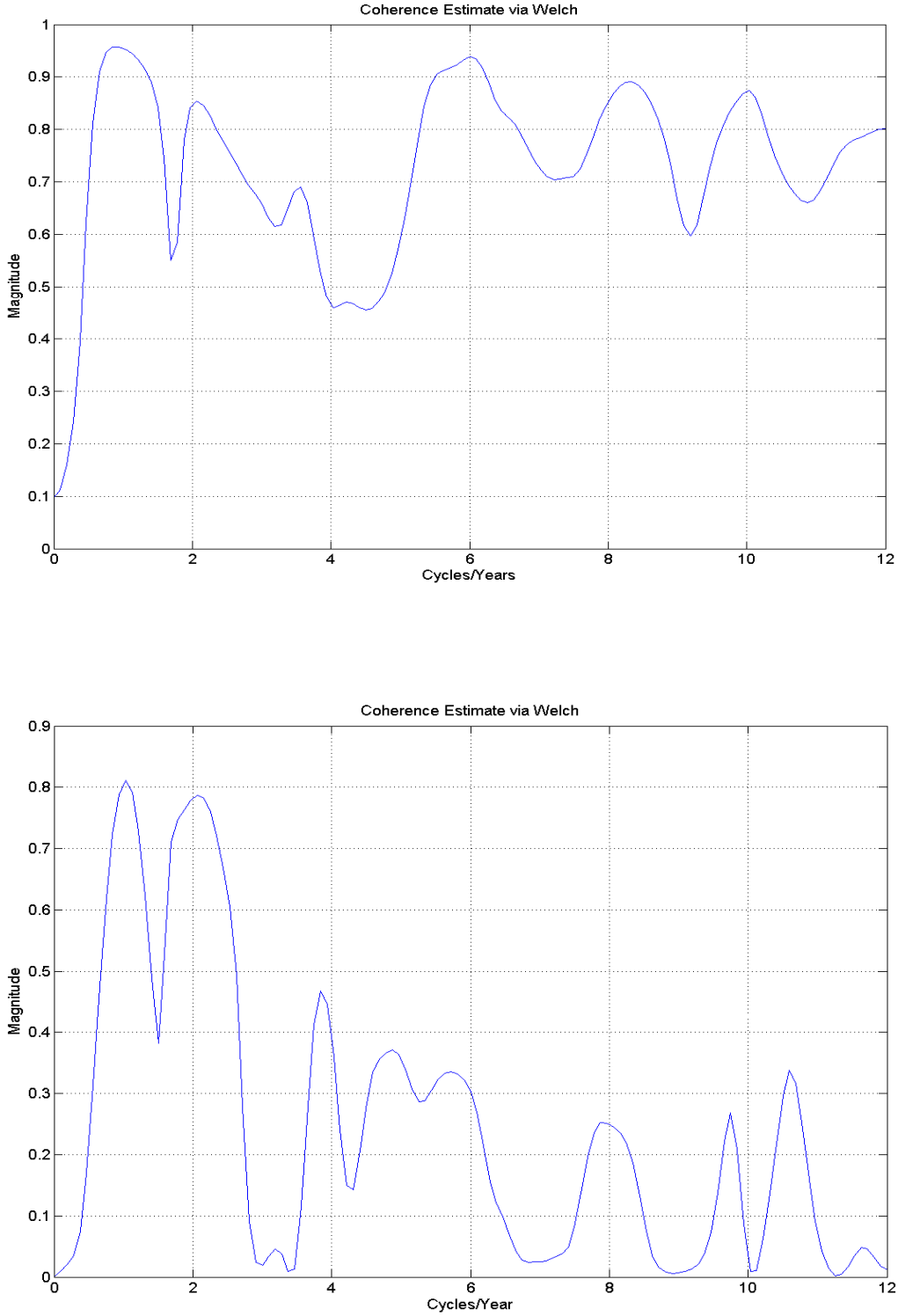

Figure 6.6 χ_3 mass (top) and motion (bottom) coherence estimates

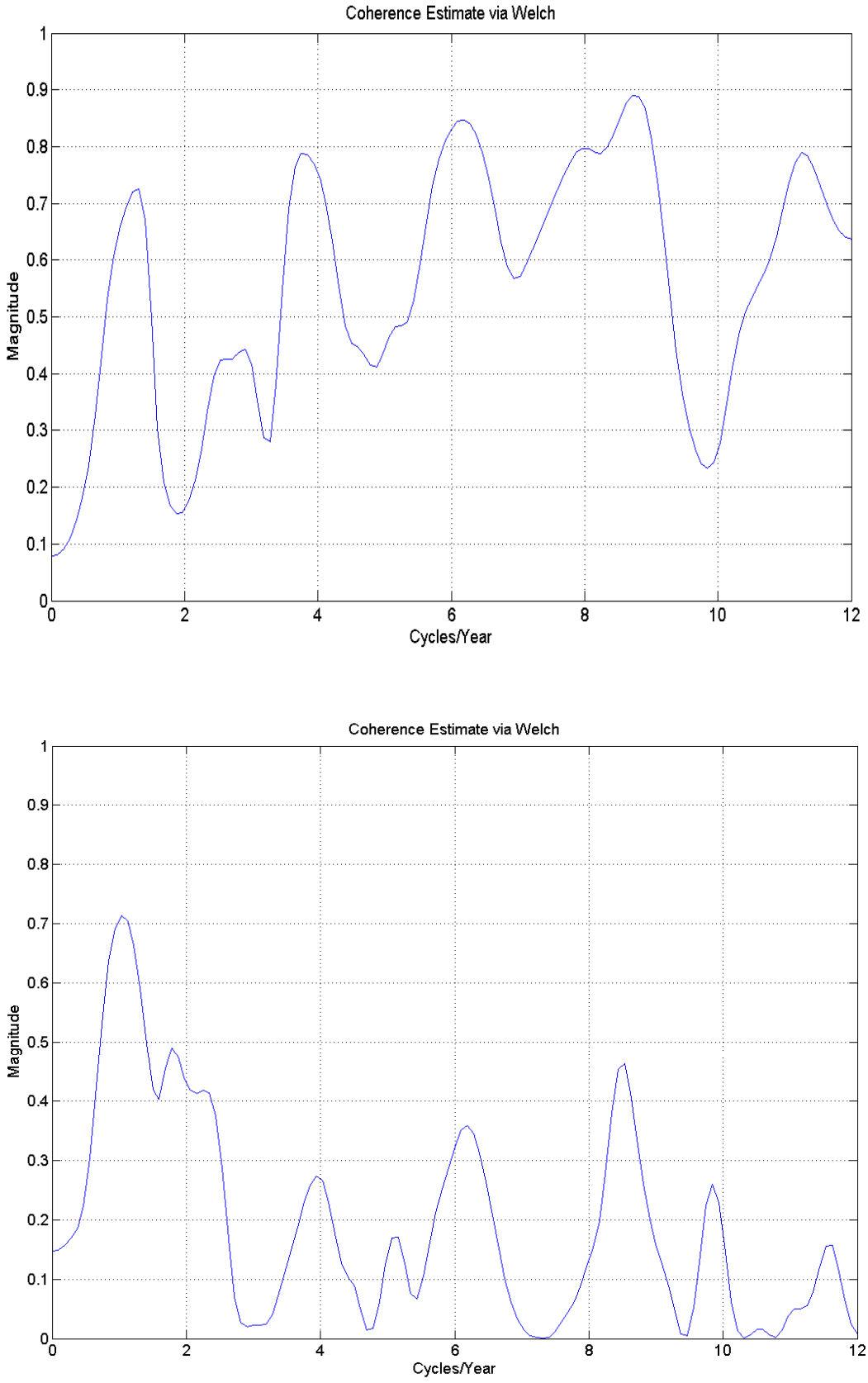

Figure 6.7 χ_1 mass (top) and motion (bottom) coherence estimates

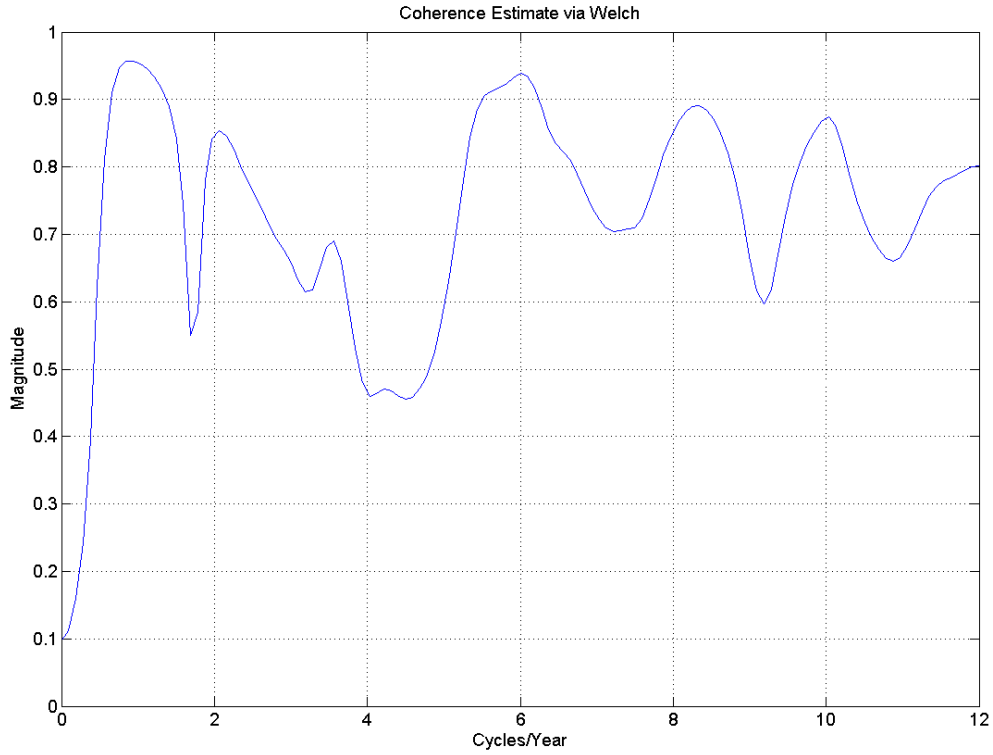

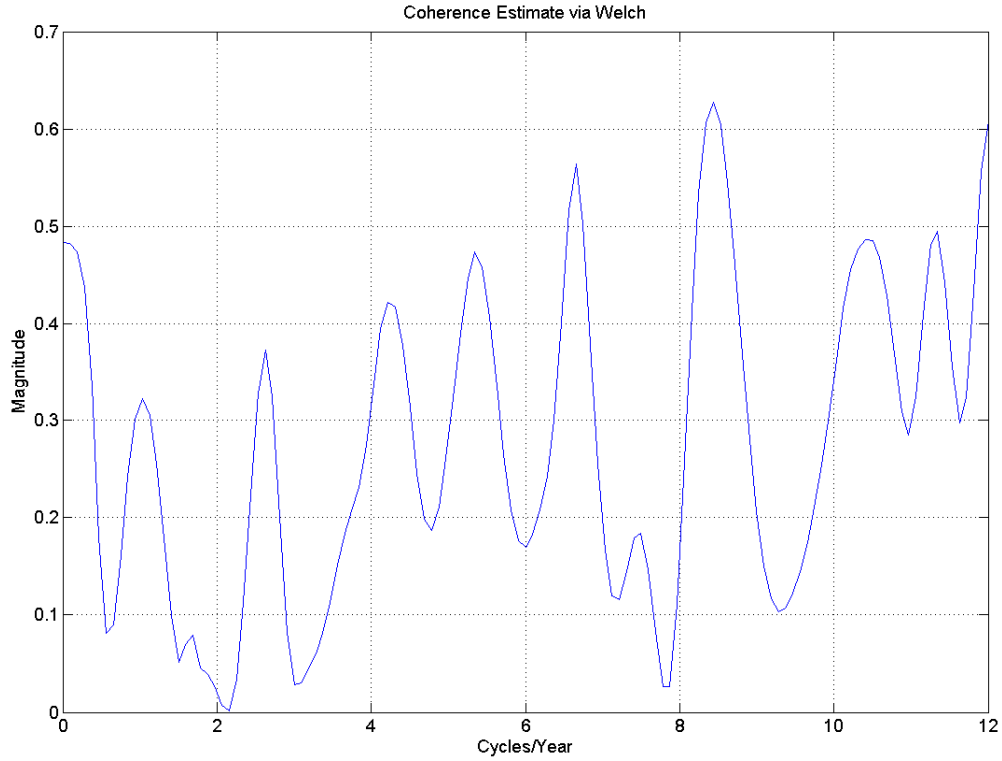

Figure 6.8 χ_2 mass (top) and motion (bottom) coherence estimates

The coherence of the mass terms are of particular importance as these will later be used to derive the degree-2 gravity field harmonics currently derived directly from the integration of the LAGEOS orbits. The data used to compute these coherence values are the weighted 15 day averages of the excitation functions. This has been done so that they are comparable with the 15 day estimates of the gravity field produced from *FAUST* and as such only up to 12 cycles per year are calculated.

The estimates of coherence for χ_3 shown in Figure 6.6 show that the long term temporal variations seem to have good agreement across the vast majority of the frequencies shown and that this coherence may be significant especially at the annual signal.

Once again this supports the use of χ_3 in the orbit determination process and shows that the values estimated from LAGEOS agree with those computed using the models. The motion term also shows good correlation at the annual and semi annual frequencies but is much less coherent at frequencies greater than two cycles a year. The lower coherence of the motion term is unexpected as the excitation functions seem to match well. Once again this may be due to the AAM being the dominant feature in this particular signal.

Figure 6.7 shows the coherence estimates of χ_1 in cycles per year. As shown previously when investigating the coherence of the combined excitation functions, χ_1 does not agree as well as the other two excitations at the annual and semi annual terms. Once again we see that this is the case for both the mass and motion terms from χ_1. There does however seem to be good coherence on the mass term of χ_1 at slightly higher frequencies but it does seem that using χ_1 to estimate the gravity field harmonics may be less successful when using χ_1 than with χ_3.

Finally, comparing the mass and motion terms estimated for χ_2 there is once again excellent agreement between the low frequency terms in the coherence estimates of the mass term, especially at the dominant yearly signal that is very evident in Figure 6.8. The motion term however shows the opposite effect, showing that the coherence between the two sources of χ_2 do not agree well at any of the low frequency terms. This phenomenon is probably due to the dominant signal in χ_2 data being the mass term and

small differences in the mass term displaying as relatively large differences when analysing χ_2 from the different sources.

This analysis shows that if one of the signals is dominated by either the mass or motion term either from AAM, OAM, HAM, or a combination of these, that small differences between the signals in the dominant signals are transferred as relatively large differences in the less dominant signal.

From the point of view of the next step in this research, which is to investigate the usefulness of using the relationships between these excitation functions to derive gravity terms in a iterative orbit determination process it is positive to see that two (χ_2 and χ_3) out of the three mass terms estimated from polar motion and LOD (after removing the estimates of the motion terms from the models) seem to match each other quite well. χ_1 does not show the same level of coherence as the other two excitation functions and therefore would probably be expected to have a less positive effect on the orbit determination process. As shown in Chapter 4, the motion terms for χ_1 are have a less well defined annual signal. Therefore it follows that using this term may give less agreement on the annual and semi annual time scales.

6.3 Comparison of Degree-2 Gravity Field Harmonics

Previous studies comparing degree-2 gravity field harmonics from various sources to those derived from ERPs have shown good agreement between data sets (Gross et al., 2004; Chen et al., 2000; Chen and Wilson, 2003b).

The relationship between the excitations due to mass variations and the degree two spherical harmonics of the Earth's gravity field are given by Chen and Wilson (2003b).

$$\Delta C21 = -\left(1+k_2^{'}\right)\cdot\sqrt{\frac{3}{5}}\cdot\frac{(C-A)}{1.098R^2M}\cdot\chi_1^{mass}$$
$$\Delta S21 = -\left(1+k_2^{'}\right)\cdot\sqrt{\frac{3}{5}}\cdot\frac{(C-A)}{1.098R^2M}\cdot\chi_2^{mass} \qquad \textbf{(6.5)}$$
$$\Delta J2 = -\left(1+k_2^{'}\right)\cdot\frac{3}{2\sqrt{5}}\cdot\frac{C}{0.753R^2M}\cdot\chi_3^{mass}$$

Where

M = mean mass of the Earth

R = mean radius of the Earth

C = Earth's Polar moment of inertia of the Earth

A = Earths Equatorial moment of inertia of the Earth

$k_2^{'}$ = the degree-2 Love number (-0.301) which accounts for the elastic deformational effects on gravitational change.

In equation 6.5 we have used the normalised second degree tesseral harmonics C2,i and S2,i where $i = 0,1$ and the second degree zonal harmonic

$$J2 = -\sqrt{5}\,C20$$

This section will compare the degree-2 spherical harmonics of the Earth's gravity field estimated from the models, from LAGEOS derived ERP, ERP from the a-priori combined C04 time series and from harmonics recovered as geophysical parameters within the orbit determination process.

Firstly the differences in the models derived using the Inverted Barometer (IB) correction, which is a loading correction done using a simple, isotatic, inverted barometer assumption (Gill, 1982) and the non IB corrected models will be analysed. The IB correction applies only to the mass terms on the AAM models. The reason for this is to establish if there are any major differences between the two models and to decide which model may be the most suited for use in the orbit determination approach.

Figure 6.9 shows the agreement between the two models that have just been mentioned. Zonal harmonic J2: the correlation between the models for this harmonic is very good (0.863). The correlation is also very good (0.881) for the S21 harmonic although relatively large differences between the models is evident at the peaks and troughs that correspond to the annual cycles on both the S21 and the J2 terms. In contrast the correlation between the mass terms from C21 is much smaller and gives evidence that C21 is less well defined in the models than J2 and S21.

Figure 6.9 and Figure 6.10 show comparisons of the two differently calculated NCEP reanalysis models with the degree-2 gravity harmonics calculated from LAGEOS as geophysical parameters. Figure 6.9 shows the non IB corrected model and Figure 6.10 shows the comparison with the IB corrected model. As expected, due to their high correlation in the previous figure the correlation between the J2 terms from the models and from SLR are very similar.

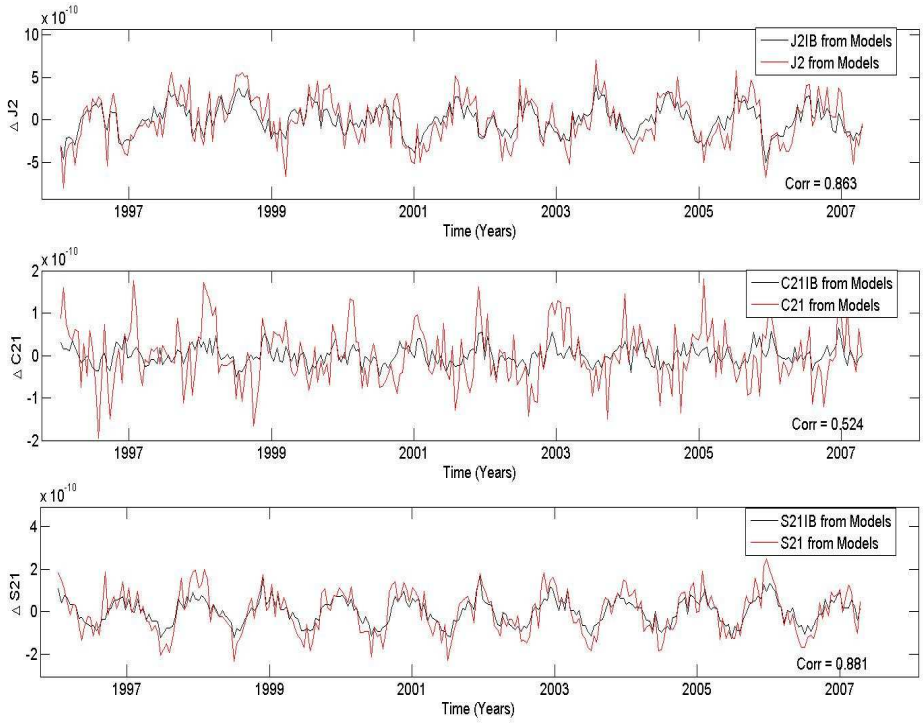

Figure 6.9 Comparison of NCEP reanalysis model using IB and non-IB derived AAM

The agreement between the S21 terms is also very similar between the models when compared with the SLR but the correlation is relatively low for both comparisons; being slightly higher for the non IB model. This seems to be due to the poor definition of the annual peaks in some instances. There does however seem to be a reasonable difference in how the values of C21 compare in the two instances presented here. Although both comparisons show very low correlation when using the non-IB corrected models the amplitude of the signal is similar in size to that of the SLR estimate C21 values. The correlation is slightly lower; although both show that the correlation is very low. There does however seem to be certain peaks in the non-IB comparison that match relatively well when compared to the IB corrected data that give hope that at those epochs the data may give a reasonable match.

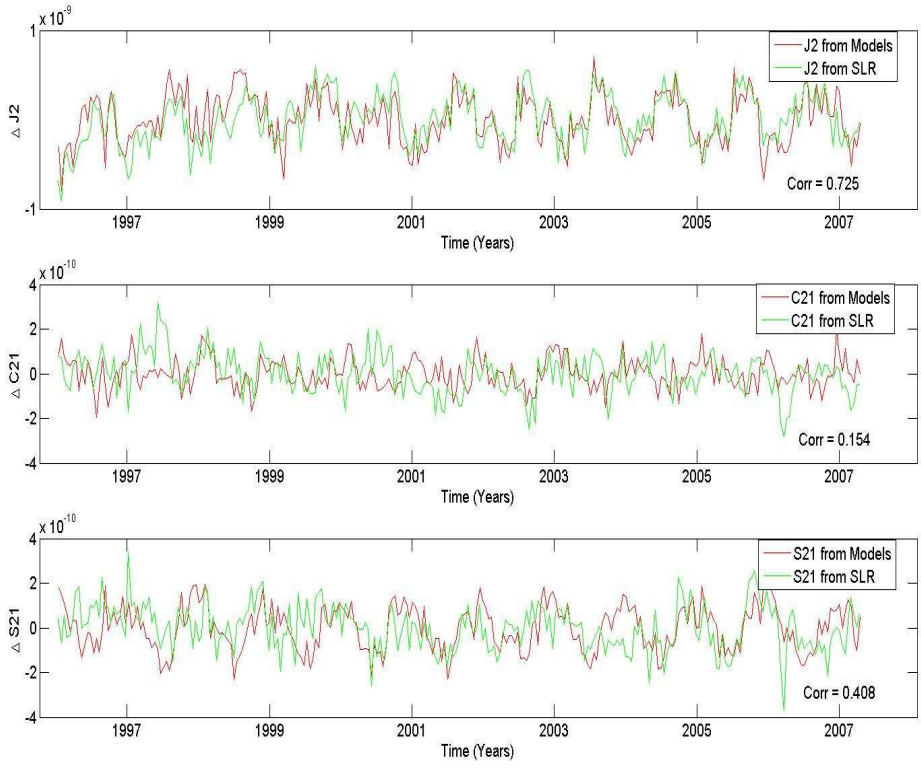

Figure 6.10 Comparison of NCEP reanalysis model using non-IB derived AAM and results derived from LAGEOS

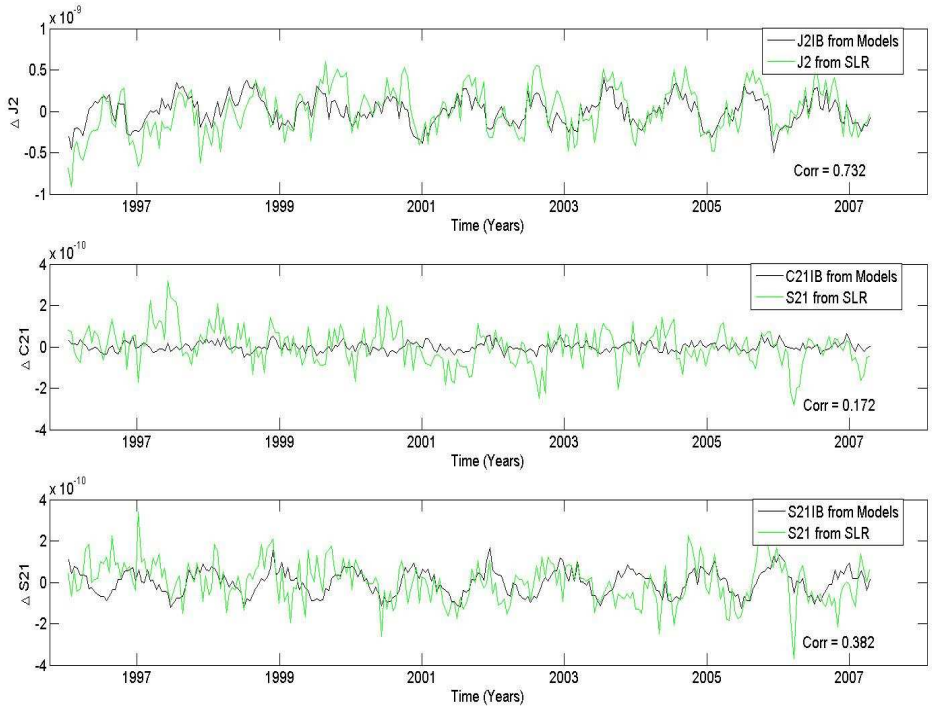

Figure 6.11 Comparison of NCEP reanalysis model using IB derived AAM and results derived from LAGEOS

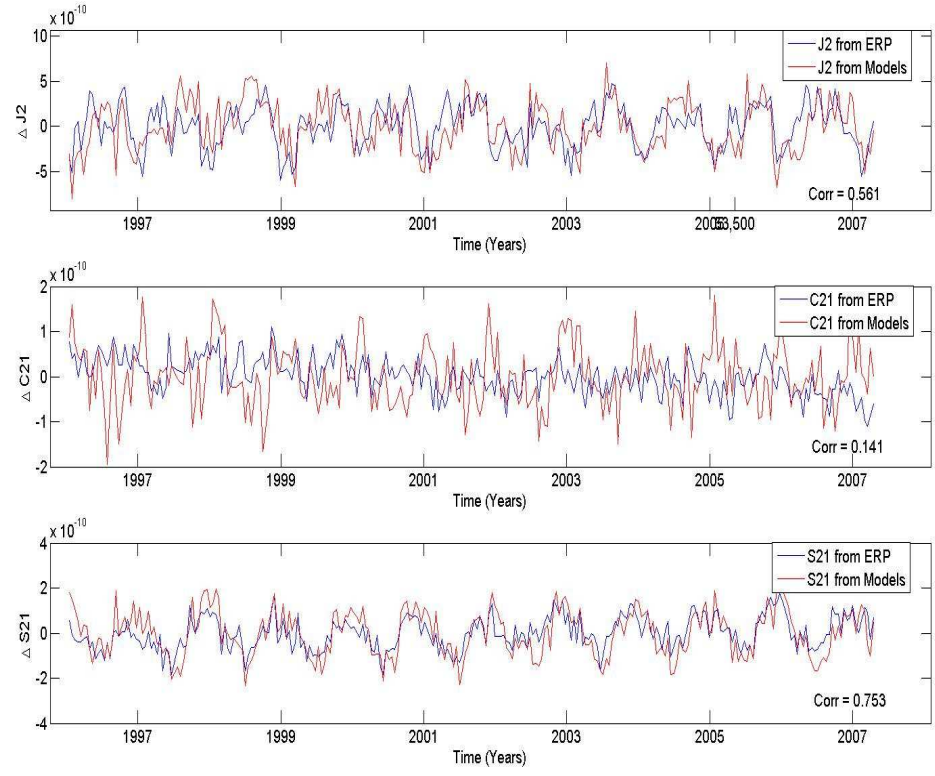

Figure 6.12 Comparison of C04 ERP excitation functions compared with the non-IB models

Figure 6.11 shows the comparison of the C04 estimated gravity field harmonics of the Earth's gravity field compared with the same values computed using the non IB models. Correlation is very good for the S21 term, but is slightly lower for J2. This is probably because the contribution of the motion term to J2 is much larger than the mass term therefore small errors in the motion term model mean relatively large errors when this is used to estimate the mass term from geodetic measurements. The S21 term on the other hand is dominated by the mass term and therefore less affected by this phenomenon. Consistent with other results the correlation for the C21 term is low probably due to the less well defined annual and semi annual terms in the model.

The estimates of changes in J2, C21 and S21 are now compared between ERP, SLR and the non-IB sources for the reason explained above. Figure 6.12 shows a comparison of the C04 derived estimates of the degree-2 harmonics and the LAGEOS estimated gravity field harmonics from *FAUST*. As expected the agreement is most well defined in the J2 and S21 components of the harmonics with clear correlation apparent between dominant annual variations in these signals especially when referring to the change in J2.

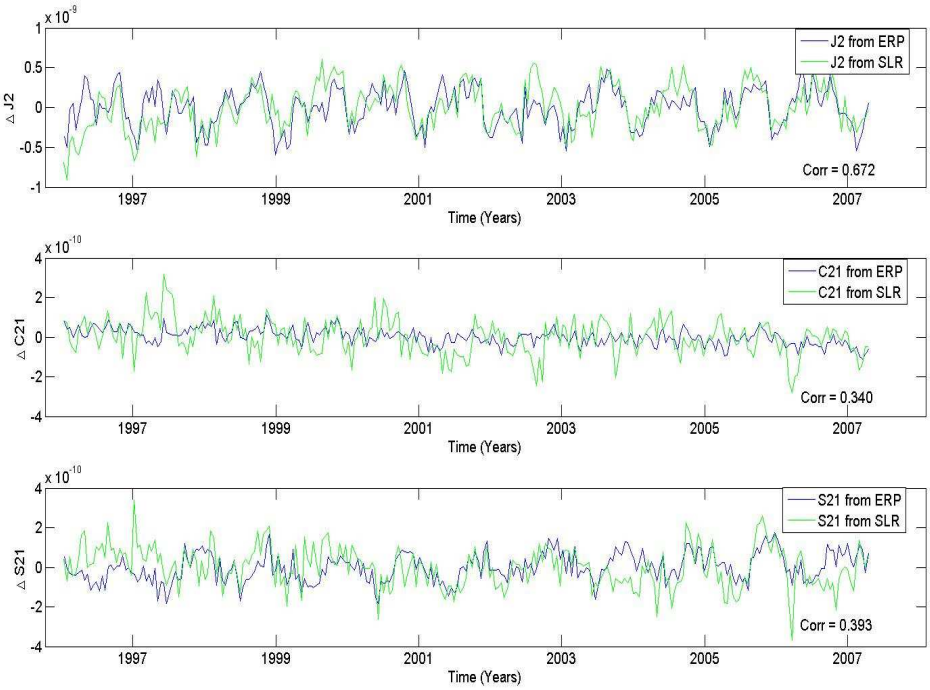

Figure 6.13 Comparison of C04 ERP excitation functions compared with the LAGEOS SLR gravity field harmonics

Finally the ERP derived gravity field estimates output from the base solution described in Chapter 4 are compared against the gravity field harmonics produced for LAGEOS orbits when solving for up to degree and order 3 gravity field harmonics. Figure 6.13 shows the comparison using the 15 day estimates of the gravity field harmonics from ERP estimates and Figure 6.14 shows the same comparison this time using the daily values of Earth rotation to compute the gravity field harmonics.

Firstly, it can be seen that, when compared to the C04 derived excitation functions using exactly the same models, the correlation of the J2 estimates in Figure 6.13 are slightly lower. This is most likely due to the differences that display as peaks in the time series. These are most likely caused by badly conditioned orbits, the removal of which would most likely raise the correlation coefficient to something similar to that of the C04 comparison.

The correlation of the S21 component has been sustained within *FAUST* when compared to the C04 derived excitation functions. Although there are several places where there are also differences seen as large peaks in this time series Figure 6.13. Finally the changes in C21 that are estimated from LAGEOS also display very similar characteristics to the estimates calculated from the C04 values, also with some large errors. It follows then that at the epochs of the time series that match well it would be expected that the gravity estimates from ERP may improve the orbit solution but there may be cases when the orbit is made worse by using ERP derived estimates of the gravity field harmonics.

The correlations seen in Figure 6.14 are comparable to ERP from GPS and GPS measures of the time variability (Gross et al., 2004) where correlations of 0.27, 0.22 and 0.61 were obtained for C20, C21 and S21 respectively. The two studies reveal better agreement in the degree-2 order 1 harmonics and show good agreement in the J2 and S21 terms on the dominant annual signals compared to GPS. In both the GPS and SLR results S21 exhibits a clear annual signal in response to the winter high in atmospheric pressure over Siberia (Gross et al., 2004). The poor correlation of C21 generally appears to reflect the relative contribution of mass to motion in the excitation functions and may indicate that the meridional motion terms are relatively poorly determined. In contrast, the relatively high correlation with the SLR J2 is perhaps unexpected given the

dominance of the atmospheric angular momentum in the excitation function. Despite the relatively low contribution of the mass component, the good agreement shows that the effects of the zonal atmospheric winds have been modelled sufficiently that it may be possible to determine small mass variations. The disparity between the SLR and GPS second degree zonal results points to an error in the GPS results rather than a major problem with the zonal winds as intimated in Gross et al., 2004.

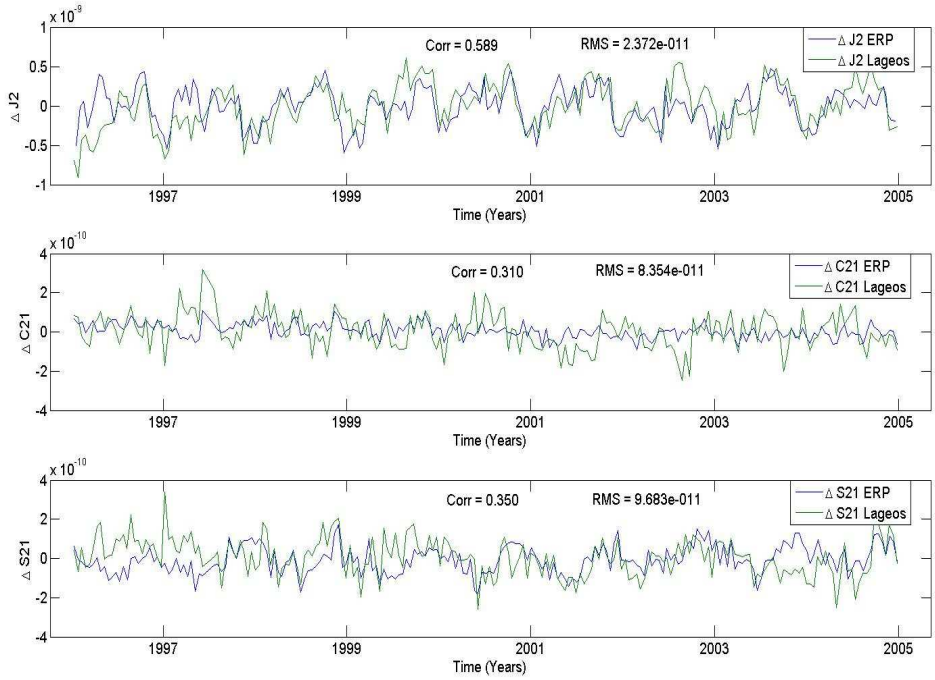

Figure 6.14 Comparison of SLR estimated ERP (15 day average) and SLR estimated gravity harmonics

It should be noted that better correlations for J2 were obtained in Hancock and Moore, 2007 but that the data has been compared over a longer period of time in this thesis. It may be that the agreement at the beginning of the time series seen in Figure 6.14, which seems to correlate the least, has contributed to this lower correlation value.

As the main purpose of this thesis is to investigate the possibility of using daily ERP values to calculate small mass changes in the orbit determination process, Figure 6.15 shows the daily estimates of J2, C21 and S21 from the base solutions ERP output plotted against the gravity harmonic estimates from LAGEOS. It is now much more difficult to see the correlation between the signals due to the noise in the ERP derived gravity field harmonics. This noise could well describe the high frequency variations in

the degree-2 harmonics and improve the orbits or it may be additional noise that causes the orbit solution to become worse. Looking back at the comparisons of χ_1, χ_2 and χ_3 in Figure 6.1 and Figure 6.2 it looks more likely that in the case of C21 and S21 that this is perhaps noise. J2, however, has given evidence in this chapter that it may be modelled well enough - despite the dominance of the motion term - to describe the daily mass fluctuations within the Earth system.

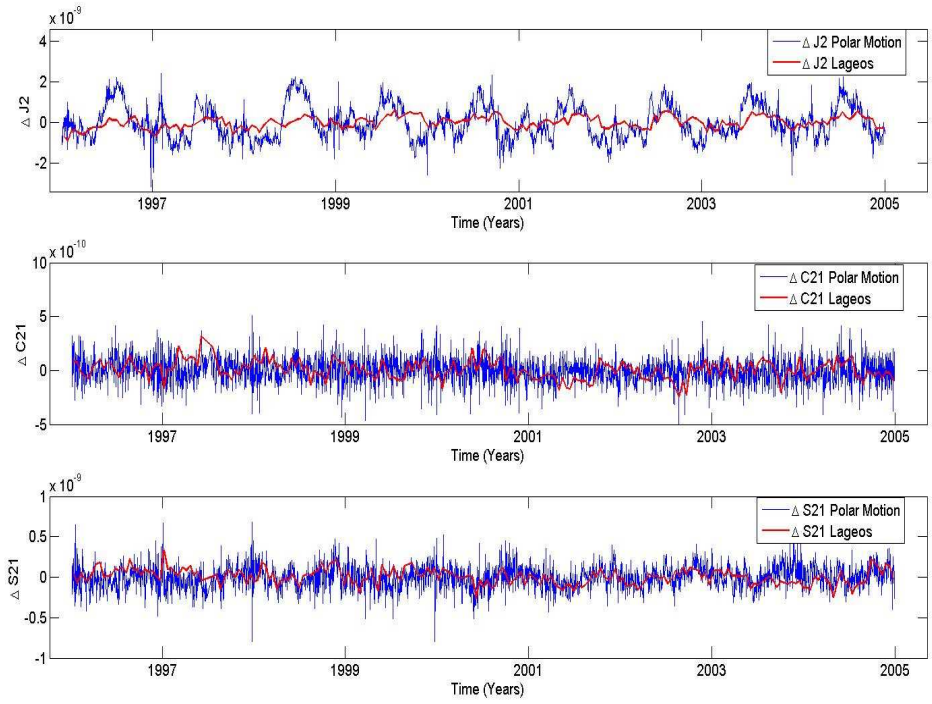

Figure 6.15 Comparison of SLR estimated ERP (daily values) and SLR estimated gravity harmonics

6.4 Conclusion

This chapter has investigated the correlation and coherence of the excitation functions, χ_1, χ_2 and χ_3 and the degree-2 gravity harmonics, J2, C21 and S21 of the Earth's gravitational field derived from models, as well as excitation estimates from ERPs and gravity field harmonics estimated as geophysical parameters in precise orbit determination. The results have shown good correlation between the ERP estimates of χ_2 and χ_3 and the models but less agreement between χ_1 and the models. Comparisons between the models and SLR derived gravity field harmonics show very good

correlation between the J2 terms and some correlation in the S21 term. The C21 term correlates the least. The poor correlation of C21 generally appears to reflect the relative contribution of mass to motion in the excitation functions and may indicate that the meridional motion terms are relatively poorly determined.

Comparing the ERP derived gravity field harmonics against the LAGEOS estimated harmonics shows promising agreement between the J2 terms, even though the correlation is lower than expected (0.59). This is most likely due to the large differences at certain epochs of the time series. This chapter shows that J2 is the most promising candidate for use in the orbit determination process and that C21 is the least likely to have a positive effect on the results.

Chapter 7

7 Using Angular Momentum Models to Estimate Gravity from ERPs in an Orbit Determination Process

7.1 Introduction

In this chapter the effects of using angular momentum models to remove the motion term from χ_1, χ_2 and χ_3 derived from ERPs estimated in LAGEOS within the iterative orbit determination process (see equation 6.3) are investigated. This will be undertaken in several stages. In the first instance, as the results of using χ_3 motion from models to obtain χ_3 mass from LOD estimates converted to the J2 spherical harmonic of the Earth's gravity field have the best agreement with both the models and the LAGEOS derived gravity field harmonics, estimates of J2 will be introduced to the orbit determination process independent of the other degree-2 harmonics. Firstly they will be calculated as a single correction over the 15 day arc, to mirror the timescales on which J2 has been derived as a geophysical parameter within *FAUST* and then this will be extended to calculate a daily correction to J2 over the 15 day arc. Following the analysis of J2, orbits will be processed utilizing all three degree-2 harmonics, C21, S21 and J2; firstly as a 15 day average and then as daily values across the 15 day arcs. The results of these orbit estimations will be compared to assess whether there is any advantage to using estimates of the degree-2 harmonics in this manner.

7.2 Use of AM Data and Gravity Mass Change in Orbit Determination

Space geodesy is limited in its ability to provide mass changes over short time periods (less than 15 days) even at low spatial resolutions, due to the satellite's low sensitivity to the Earth's gravity field and to the high correlation between harmonics (especially degrees 2 and 4) (Hancock and Moore, 2007). However space geodesy does provide high resolution (here daily but in some cases, such as with GPS, even more frequent) ERP data.

7.2.1 Orbit Determination Procedure

The low sensitivity of orbits to the gravity field variability or the high correlation between the harmonics limits the time period over which mass change, even at low spatial resolutions, can be recovered from space geodesy. However, the relatively high temporal resolution of ERPs does raise the possibility of simultaneously recovering and using higher temporal frequencies for the degree-2 harmonics from the ERP data within an orbital determination procedure. The methodology will require that angular momentum data is available but this is not a major concern as geophysical studies utilizing geodetic satellites are typically retrospective.

To investigate whether this methodology can lead to enhanced orbital accuracies, the variability in the degree-2 gravity field harmonics inferred from ERP parameters within the orbit determination is utilised. However, it has already been observed in Chapter 6 that the mass components of the second degree first order harmonics from ERPs modified for the motion have low correlations with the mass variations determined directly from the orbital tracking. Consequently, we cannot anticipate any improvement with C21 and S21 despite the high contribution of mass (>50%) to the excitations. To ascertain this we undertook an analysis in which a single correction to the second degree harmonics was recovered from the ERPs over each 15 day LAGEOS arc.

The method used comprised the following steps (Figure 7.1):

1. Consider a-priori ERP values
2. Form 15 day average of ERPs
3. Read in angular momentum from NCEP model and form 15 day average
4. Remove motion and secular core-mantle interaction terms from ERPs
5. Derive change in second order harmonics J2, C21 and S21,
6. Compute orbit and estimate orbital parameters
7. If convergence achieved stop; otherwise reiterate starting at step 2.

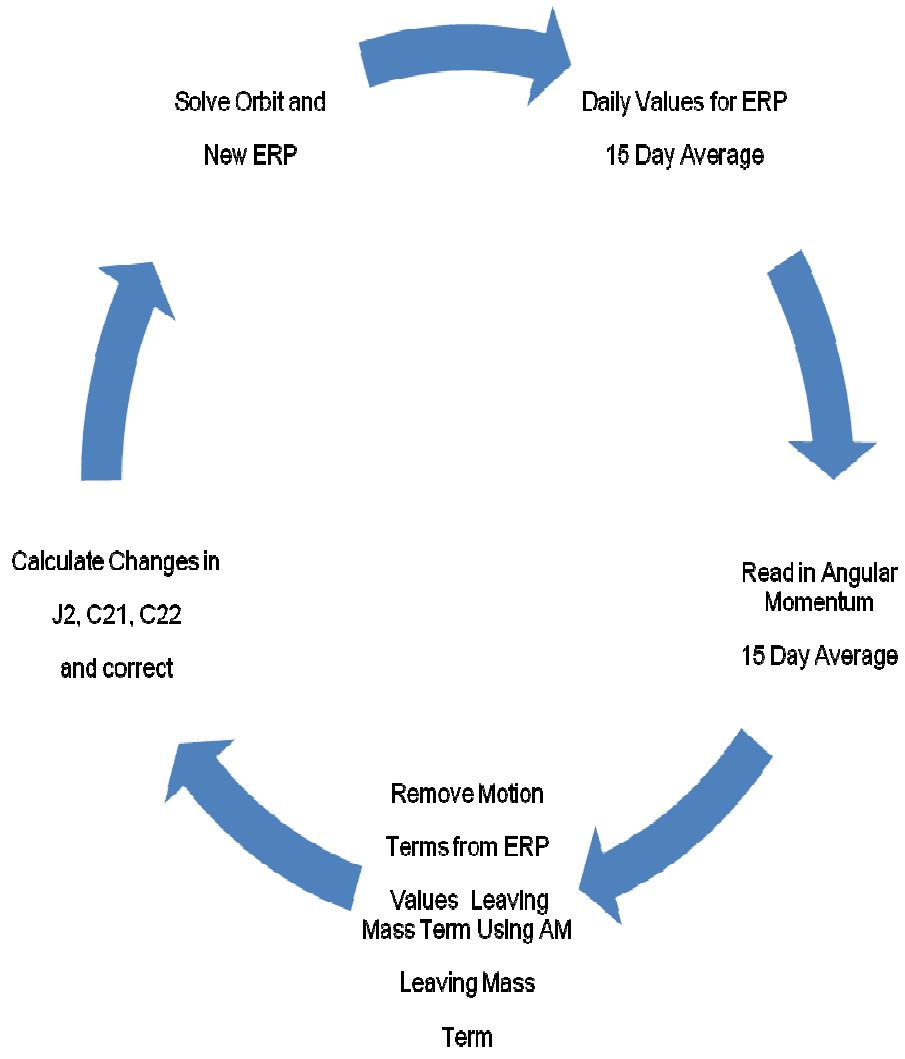

Figure 7.1 Schematic of orbit determination process using angular momentum.

7.3 Precise Orbit Determination Analysis

As described previously, precise orbits of LAGEOS I and LAGEOS II have been calculated using *FAUST*. A base solution was calculated first (for details see Chapter 5). In the first instance 15 day arcs were calculated using no global parameters (i.e. no gravity, station coordinates or ERPs were solved for. State vectors, solar radiation pressure and two along track corrections are estimated over 5 day arcs calculated from July 1996 until October 2007. All available data in the MERIT II format was used. Any station with less than 20 observations over the whole arc or an average RMS error value over 5 cm for the total arc was discarded from the solution at this point. These orbits were iterated until convergence. These converged orbits would then provide the starting point for the next stage of orbit determination.

Using the previously converged orbits as a starting point a base solution was then determined for the purpose of later comparison. State vectors, solar radiation pressure and 2 along track corrections are estimated over 5 day arcs but this time also solving for the global parameters of station coordinates and daily ERPs (XP, YP and LOD) estimated over the 15 day arc and iterated until the solution converges. Daily values for UTC are also introduced at this point but these are kept fixed to help constrain the LOD estimates.

Starting again with the previously described converged orbits without any global parameters, the same orbits were solved for again using the modified version of *FAUST* that uses ERPs to calculate the low degree spherical harmonics of the Earth's gravity field. This has been carried out using four different scenarios.

1. Using only LOD to estimate an average value for J2 over the 15 day arc
2. Using only LOD to estimate an average value for J2 on a daily basis
3. Using XP, YP and LOD to estimate values for C21, S21 and J2 over the 15 day arc
4. Using XP, YP and LOD to estimate values for C21, S21 and J2 on a daily basis

Due to the analysis performed in Chapter 6 that shows that agreements between corrections to J2 have relatively high correlation compared with S21 and C21, LOD will be used independently to estimate a correction to J2. This will assess whether J2 on its own can give higher resolution estimates that will improve the estimated orbit. This will be done firstly with an averaged correction over the 15 day arc, to assess how well it compares with results from deriving gravity as a geophysical parameter in an iterative process, and then, secondly, calculating daily corrections. These tests will use all three parameters C21, S21 and J2 with the results expected to be less promising due to the lower correlations between the models and the SLR results. The results and comparisons of each of the scenarios with respect to the base solution are shown in Figure 7.2 – 7.9.

Figure 7.2 shows a comparison of the frequency of post-fit residual RMS error fits of the orbits derived from J2 gravity estimates from LOD only, averaged over the 15 day arc against the base solution grouped together in 2cm blocks. The post-fit residual RMS error values of each of the test solutions have been subtracted from the post-fit residual RMS error values of the base solutions. Thus, negative values imply that the test solution is an improvement on the base solution while positive values show that the test solution has been degraded by the introduction of gravity estimates from ERP parameters.

As can be seen from Figure 7.2 calculated values of J2 using estimated values of LOD from LAGEOS averaged over a 15 day period improves the overall solution with respect to the base solution. From the previous analysis in Chapter 6 this is what would have been expected as the estimates of J2 from LAGEOS derived ERPs have fairly good agreement with both the J2 estimates from the models (correlation of 0.450) and the J2 estimates from LAGEOS (correlation of 0.589). Also Figure 7.2 shows that by calculating a value for J2 on a daily basis decreases the accuracy of the overall solution on the majority of the 15 day arcs and gives a worse solution than when solving for a single J2 correction over the 15 day arc. Once again previous analysis has shown this to be the likely outcome of this test as a comparison of daily J2 estimates from ERPs and daily values from the models in Chapter 6 has shown that the agreement between the two different estimates is far less due to the much noisier data apparent in the daily estimates of J2 when compared with J2 from LAGEOS. The overall improvement across the whole dataset when using ERPs to estimate J2 is a reduction in the mean post-fit residual RMS of 0.013 cm, this compares to a 0.714 cm increase in the average post-fit residual RMS values when using the J2 daily estimates.

In considering the changes in the post-fit residual RMS error of the estimated orbits the number of rejected observations must also be considered as this has a direct effect on the post-fit residual RMS of the orbit. Figure 7.3 shows, similar to Figure 7.2, the frequency of the number of rejected observations when using an estimated value of J2 derived from estimated LOD values averaged over 15 days, grouped together in blocks of 50 observations.

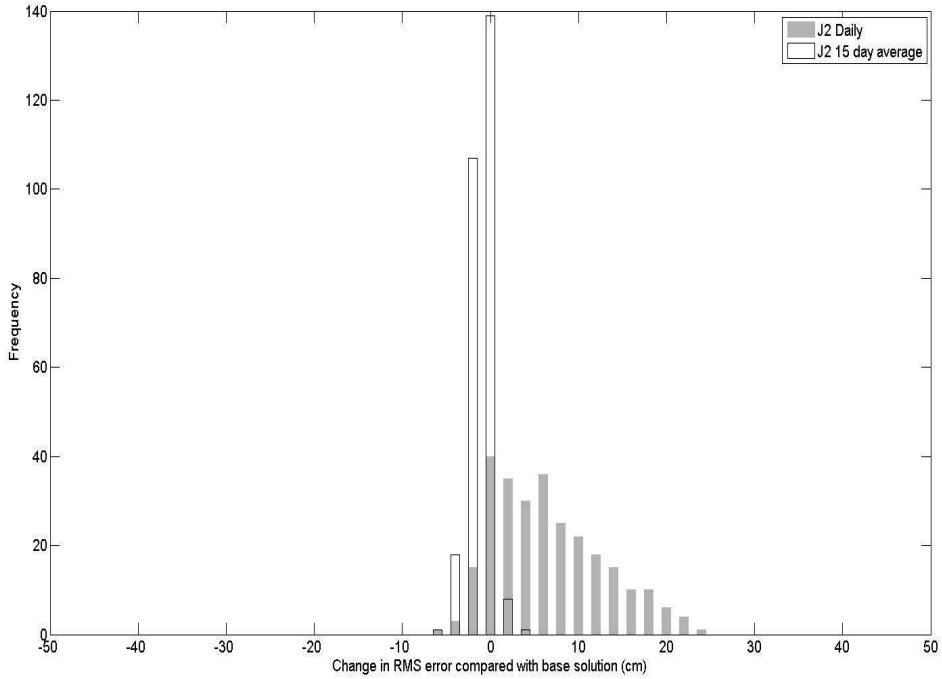

Figure 7.2 A comparison of RMS of orbits using J2 estimated from LOD on a daily basis and on a 15 day average against the base solution

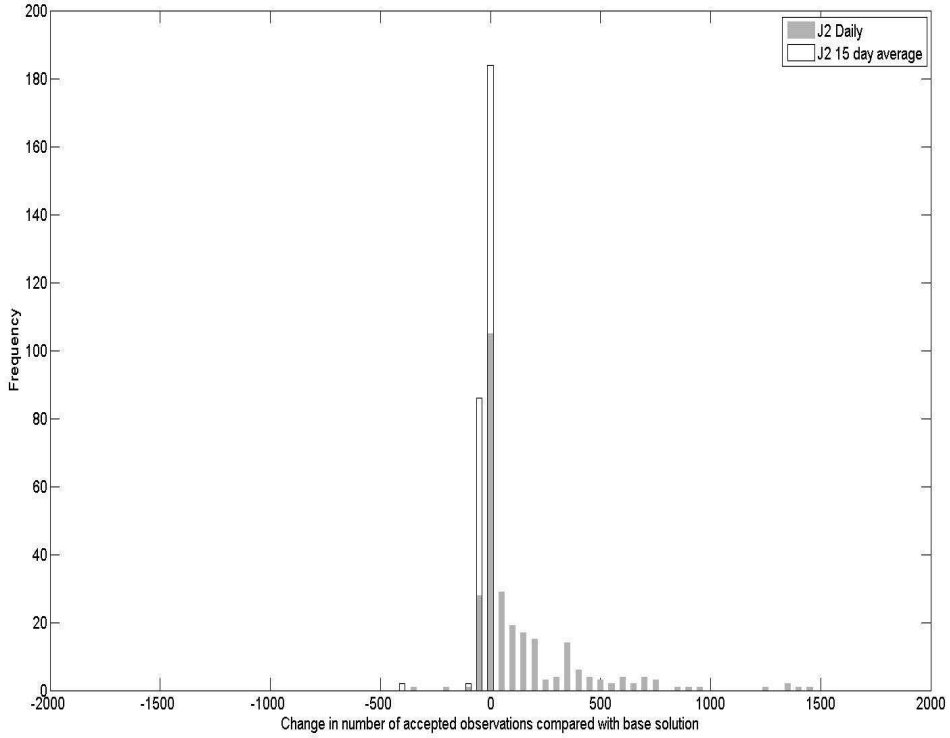

Figure 7.3 A comparison of rejected observations from orbits using J2 estimated from LOD on a daily basis and on a 15 day average against the base solution

Figure 7.3 shows that the number of rejected observations from the orbital fit when using calculated J2 are less or the same in 75% (202 of 271, 115 of which are exactly the same) of the arcs processed when compared to the base solution whereas when J2 values are estimated daily the number of arcs with a larger number of rejected observations increases greatly so that only 20% (56 of 271) reject less or the same number of observations as the base solution. Again these results reflect the analysis of the previous chapter and give evidence that 15 day estimates of J2 that show good agreement with both the models and the LAGEOS gravity field estimates for J2 provide a better fit in the orbit determination process compared with the average value for J2.

The next set of tests carried out involved estimating all three low degree harmonics C21, S21 and J2 in the orbit determination process. As previously stated two separate tests were carried out giving results with low degree gravity harmonics averaged over the 15 day arc as well as the second test where C21, S21 and J2 were estimated daily from ERP values within the orbit determination process.

Figure 7.4 shows a comparison of the frequency of post-fit residual RMS error results from these tests subtracted from the post-fit residual RMS error values of the base solution. As before negative values represent an improvement in the solution. A very similar result is achieved when compared to using J2 alone as we obtain an improved orbital estimate when using the averaged 15 day value but the solution of the orbit is degraded quite considerably when estimating the gravity values on a daily basis. The mean post-fit residual RMS value for all the arcs processed using C21, S21 and J2 with a 15 day average is 0.011 cm better than the base solution compared with 1.107 cm degraded mean post-fit residual RMS when using the daily values.

Following on from analysing the post-fit residual RMS of the orbits, we again look at the number of accepted observations when using gravity values in the solution. As before we see that when using a 15 day average the number of arcs with a larger number or the same number of accepted values is 76% (205 of 271) giving evidence for a better solution when using gravity values from ERPs in the overall solution.

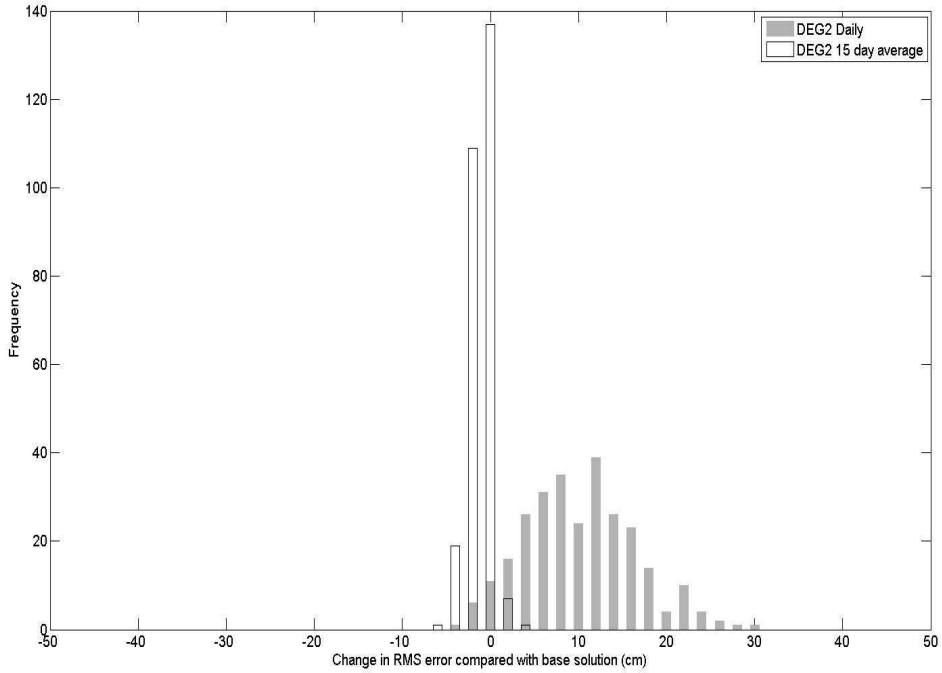

Figure 7.4 A comparison of RMS of orbits using C21, S21, J2 estimated from ERP on a daily basis and on a 15 day average against the base solution

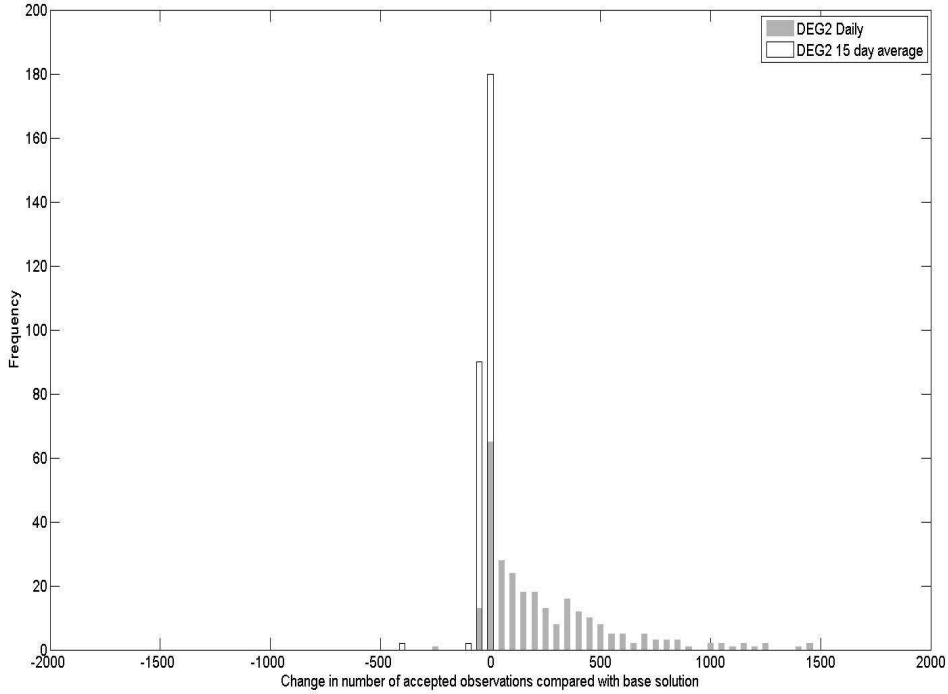

Figure 7.5 A comparison of rejected observations from orbits using C21, S21, J2 estimated from ERP on a daily basis and on a 15 day average against the base solution

Once again using daily gravity values vastly increases the number of arcs with a larger number of rejected observations in the solution. The number of arcs that accept more or the same number of observations is now just 8% (21 of 271).

Figure 7.6 shows a comparison of orbits where we have firstly calculated J2 values alone from LOD and secondly when C21, S21, J2 are derived from XP, YP and LOD; all averaged over a 15 day period. It can be seen that the solutions are very similar to each other in terms of post-fit residual RMS. The graph shows that there is a slight improvement in the number of arcs that have an improved post-fit residual RMS when using C21, S21, J2 values in the solution compared with J2 alone. The mean post-fit residual RMS of the data, however, shows that the J2 alone solution is slightly better than the combined solution with the mean of the combined solution being a 0.011 cm improvement compared with the base solution and the J2 alone orbit showing a 0.013 cm improvement over the same. The closeness suggests that the estimates of C21 and S21 may either have little effect on the results compared to J2 or that the data already has a high level of fit and thus further modelling improvements are minimal. This may cause small or zero improvements on certain arcs that have a RMS difference close to zero which may be increased slightly by C21 and/or S21 corrections that are a good fit to the data at that particular epoch.

Figure 7.7 shows that in terms of the frequency of the number of accepted observations when comparing the 15 day averaged estimates of C21, S21 and J2 to the J2 alone solution yields a similar result to that of the above RMS comparison. Once again a small improvement is visible in Figure 7.7 when using the combined solution. This equates to 76% (205 of 271) of the arcs processed in the combined solution showing either the same number of rejections or less compared with 75% (202 of 271) when using the J2 only solution. The small improvement that is seen here when using the combined solution is somewhat unexpected as from the previous comparisons of degree-2 harmonics it can be seen that C21 and S21 estimates from ERPs do not agree as well with the same estimates from other sources as the J2 estimates do. The number of orbital arcs that are showing improvements may be due to particular arcs where the match of S21, C21 and J2 is relatively good and the post-fit residual RMS of the orbit is close to 0. This may cause small improvements in the fit of the orbit over that particular arc.

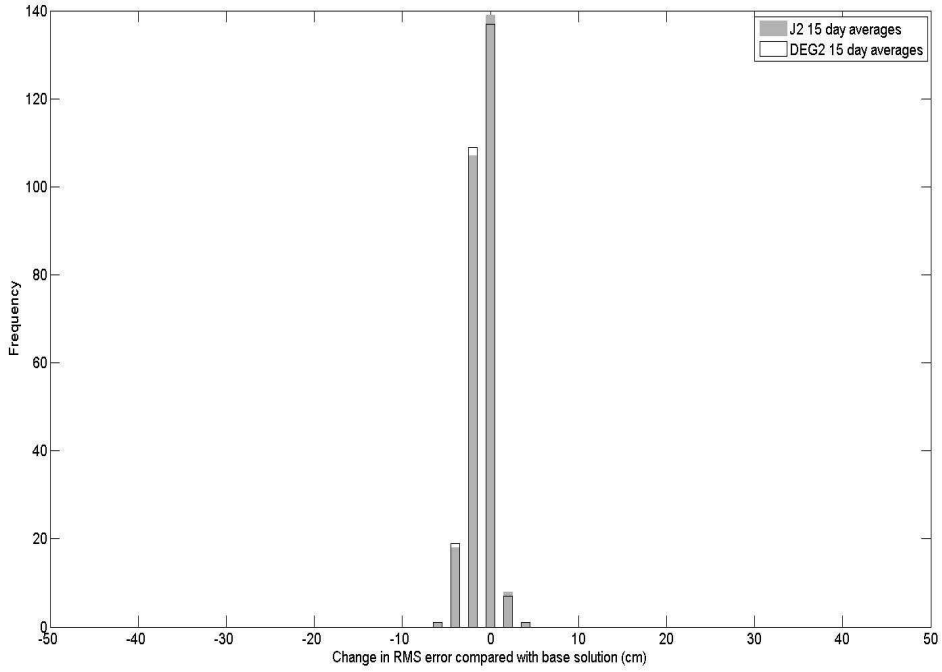

Figure 7.6 A comparison of RMS of orbits using J2 and of C21, S21, J2 estimated from ERP averaged over 15 days and against the base solution

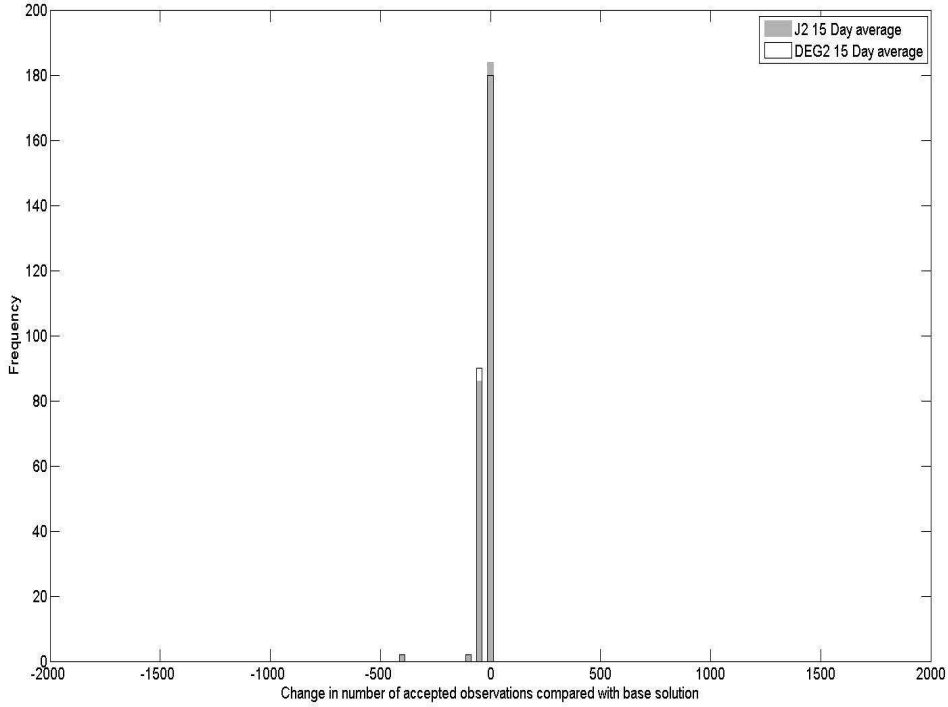

Figure 7.7 A comparison of rejected observations using J2 and of C21, S21, J2 estimated from ERP averaged over 15 days and against the base solution

Figure 7.8 shows a comparison between values for gravity spherical harmonics estimated from ERPs on a daily basis. From the previous analysis it can be seen that using daily values gives a much less well defined orbit than when using spherical harmonic values averaged over a 15 day period. Here, it can be seen that the daily values, when using all three low degree harmonics, gives a much worse solution (increase of 1.107 cm in RMS) than when using J2 gravity values alone (increase of 0.714 cm in RMS). From the analysis in Chapter 6 this result would make sense as the daily degree-2 harmonics are much noisier than their 15-day-averaged counterparts.

As all three harmonic data sets are very noisy this increased noise causes the fit of the orbit to degrade in most cases. It is also more likely that as the data is noisy on all three degree-2 harmonics that there is more chance that the orbit will be degraded when using all three estimates when compared to the J2 alone solution. The noise in this data comes from the fact that the degree-2 estimates on a daily basis do not agree well at the higher frequency terms (i.e. weekly and daily terms) in the coherence plots shown in Chapter 6. The reason for this could be that either the models from the ocean and/or atmospheric data may not be accurate enough to use to model the small mass variations on a daily basis. These models do not take into account the whole of the motion of the ocean and atmosphere in their calculations and other error sources such as improper modelling of El Nino events may also cause discrepancies in the models. On the other hand the ERPs derived from LAGEOS may not be sensitive enough to these short term variations.

This means that on a daily basis the estimated values of the degree-2 harmonics do not match well with the real mass variations of the Earth system. There are however a few arcs that show an improvement in post-fit residual RMS in both the combined solution and in the J2 alone solution. It is possible that at these particular epochs all three estimates agree well with the LAGEOS estimates by chance. Obviously there is more chance of a good match to the LAGEOS estimates of gravity if only one of the three parameters is estimated, which is the likely reason why the J2 only solution is much better than the combined solution.

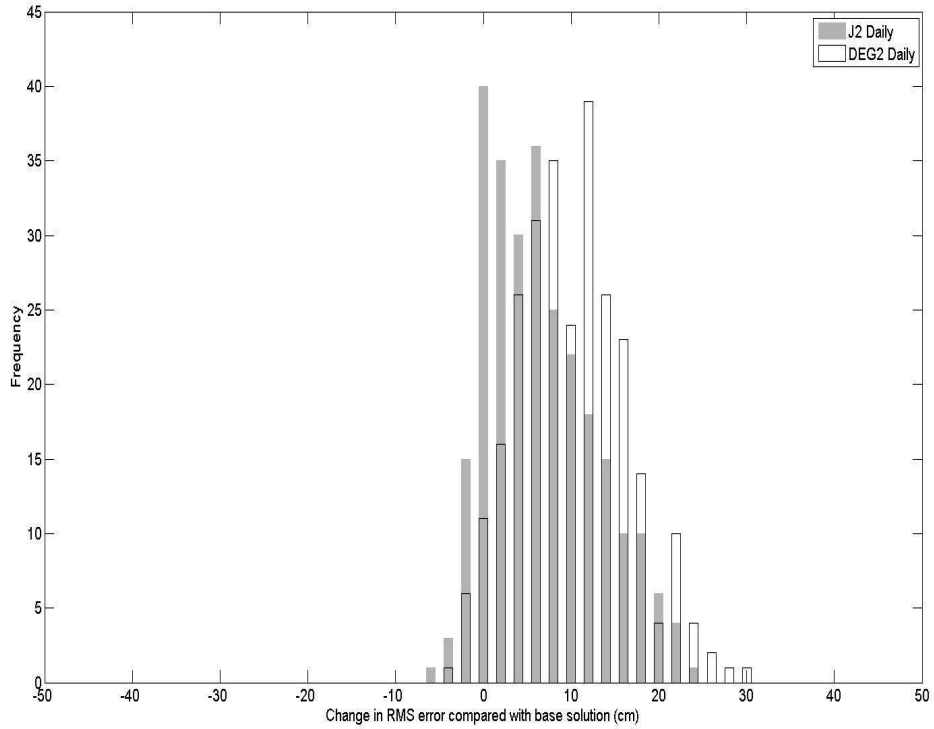

Figure 7.8 A comparison of RMS of orbits using J2 and of C21, S21, J2 estimated from ERP on a daily basis against the base solution

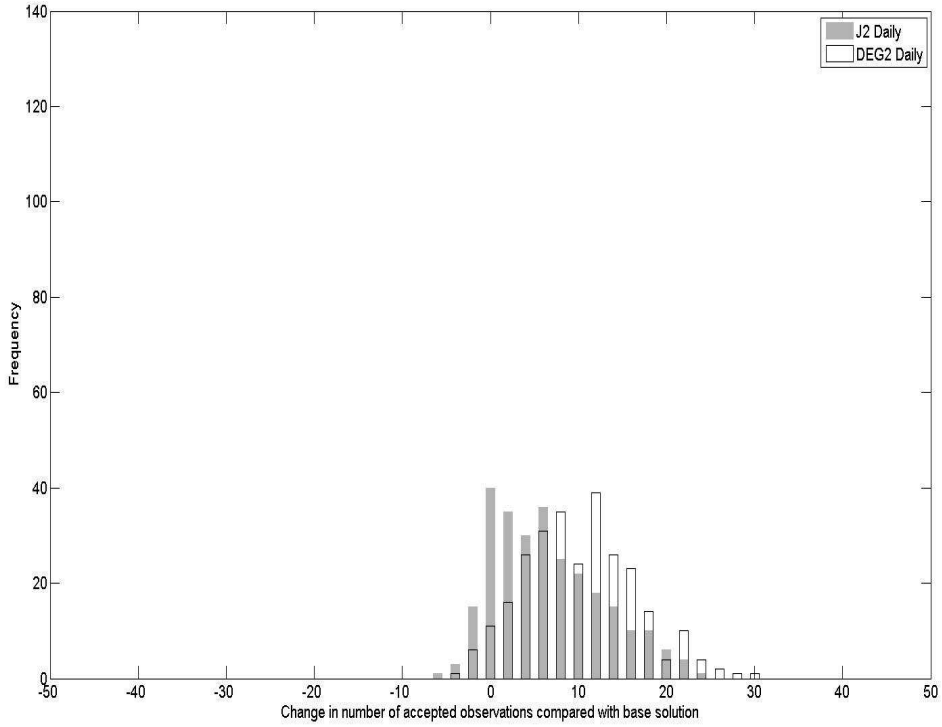

Figure 7.9 A comparison of rejected observations using J2 and of C21, S21, J2 estimated from ERP on a daily basis against the base solution

As further evidence of the conclusions generated from the previous analysis, Figure 7.9 shows that there are many more rejected observations when using all three low degree harmonics (8% or 21 of 271 arcs show an increase in the number of accepted observations) in the orbit determination process compared with using J2 alone (20% or 56 of 271 arcs show an increase in the number of accepted observations). The reason for this is once again the increased noise in the daily data.

7.4 Precise Orbit Determination - Gravity Comparison

After analysing the post-fit residual RMS and the number of accepted and rejected observations of the four different scenarios set out in section 7.2 this section will attempt to investigate the specific arcs that have shown an improvement or deterioration when using estimates of the degree-2 spherical harmonics of the Earth's gravity field from ERPs.

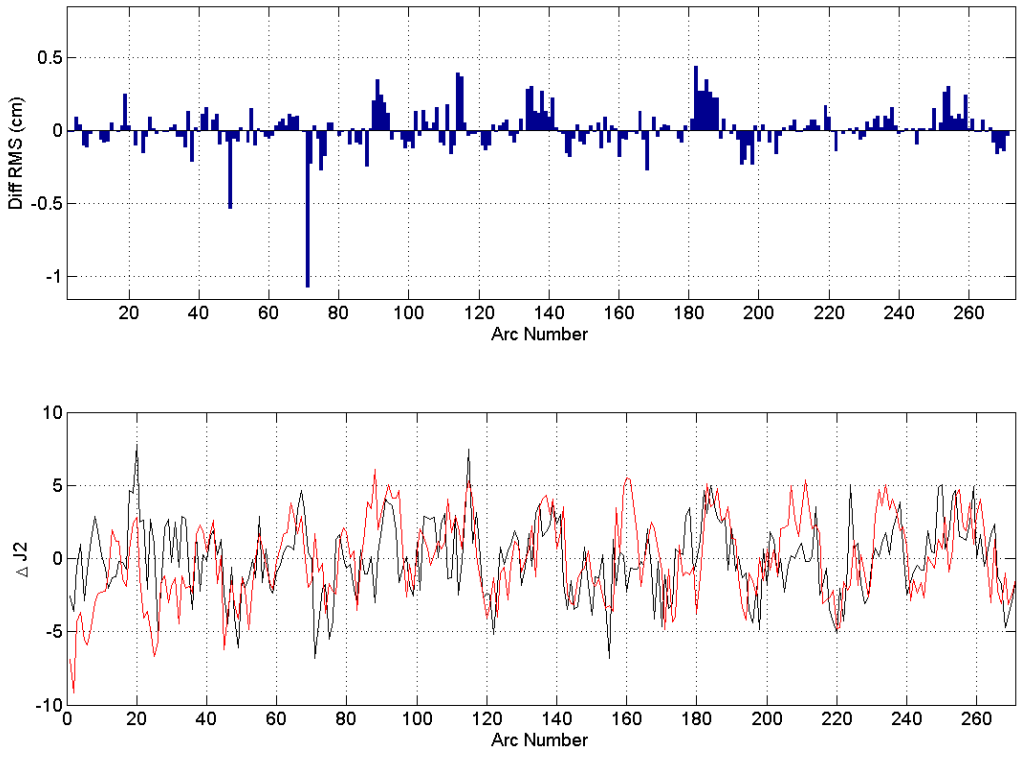

Figure 7.10 RMS difference of the J2 15 day solution with global solution from *FAUST* (top) and a comparison of the J2 from LAGEOS (red) and ERP (black)

Figure 7.10 shows the post-fit residual RMS difference arc by arc of the base solution compared with the J2 only solution along with a comparison of the low degree harmonic J2 from LAGEOS as a geophysical parameter and from the ERP estimate of J2. The positive values on this graph show improvement in the fit of the SLR range data to the orbit.

Figure 7.10 identifies several periods where improvement in the post-fit residual RMS error of the orbit is evident. There are five time periods of relatively large improvement in the post-fit residual RMS. These occur approximately at arc number 90, 115, 130, 180 and 250. All of these time periods of large improvement coincide with where the J2 comparison is particularly good. This is especially evident around arc number 180 where the peaks of the two J2 parameters almost coincide.

The time period of Figure 7.10 that shows the least agreement is at the beginning of the analysis. Here there are arcs showing much larger deterioration and the very large negative value around arc number 70 coincides with a large discrepancy between the J2 data sets. This figure gives evidence that using J2 as a 15 day average in an orbit determination process gives benefit as long as the match between the SLR derived gravity parameter J2 and the ERP estimate of the same match closely.

If there is a large discrepancy between the SLR derived gravity parameter and the J2 from ERPs then the fit deteriorates, this is likely caused by errors in the motion part of χ_3 due to domination of the motion term in χ_3. It is also interesting to note that most of the improved arcs seem to correspond to peaks in the J2 time series rather than the troughs. A similar but opposite pattern can be seen in Figure 7.11 which shows the post-fit residual RMS fit of the *FAUST* solution solving for up to degree and order 3 parameters of the Earth's gravity field. This shows that the errors in the fit of the orbits are larger at this time of year.

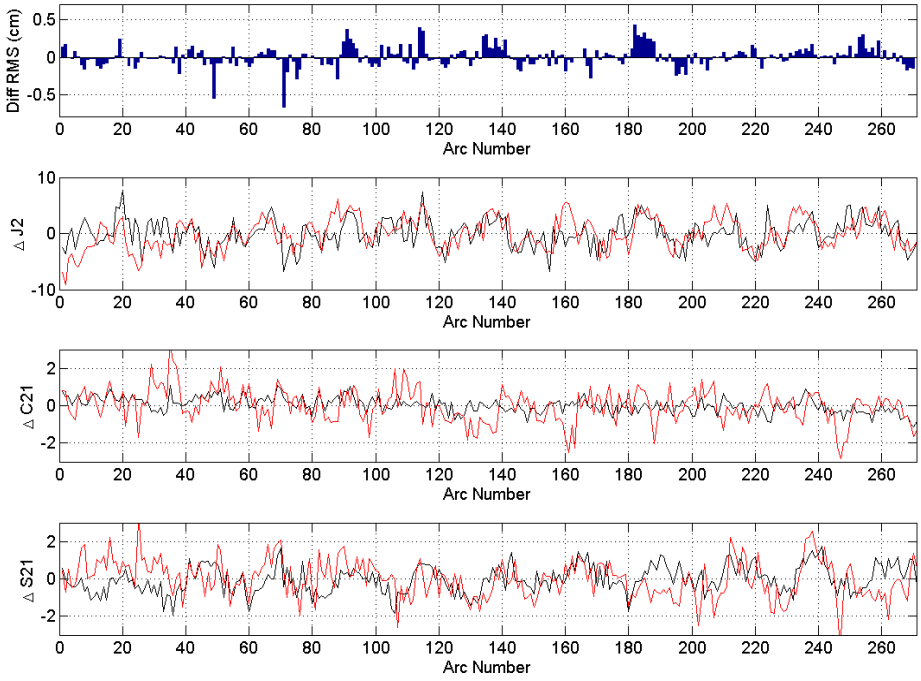

Figure 7.11 RMS difference of the degree-2 (J2, C21, S21) 15 day solution with global solution (top) and a comparison of the J2, C21, S21 from LAGEOS (red) and ERP (black)

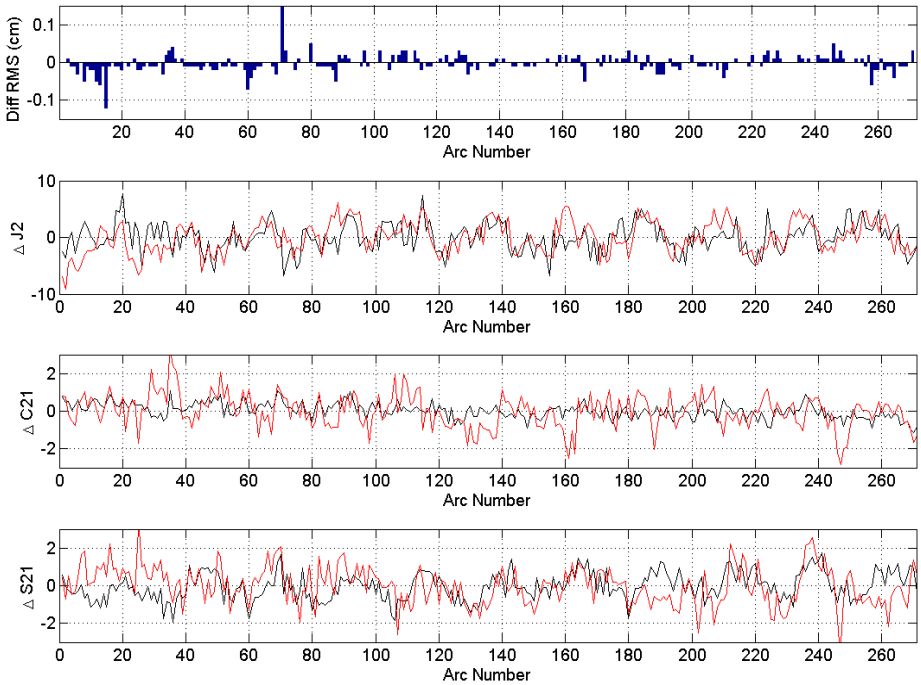

Figure 7.12 RMS difference of the degree-2 (J2, C21, S21) 15 day solution with J2 15 day solution (top) and a comparison of the J2, C21, S21 from LAGEOS (red) and ERP (black)

Following on from the comparison in Figure 7.10, Figure 7.11 shows the fit of the base solution compared to the fit of the solution using all three degree-2 spherical harmonics, along with comparisons of C21, S21 and J2 derived from LAGEOS as a geophysical parameter and from ERPs estimated in LAGEOS. The two comparisons of fit from Figure 7.10 and Figure 7.11 can be seen to be almost identical on this scale and that the relatively large improvements in the fit of the orbits are still evident around the same five time periods as mentioned above. Some of the arcs show good agreement on at least two out of the three gravity parameters in these areas, such as J2 and S21 at arc number 180 and just after and J2 and C21 at arc 250. Finding an arc where all three parameters match well with their LAGEOS derived counterpart is difficult, which would be exactly what we would expect from previous analysis. It is however difficult to see any real effect caused by introducing the two additional parameters from Figure 7.11

Figure 7.12 shows the post-fit residual RMS error from the fit of the orbits that use J2 only from ERPs and C21, S21 and J2 from ERPs. Positive values show an improvement when using the C21, S21 and J2 combined solution; negative values show deterioration of the solution. There are two time periods that are immediately apparent. The initial period has already been shown to give mixed results for J2 alone and can clearly be seen to have been degraded further by the addition of C21 and S21. Inspection of the data reveals that the match of S21 for these arcs is particularly bad and the match of C21 does not agree well either. Also of note is that the large error seen previously at arc number 70 has improved as the match of both C21 and S21 at this particular epoch are good especially when compared to the match of the J2 data. Arcs after number 260 show large amounts of degradation most likely due to the poor match of the S21 data at these epochs.

This analysis shows that when two of the three parameters have good matches to their respective counterparts derived from SLR orbits it is likely that the post-fit residual RMS of the orbit is improved. It also shows that the improvement seems to be dominated by the match of the J2 component to the data as the comparison in Figure 7.10 and Figure 7.11 do not show many visible changes, indicating that J2 is more

important in defining the orbit than C21 and S21. This may be a result of the J2 correction being larger than the correction to C21 and S21 respectively.

It should also be noted that the correlations between the LAGEOS-derived degree-2 harmonics of the gravity field and the ERP-estimated degree-2 harmonics have dropped from 0.589, 0.310 and 0.350 for J2, C21 and S21 respectively to 0.419, 0.210 and 0.221 after the orbits have converged in this orbit determination process.

7.5 Conclusion

The analysis has shown that the overall estimated orbits are affected by the addition of gravity parameters C21, S21 and J2 derived from estimates of XP, YP and LOD in the orbit determination process. This effect can be positive or negative dependent on the agreement of the ERP-estimated gravity values with the LAGEOS-estimated low degree spherical harmonics, which are assumed as truth at a particular epoch. If the ERP estimated low degree gravity harmonics match well with the LAGEOS estimated low degree gravity harmonics at a particular epoch then the orbit will improve when comparing with the base solution (as described in Chapter 6, otherwise the orbit will degrade as well as the number of accepted observations decreasing.

It has been shown that there is not much difference in using J2 estimates from ERP parameters on its own and in using a combined solution using values of C21 and S21 in addition to J2. This was slightly unexpected due to the relatively low correlations of both C21 and S21 to the counterparts derived from the models and especially from LAGEOS. On detailed inspection of the specific arcs that show improvement it is evident that these improvements occur for orbits where J2 gives a small detrimental effect on the post-fit residual RMS that is compensated by reasonable agreement in the C21 and/or S21 parameters that can turn that detrimental effect into a positive. It has also been shown that the J2 parameter seems to have more influence on the orbits than the other degree-2 coefficients.

Finally, it has been shown that using daily estimates of J2, C21 and S21 has a large detrimental effect on the post-fit residual RMS of the orbits. This is due to the noisy nature of the signals and, although a small percentage of arcs show an improvement

using this method, it is not practically useful to use this method in orbit determinations at the current time. This effect may be due to inaccuracies in the models or the insensitivity of LAGEOS to these high frequency variations.

Chapter 8

8 Geocentre motion from SLR, GPS and Geophysical Models

8.1 Introduction

The geocentre is the centre of mass of the whole Earth, which means the combined centre of mass of the solid Earth, atmosphere, oceans, hydrosphere and cyrosphere. The distribution of mass within the Earth system is the cause of geocentre motion, which is defined as the displacement of the centre of mass of the Earth from the International Terrestrial Reference Frame (ITRF) origin. This chapter will derive geocentre motion from SLR, GPS and geophysical models and show a comparison of the three methods.

8.2 Background

From Wahr et al. (1998) let $\Delta\sigma(\phi,\lambda)$ be the mass unit area centred at latitude ϕ and longitude λ on the Earth's surface. Expansion gives (Moore and Wang, 2003):

$$\Delta\sigma(\phi,\lambda) = R\rho_{\omega}\sum_{l=0}^{\infty}\sum_{m=0}^{l}\bar{P}_{l,m}(\sin\phi)\left(\Delta\hat{C}_{lm}\cos m + \hat{S}_{lm}\sin m\right) \qquad \textbf{(8.1)}$$

Where

R = radius of the Earth

ρ_{ω} = water density

$\bar{P}_{l,m}$ = the associated Legendre polynomial of degree *l* and order *m*

$\Delta\hat{C}_{lm}$ and $\Delta\hat{S}_{lm}$= dimensionless Stokes coefficients

According to Wahr et al. (1998) using the orthogonality of the Legendre polynomials these harmonics can be evaluated by

$$\begin{Bmatrix}\Delta\hat{C}_{lm}\\ \Delta\hat{S}_{lm}\end{Bmatrix} = \frac{1}{4R\pi\rho_{\omega}}\int_0^{2R}d\lambda\int_{-\frac{\pi}{2}}^{\frac{\pi}{2}}\Delta\sigma(\phi,\lambda)\,\bar{P}_{l,m}\begin{Bmatrix}\cos m\lambda\\ \sin m\lambda\end{Bmatrix}\cos\phi\,d\phi \qquad \textbf{(8.2)}$$

These are related to the gravity field harmonics by Wahr et al. (1998)

$$\begin{Bmatrix}\Delta C_{lm}\\ \Delta S_{lm}\end{Bmatrix} = \frac{3\rho_{\omega}}{\rho_{av}}\frac{1+k_l'}{2l+1}\begin{Bmatrix}\Delta\widehat{C}_{lm}\\ \Delta\widehat{S}_{lm}\end{Bmatrix} \qquad \textbf{(8.3)}$$

where

ρ_{av} = density of the Earth

k_l' = load Love number of degree *l* (Farrell, 1972)

The loading associated with equation 8.1 deforms the elastic Earth and displaces points on the surface by distances S_r, S_θ and S_λ, where:

$$\begin{aligned} S_r &= \frac{GM}{gR}\sum_{l=1}^{\infty}\sum_{m=0}^{l} h_l \bar{P}_{l,m}(\sin\phi)\left(\Delta\widehat{C}_{lm}\cos m\lambda \hat{S}_{lm}\sin m\lambda\right)\\ S_\theta &= \frac{GM}{gR}\sum_{l=1}^{\infty}\sum_{m=0}^{l} l_l \frac{\partial\bar{P}_{l,m}}{\partial\phi}(\sin\phi)\left(\Delta\widehat{C}_{lm}\cos m\lambda \hat{S}_{lm}\sin m\lambda\right) \qquad \textbf{(8.4)}\\ S_\lambda &= \frac{GM}{gR\cos\phi}\sum_{l=1}^{\infty}\sum_{m=0}^{l} l_l \bar{P}_{l,m}(\sin\phi)\left(-mn\widehat{C}_{lm}\sin m\lambda \hat{S}_{lm}\cos m\lambda\right)\end{aligned}$$

*w*here

h_l = Degree-1 Love number

l_l = Degree-1 Shida number

Observations of the Earth's geocentre are important for two main reasons 1) most fundamentally, they are important for defining the origin of the ITRF and 2) for analyzing mass transports over the Earth (Kang et al., 2009).

To be able to describe the motion of the geocentre a terrestrial reference frame needs to be defined with the centre of figure (CF) as the origin. The centre of mass (CM) of the whole Earth system (solid Earth, atmosphere, oceans, hydrosphere, cyrosphere) is defined as the geocentre of the Earth. Thus the gravitational harmonics of degree-1 in equation 8.3 are zero for *l* = 1 where, $k_1' = -1$. The contribution of the non-zero $\Delta\widehat{C}_{lm}$ and $\Delta\hat{S}_{lm}$ terms for m = 0,1 in the external gravity field coefficients from equation 8.3 is seen as a displacement (X_g,Y_g,Z_g) in the position of the satellite tracking stations (Moore and Wang, 2003) where Trupin et al. (1992) give:

$$X_g = R\sqrt{3}\left(1-\frac{h_1+2l_1}{3}\right)\frac{\rho_\omega}{\rho_{av}}\Delta\hat{C}_{11}$$
$$Y_g = R\sqrt{3}\left(1-\frac{h_1+2l_1}{3}\right)\frac{\rho_\omega}{\rho_{av}}\Delta\hat{S}_{11} \qquad \textbf{(8.5)}$$
$$Z_g = R\sqrt{3}\left(1-\frac{h_1+2l_1}{3}\right)\frac{\rho_\omega}{\rho_{av}}\Delta\hat{C}_{10}$$

8.3 Comparison of Geocentre Motion from GPS, SLR and Geophysical Models

There are two established definitions of geocentre variation (Dong et al., 2003). One is the offset of vector CF relative to CM and secondly the opposite of this. The amplitudes of these two variants will obviously be the same but their phases will differ by 180^o. This offset can be observed by space geodetic techniques by measuring the tracking network relative to the centre of the tracked orbits or it can be inferred by observing the deformation of the solid Earth due to surface mass loads (Kang et al., 2009). Space geodetic techniques have shown this movement to be of the order of a few millimetres over timescales from diurnal to semi-diurnal (Eanes et al., 1997) to seasonal (Chen et al., 1999).

Geocentre motion has been computed from SLR, GPS and geophysical models. The method for performing these calculations is described below and a comparison of the results of these computations from the different sources is compared.

8.3.1 Analysis Procedure

To account for the tectonic motion of the GPS sites a secular model has been removed from the GPS site displacements. this correction has also been applied to the SLR data. For SLR and GPS, site displacements and gravity field variation (degree-1 only for GPS) map onto the same set of surface load coefficients in a “unified approach” (Lavallee et al., 2006).

For GPS we use a set of modified spherical harmonic basis functions which incorporate the land-ocean distribution, mass conservation and self equilibration of the oceans (Clarke et al., 2007). The modified basis functions give a more stable, precise and accurate fit in tests using synthetic data and are less subject to aliasing errors.

The load coefficients for GPS have been estimated from the weekly GPS Solution Independent Exchange (SINEX) files (re-analysed) from the International GNSS servies (IGS) analysis centre at the Scripps Institute of Oceanography (SIO) [ftp://garner.ucsd.edu/pub/combinations]. The files were downloaded in 2007 further details on the data set can be found in Nikolaidis, 2002. This processing was carried out and provided by Dr David Lavellee using the TANYA software that was developed by Dr Lavellee.

The load model is a combination of hydrology, ocean bottom pressure and atmospheric pressure data. The hydrology data has been taken from the Land Dynamics model (LaD) (Milly and Shmakin, 2002). The ocean bottom pressure model is taken from the ECCO model and is based on an earlier MIT global ocean circulation model (Marotzke et al., 1999), details of which are given by Chen and Wilson (2003b). The atmospheric pressure model data is from the NCEP reanalysis (Kalnay et al., 1996). The geophysical data from these models have been expanded into load spherical harmonics by numerical integration using equation 8.2.

8.3.2 SLR orbit results

FAUST has been used to calculate the orbits of LAGEOS I and LAGEOS II over the period 1996 – 2008. In this analysis the orbits have been calculated using 7 day arcs and using the processing conventions already described in this thesis and also in Moore et al. (2005).

The parameters estimated in the orbit determination process were:

- State vector – initial position and velocity
- Two along track accelerations
- Solar radiation pressure (See Figure 8.2)
- Daily ERPs
- Gravity field harmonics up to degree and order 4
- Station coordinates
- UT1-UTC fixed at the IERS C04 value

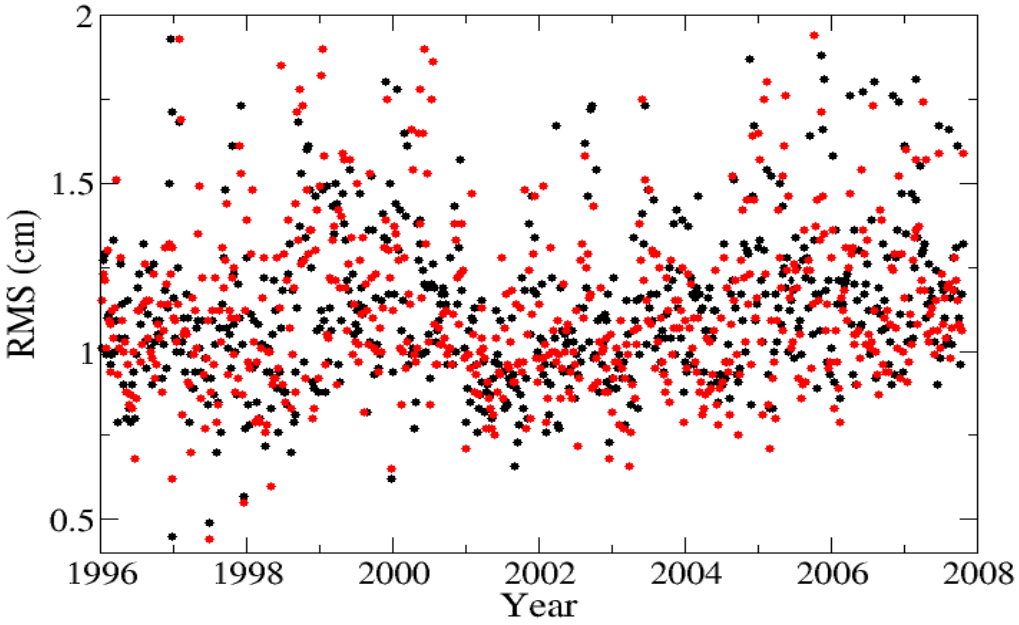

Figure 8.1 RMS fit of orbits from *FAUST*: LAGEOS I (black) and LAGEOS II (red)

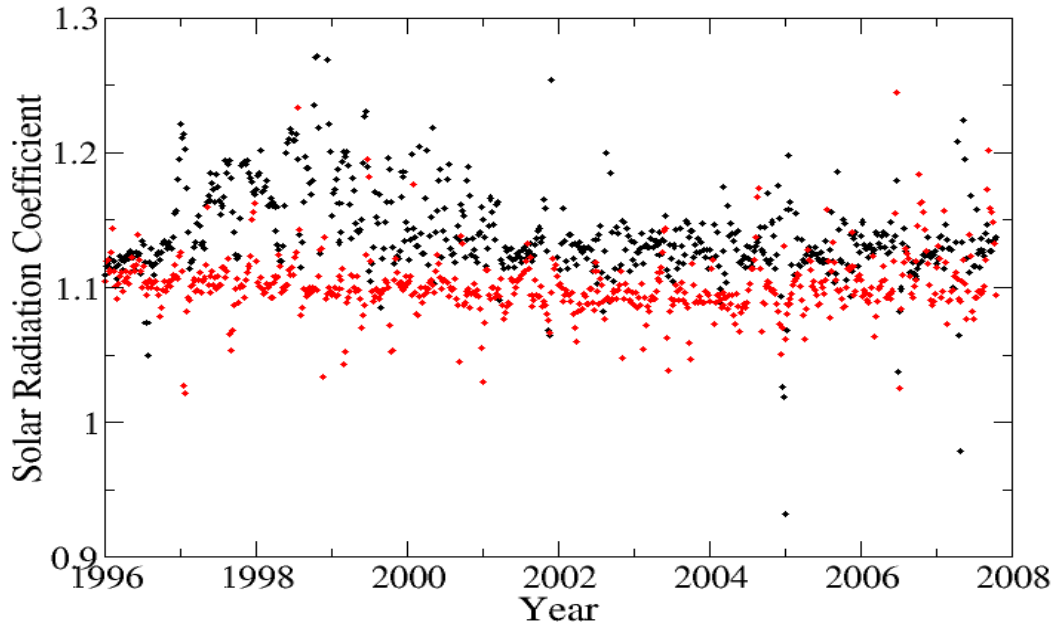

Figure 8.2 Solar radiation pressure from *FAUST* for LAGEOS I (black) and LAGEOS II (red)

Station dependant weights have been chosen according to the quality of the data from that station between 10 cm and 30 cm. These weights have been chosen by analysing data from the ILRS (ILRS, 2007). The tracking residuals for all the orbits combined are approximately equal to 1.1 cm (Figure 8.1).

8.3.3 Geocentre motion

The plots shown in Figure 8.3, Figure 8.4 and Figure 8.5 show the geocentre X, Y, Z coordinates respectively as derived from *FAUST* compared to the estimates of the same parameters from the ILRS combination SLR contribution to ITRF2005.

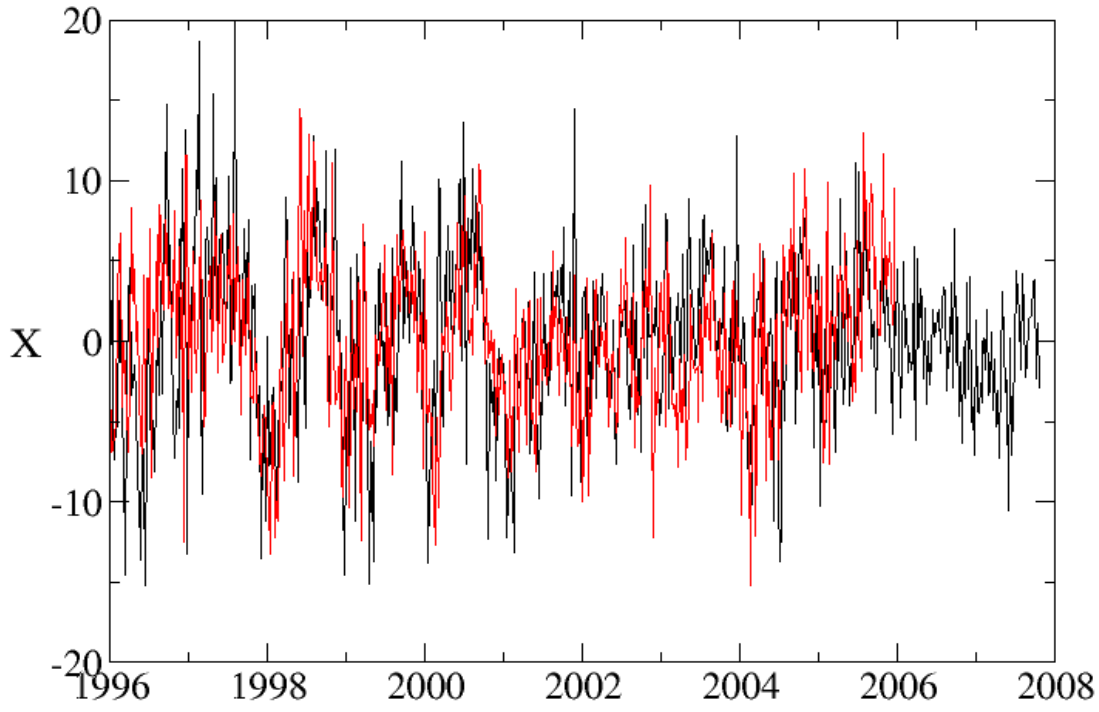

Figure 8.3 X component of geocentre motion from LAGEOS observations computed using *FAUST* (black) and ILRS combination (red) in mm

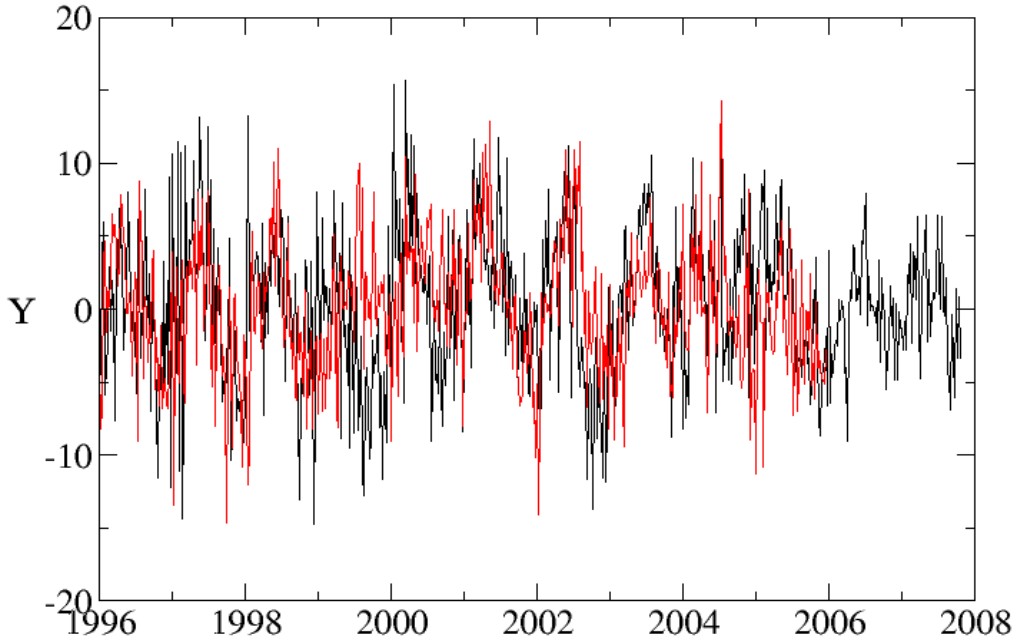

Figure 8.4 Y component of geocentre motion from LAGEOS observations computed using *FAUST* (black) and ILRS combination (red) in mm

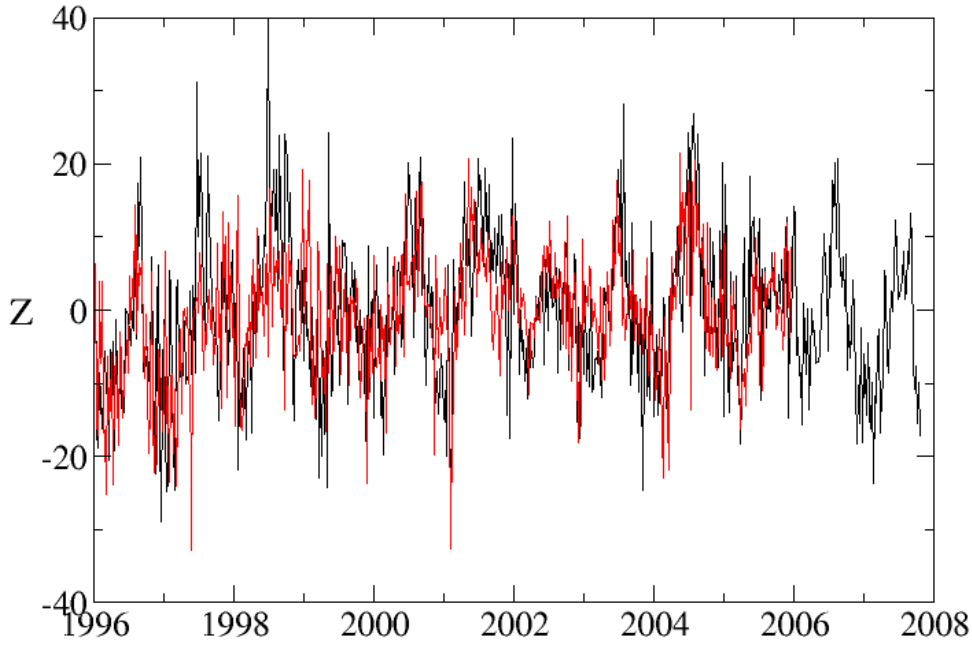

Figure 8.5 Z component of geocentre motion from LAGEOS observations computed using *FAUST* (black) and ILRS combination (red) in mm

These comparisons show good agreement between the estimates of the geocentre derived from LAGEOS I and II with *FAUST* and with the combined solution from the ILRS. This gives a good indication that the results from *FAUST* are reasonable.

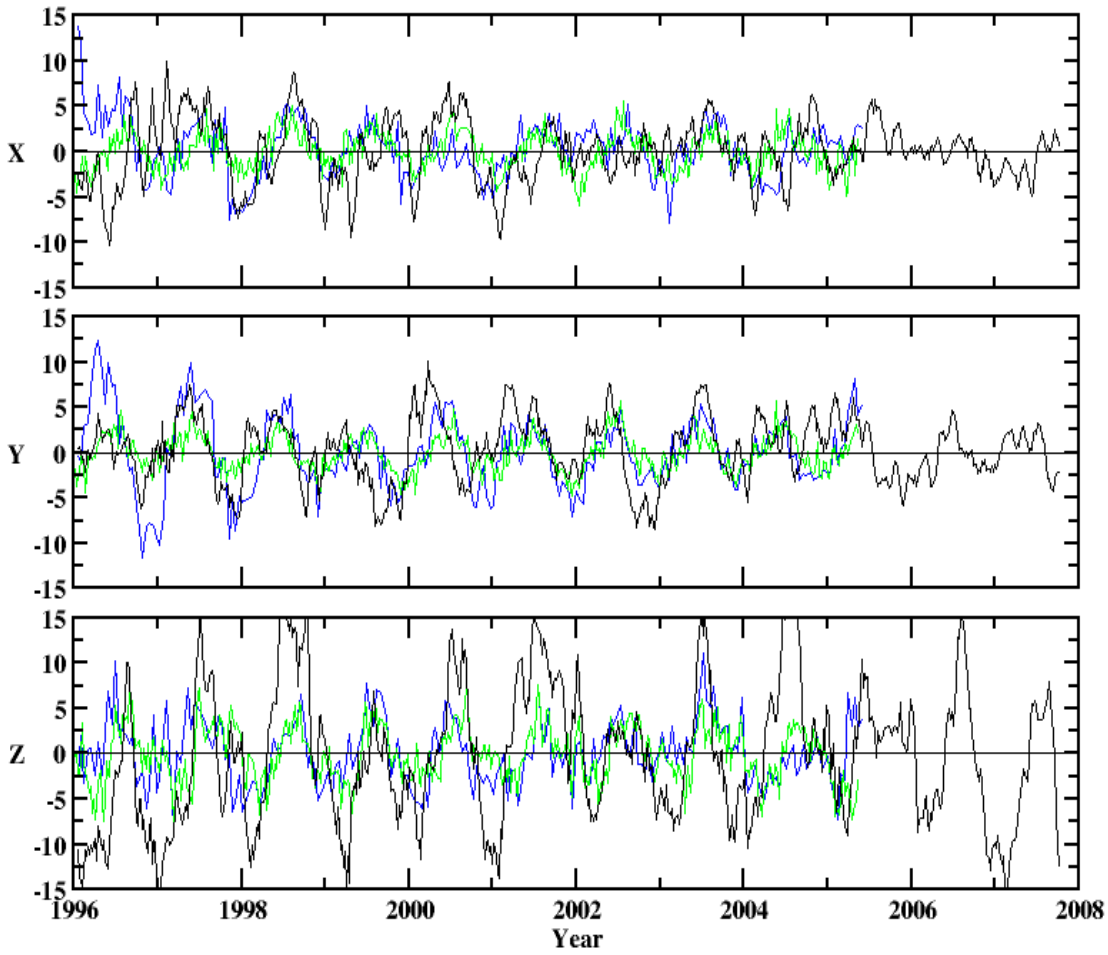

Figure 8.6 Estimated degree-1 load coefficients here expressed as geocentre motion (CF relative to CM) time series (mm) for SLR (black), GPS (blue) and the loading model (green)

Figure 8.6 shows a comparison of geocentre motion in mm for solutions estimated from SLR, GPS and geophysical models for the period 1996 to mid 2005 with the SLR estimates available until 2008.

Table 8.1 shows the estimated amplitude and phase for the dominant annual and semi annual terms of the geocentre motion estimated through a least squares process.

	Annual				Semi-Annual			
	Amp	**+/-**	**Phase**	**+/-**	**Amp**	**+/-**	**Phase**	**+/-**
Loading Model								
X	**2.3**		**209**		**0.1**		**17**	
Y	**2.2**		**158**		**0.3**		**3**	
Z	**3.2**		**241**		**1.4**		**38**	
SLR								
X	**2.1**	**0.3**	**233**	**4**	**0.9**	**0.3**	**152**	**20**
Y	**3.0**	**0.3**	**123**	**5**	**0.4**	**0.3**	**73**	**40**
Z	**3.2**	**0.7**	**205**	**5**	**2.4**	**0.7**	**4**	**17**
GPS								
X	**2.1**	**0.3**	**211**	**9**	**0.3**	**0.3**	**78**	**56**
Y	**3.9**	**0.3**	**148**	**4**	**0.5**	**0.3**	**28**	**31**
Z	**2.7**	**0.3**	**201**	**7**	**0.7**	**0.3**	**356**	**25**

Table 8.1 Estimated geocentre motion annual and semi-annual components (mm)

These comparisons show that there is good agreement in general terms between the X and Y components from all three sources. Agreement is greater on the annual term both in phase and in amplitude. The Z term also shows good agreement on the annual term in phase and in amplitude but the semi annual term demonstrates itself as a much larger term from the SLR data and this can easily be identified from
Figure 8.6. This may be due to possible aliasing from other geophysical signals, geodynamics or sampling.

The differences in these estimates are most likely due to modelling errors in the orbits as well as the amount of data used in the estimates. For example the sparseness of the SLR station network Figure 5.4 compared to GPS and the fact that the quality of the

data from these stations varies over the globe will contribute to errors in the geocentre estimates.

8.4 Conclusion

Realisation of the geocentre is an important part of the monitoring of mass redistribution within the Earth system and it is important for defining the origin of the International Terrestrial Reference Frame (ITRF). It is possible to measure geocentre motion from a variety of geodetic techniques.

Geocentre estimates from SLR, GPS and geophysical models have been estimated and compared. The estimates from LAGEOS I and LAGEOS II data calculated using *FAUST* have been shown to be comparable with the combined solution from the ILRS. The comparisons of data from SLR, GPS and the models have shown that there is good agreement between the different sources on the annual term for both phase and amplitude, especially for the X and Y terms. Agreement declines for the semiannual term and for the Z term from SLR in particular.

Chapter 9

9 Conclusion

9.1 Discussion

As has been stated in this thesis, the Earth can be thought of as a closed system in terms of angular momentum, and therefore mass components (i.e. atmosphere, oceans, continental water storage (hydrology), core and mantle) in one reservoir of the Earth system are exchanged with others (Salstein, 1993). Mass redistribution within the Earth system is caused by geophysical processes. This movement of geophysical fluid (mass) causes variations in the Earth's rotation, gravity field and geocentre. As geodetic techniques have improved in quantity and quality over time, especially over the last 50 years or so, the manifestations of these mass distributions have been observed to unprecedented accuracy over an array of timescales.

Variations in Earth rotation are affected by this exchange of mass in two ways. Firstly, the movement of geophysical fluids causes torques on the surface of the Earth and second the change of mass across the Earth causes changes in the Earth's inertia tensor (as described in Chapter 3). From this knowledge it can be said that the Earth obeys the law of "conservation of angular momentum" (Chao et al., 2000).

The gravity field of the Earth is very closely linked to the same geophysical process within the Earth system as it too is affected by the redistribution of mass around the globe. These processes cause changes in the Earth's gravity field through Newton's gravitational law. This law states that a body creates its own gravity field according to the distribution of mass within that particular body.

Finally, changes in the Earth's geocentre obey the law of "conservation of linear momentum". This law states that the centre of mass of the solid Earth plus the geophysical fluids such as the atmosphere and oceans etc obeys the law of celestial mechanics in its translational motion around the solar system.

The main theme of this thesis relates to the redistribution of mass within the Earth system and how this relates to precise orbit determination and the parameters that can be estimated as part of the orbit determination process. As seen in Chapter 4, there are several reservoirs of mass whose redistribution contributes to the changes in the rotation of the Earth. Most of these reservoirs' movements are modelled and data is readily available from several organisations across the world. Some of this data is shown in Chapter 4. This data, when converted to excitation functions, shows the differences between the mass and motion effects of these mass redistributions on the Earth's variable rotation. These excitation functions show that the Z term that relates to the LOD is dominated by the atmospheric motion term and that all other terms have a relatively small effect on changes in LOD. The X and Y terms are much more similar in size when comparing the mass and motion terms as well as the contribution of atmosphere and oceans to the excitation are of similar size with the hydrological angular momentum contributing slightly less to changes in the poles. It has been shown that models developed by different organisations show good agreement on all of the mass terms and on the Z motion term. However agreement is sketchy between the X and Y motion terms giving evidence that these models are the least well defined.

The Newcastle University's POD software *FAUST* (Moore et al., 1999; Boomkamp, 1998) has been modified to allow the estimation of daily ERPs (XP, YP, LOD). *FAUST* was then utilised to compute the orbits of LAGEOS I and LAGEOS II from 1996 – 2007 in several different scenarios, firstly solving for ERPs and the coordinates of all stations used within the orbit determination process, secondly solving for the same with the addition of low degree gravity field variations (up to degree and order 3), thirdly solving for gravity field variations up to degree and order 4. The results of estimated parameters from these different scenarios have been compared and shown to be reasonable when compared with similar parameters from other sources such as a comparison with orbit determination software used at the NERC geodesy facility and also by comparing with data available on the web through the ILRS.

Chapter 6 describes how ERPs can be converted into excitation functions of the Earth's variable rotation. As described previously the Earth's rotation is affected in two ways (torques and mass changes) and from different geophysical reservoirs. Because of this the excitation functions computed from ERPs contain the contributions to excitation

from all of these sources. To compare the models and the *FAUST*-derived excitation functions (from ERPs) the models were combined and the long term trends and means removed from the data. Very good agreement was found between the LOD derived excitation function and the combined Z term χ_3 from the models (when averaged over 15 days), this is most likely due to the dominance of the atmosphere in this particular term and gives evidence that the Z motion term is relatively well defined in the models and from SLR. The agreement is less on χ_1, χ_2 or the X and Y terms respectively. This may be because the modelled contribution of the motion terms is less well defined for χ_1 and χ_2, as shown in Chapter 4. The agreement, evidenced by the much lower correlation values (0.068, 0.155, 0.671 compared to 0.683, 0.694, 0.885 for χ_1, χ_2 and χ_3 respectively) also degrades greatly when using daily values of χ_1, χ_2 and χ_3.

In addition to this the coherence functions of each of the excitation functions were calculated to see how well the excitations from the models and from ERPs compare at different frequencies. The results of this analysis has shown that both χ_2 and χ_3 have very good agreement at the dominant annual and semi annual terms but that this agreement drops as the frequency increases. χ_1 does not show such good agreement and the same dominant periods and once again the agreement drops away as frequency increases. The excitation functions calculated from ERPs have also been split into the effects caused by mass redistributions and those caused by motion (torques). This has been performed by using the modelled motion and mass terms to remove each respective element to leave the excitation residuals which should correspond to the opposite effect, depending on the accuracy of the models and of the total excitation estimated from the ERPs. As would be expected it was found that the motion term for χ_3 showed an excellent match between model and ERPs due to the domination of this term. The other two motion terms do not match as well although there are some areas in the χ_1 term that match well. The fact is that the relatively poor agreement in these terms is what would be expected following the comparison of models from different data centres compared previously. Also as we may expect the mass term for χ_3 has the least agreement of the three terms, with the dominant annual signal on χ_2 showing good agreement.

Coherence analysis of the data shows that there is very good agreement between the dominant annual and semi annual terms in the data for χ_2 on the mass term (less so on the motion term as this term seems to be harder to define) and χ_3 on both the mass and the motion terms; this is perhaps not so expected due to the dominance of the motion term .

The excitation functions can be converted to corrections to low degree spherical harmonics (J2, C21, S21) of the Earth's gravity field by using the relationship given by Chen and Wilson (2003b). Matching these spherical harmonics calculated from different sources, averaged over 15 days, has shown that in general J2 has the best agreement between the different sources and S21 has agreement particularly with the dominant annual signal, C21 is in least agreement from the different sources which suggest it is perhaps poorly defined from one or more of the sources. This general pattern is followed when comparing the J2, C21 and S21 estimated from ERPs from LAGEOS, with LAGEOS directly-estimated J2, C21 and S21. When comparing the daily estimates the agreement reduces drastically and it is questionable whether it adds any more value to the data.

Chapter 6 has shown that it is possible to use ERPs to calculate J2, C21 and S21 and that the agreement is relatively good between all of the harmonics, although it is particularly good for J2 and at its lowest on C21.

Space geodesy is limited in its ability to provide mass changes at short time periods (less than 15 days) even at low spatial resolutions, due to the satellites' low sensitivity to the Earth's gravity field and to the high correlation between harmonics (especially degrees 2 and 4) (Hancock and Moore, 2007). However space geodesy does provide high resolution (here daily but in some cases, such as with GPS, even more frequent) ERP data.

The low sensitivity of orbits to the gravity field variability or the high correlation between the harmonics limits the time period over which mass change, even at low spatial resolutions, can be recovered from space geodesy. However, the relatively high temporal resolution of ERPs does raise the possibility of simultaneously recovering and

using higher temporal frequencies for the degree-2 harmonics from the ERP data within an orbital determination procedure.

This theory has been tested in Chapter 7 by using the angular momentum models described in Chapter 5 to compute and remove the excitation caused by motion and surface torques from the ERPs. A strategy was carried out to use this in the orbit determination process by converting the ERPs to excitation functions and then using the NCEP reanalysis atmospheric angular momentum model and the ECCO ocean circulation model to remove the motion excitation from the ERP excitation to leave the mass excitation. These mass excitations from LOD were then converted to J2 and the correction applied to the average value of J2 beginning with correction over one 15 day arc. This process was repeated for several different scenarios which were:

- J2 only one correction over a 15 day arc
- J2 only one correction a day
- J2, C21 and S21 one correction over a 15 day arc
- J2, C21 and S21 one correction per day

The results of these experiments have shown that using one correction over a 15 day arc gives an improvement to the orbits over the whole period (1996 – 2007), with a slightly better improvement achieved when using J2 only. The degradation of the orbits when using all three corrections is likely due to the fact that they do not often all have good agreement with the models or SLR derived gravity at the same epochs showing that it is probable that at least one of the estimates at that epoch may be wrong and corrupt the solution at that particular epoch.

When utilising the high frequency (daily) ERPs to compute high frequency low degree harmonics the fit of the orbit is much poorer. From the analysis in Chapter 6 of this thesis this is likely to be due to the noisiness of the daily ERP-derived gravity field parameters, with this noisy data likely to be caused by either modelling errors or/and errors in the determination of the ERPs within the LAGEOS orbit determination process. It has already been shown that the motion terms (from the excitation functions) used to calculate S21 and C21 are poorly defined and that the excitation function used to derive

J2 is dominated by the motion signal meaning that any relatively small errors in the motion part of the excitation function will display as relatively large errors in the residual mass excitation function (left over).

This analysis has shown that it is possible to derive the gravity field harmonics J2, S21 and C21 from ERPs and angular momentum models and that, averaged over a 15 day period, they compare relatively well with the same parameters estimated directly from the least squares orbit determination process. However, it has also been shown that, using the methods in this thesis, using higher frequency gravity harmonics has a negative effect on the orbit determination procedure and that these daily estimate parameters do not compare well with other sources of the same data.

Data from *FAUST* estimated orbits of SLR data to LAGEOS I and LAGEOS II has also been used to estimate the geocentre motion of the Earth. It has been shown that the geocentre estimate from SLR, GPS and geophysical models are comparable although the agreement varies between the various methods and also for the various parameters. These variations could be due to the differences in the various data networks and errors in the specific measurement methods.

9.2 Future Work and Recommendations

The main aims of this thesis were to investigate the usefulness of using Earth Rotation Parameters within the orbit determination process to establish higher frequency estimates of the low degree spherical harmonics of the Earth's gravity field. Also investigated was the ability of SLR to determine mass redistribution through estimates of the Earth's geocentre motion. These aims have generally speaking been met but there are several areas that could be looked at more closely to extend and improve the research in this thesis.

As new models of atmospheric and oceanic data become available, analysis of this data could be performed to understand if these new models offer any advantage over the old models that might enhance the novel method investigated in this thesis. In addition to this it might be worth investigating methods of removing the secular term in the data. A more intensive investigation of the geophysical models used in the process could be

undertaken to evaluate which models give the best performance. For example if core angular momentum data is available, this could be used to remove the secular part of the data.

In this thesis two scenarios were assessed when investigating the usefulness of using angular momentum models to calculate gravity field estimates for the low degree harmonics from ERPs in a unified process. Firstly, J2 alone was evaluated, and then corrections to J2, C21 and S21 were calculated and evaluated. It would be useful to investigate the effects of each of the corrections on the orbits individually. This may aid in understanding the reasons why some arcs are affected positively by the corrections and others not so, or at least give evidence for which of these parameters is most likely causing the errors.

Also, as mentioned in this thesis, one of the problems in solving for gravity field harmonics by integration is the high correlations between some of the harmonic parameters. This is especially true for the degree-2 and degree-4 harmonics. By solving for degree-2 harmonics in the method described in this thesis, the advantage of this method in removing these correlations can be investigated.

The usefulness of solving for one correction every 15 days and solving for a daily correction to the degree-2 spherical harmonics of the gravity field has shown that daily corrections mostly make the solution worse and corrections averaged over the 15 day period improve the orbits. An investigation of where the breakeven point is would be useful as it would provide information regarding the frequency of gravity estimates available from this method that would provide estimates of the gravity field that may be close to the truth at higher frequencies.

The lengths of the arcs could also be varied to investigate whether changes to the arc length will have a positive effect on the determination of the orbits. Along the same lines the method of rejecting observations and methods for weighting the SLR data could be investigated to determine a more robust method for selecting the data to be used in the determination of the global parameters.

This method could also be tested within the GPS or GNSS method for determining gravity field harmonics and ERPs. GPS allows even higher frequency ERP determination and may be more accurate in defining the ERPs than SLR.

It has been shown that geocentre estimates derived using the changes in the station coordinates from SLR stations around the globe from *FAUST* are comparable with geocentre variations calculated from GPS and from geophysical models. However these comparisons have shown some discrepancies, especially in the Z term. It is well known that some SLR stations have better quality data than others. Therefore a method for improving the geocentre solution from SLR is to improve the method of weighting the measurements.

References

Baldwin, M. P., Gray, L. J., Dunkerton, T. J., Hamilton, K., Haynes, P. H., Randel, W. J., Holton, J. R., Alexander, M. J., Hirota, I., Horinouchi, T., Jones, D. B. A., Kinnersley, J. S., Marquardt, C., Sato, K. and Takahashi, M. (2001) 'The quasi-biennial oscillation', *Reviews of Geophysics,* 39, (2), pp. 179-229.

Barnes, R. T. H., Hide, A., White, A. and Wilson, C. A. (1983) 'Atmospheric Angular Momentum Fluctuations, Length of Day Changes and Polar Motion', *Proc. R. Soc. Lon,* 387, pp. 31-73.

Barnes, W. L., Xiong, X. and Salomonson, V. V. (2003) 'Status of Terra MODIS and Aqua MODIS', *Advances in Space Research,* 32, (11), pp. 2099-2106.

Barnett, T. P., Latif, M., Kirk, E. and Roeckner, E. (1991) 'On ENSO Physics', *J. Climate.,* 4, (487-513).

Bizouard, C. and Gambis, D. (2009) *The combined Earth Orientation Solution C04.* Paris: IERS Earth Orientation Centre

Blakely, R. (1995) *Potential Theory in Gravity and Magnetic Applications.* Cambridge U. Press, Cambridge.

Bomford, G. (1980) *Geodesy.* Clarendon Press.

Boomkamp, H. J. (1998) *Combination of altimetry data from different satellite missions.* thesis. Aston University.

Brzezinski, A. (2002) 'Oceanic Excitation of Polar Motion and Nutation: An Overview', *IERS Technical Note 30*.

Brzezinski, A., Bizouard, C. and Petrov, S. D. (2002) 'Influence of the atmosphere on earth rotation: What new can be learned from the recent atmospheric angular momentum estimates?', *Surveys in Geophysics,* 23, (1), pp. 33-69.

Brzezinski, A. and Nastula, J. (2002) 'Oceanic excitation of the Chandler wobble', *Advances in Space Research,* 30, (2), pp. 195-200.

Carter, W. E., Robertson, D. S. and Mackay, J. R. (1985) 'Geodetic radio interferometric surveying: applications and results', *Journal of Geophysical Research,* 90, (B6), pp. 4577-4587.

Cazenave, A., Mercier, F., Bouille, F. and Lemoine, J. M. (1999) 'Global-scale interactions between the solid Earth and its fluid envelopes at the seasonal time scale', *Earth and Planetary Science Letters,* 171, (4), pp. 549-559.

Chao, B. F. (1984) 'Interannual length-of-day variation with relation to the Southern Oscillation/ El Nino', *Geophysical Research Letters,* 11, (5), pp. 541-544.

Chao, B. F. (1989) 'Length-of-day variations caused by El Nino Southern Oscillation and Quasi-Biennial Oscillation', *Science,* 243, (4893), pp. 923-925.

Chao, B. F. and Au, A. Y. (1991) 'Atmospheric excitation of the Earth's annual wobble: 1980-1988', *Journal of Geophysical Research,* 96, (B4), pp. 6577-6582.

Chao, B. F. and Gross, R. S. (1987) 'Changes in the Earth's rotation and low-degree gravitational field induced by earthquakes', *Geophysical Journal of the Royal Astronomical Society,* 91, (3), pp. 569-596.

Chao, B. F. and O'Connor, W. P. (1988) 'Global surface-water-induced seasonal variations in the Earth's rotation and gravitational field', *Geophysical Journal,* 94, (2), pp. 263-270.

Chao, B. F., O'Connor, W. P., Chang, A. T. C., Hall, D. K. and Foster, J. L. (1987) 'Snow load effect on the earth's rotation and gravitational field, 1979-1985', *Journal of Geophysical Research,* 92, (B9), pp. 9415-9422.

Chao, B. F. and Ray, R. D. (1997) 'Oceanic tidal angular momentum and Earth's rotation variations', *Progress In Oceanography,* 40, (1-4), pp. 399-421.

Chao, S. B., Dehant, V., Gross, R. S., Ray, R. D., Salstein, D. A., Watkins, M. M. and Wilson, C. R. (2000) 'Space Geodesy Monitors Mass Transports in Global Geophysical Fluids', *Eos, Tranactions, American Geophysical Union,* 81, (22), pp. pp 247, 249-250.

Chen, J. L. and Wilson, C. R. (2003a) 'Low degree gravitational changes from earth rotation and geophysical models', *Geophysical Research Letters,* 30, (24), pp. SDE 6-1 - SDE 6-4.

Chen, J. L. and Wilson, C. R. (2003b) 'Low degree gravitational changes from earth rotation and geophysical models', *Geophys. Res. Lett.,* 30, (24), pp. 2257.

Chen, J. L. and Wilson, C. R. (2005) 'Hydrological excitations of polar motion, 1993-2002', *Geophysical Journal International,* 160, (3), pp. 833-839.

Chen, J. L., Wilson, C. R., Eanes, R. J. and Nerem, R. S. (1999) 'Geophysical interpretation of observed geocenter variations', *Journal of Geophysical Research B: Solid Earth,* 104, (B2), pp. 2683-2690.

Chen, J. L., Wilson, C. R., Eanes, R. J. and Tapley, B. D. (2000) 'A new assessment of long-wavelength gravitational variations', *Journal of Geophysical Research B: Solid Earth,* 105, (B7), pp. 16271-16277.

Cheng, M. and Tapley, B. D. (1999) 'Seasonal variations in low degree zonal harmonics of the Earth's gravity field from satellite laser ranging observations', *Journal of Geophysical Research B: Solid Earth,* 104, (B2), pp. 2667-2681.

Cheng, M. K., Shum, C. K. and Tapley, B. D. (1997) 'Determination of long-term changes in the Earth's gravity field from satellite laser ranging observations', *Journal of Geophysical Research B: Solid Earth,* 102, (B10), pp. 22377-22390.

Clarke, P. J., Lavallee, D. A., Blewitt, G. and van Dam, T. (2007) 'Basis functions for the consistent and accurate representation of surface mass loading', *Geophysical Journal International,* 171, (1), pp. 1-10.

Cox, C. M. and Chao, B. F. (2002) 'Detection of a large-scale mass redistribution in the terrestrial system since 1998', *Science,* 297, (5582), pp. 831-833.

Dickey, J. (1992) 'Atmospheric excitation of the Earth's rotation: Progress and prospects via. space geodesy', *Space Geodesy and Geodynamics, American Geophysical Union Monograph*.

Dickey, J. (1993) 'Atmospheric Excitation of the Earth's Rotation: Progress and Propects Via Space Geodesy', *Contributions of Space Geodesy to Geodynamics: Earth Dynamics,* Geodynamics 24, pp. 55-70.

Dickey, J. O. and Eubanks, T. M. (1985) 'Earth Rotation and Polar Motion: Measurements and Implications', *IEEE Transactions on Geoscience and Remote Sensing,* GE-23, (4), pp. 373-384.

Dong, D., Gross, R. S. and Dickey, J. O. (1996) 'Seasonal variations of the Earth's gravitational field: an analysis of atmospheric pressure, ocean tidal, and surface water excitation', *Geophysical Research Letters,* 23, (7), pp. 725-728.

Dong, D., Yunck, T. and Heflin, M. (2003) 'Origin of the International Terrestrial Reference Frame', *Journal of Geophysical Research B: Solid Earth,* 108, (4), pp. ETG 8-1 - 8-10.

Eanes, R. J. (1994) 'Diurnal and Semidiurnal Tides from TOPEX/POSEIDON Altimetry', *Eos, Tranactions, American Geophysical Union*, pp. 75(16):108.

Eanes, R. J., Kar, S., Bettadapur, S. and Watkins, M. (1997) 'Low-frequency geocenter motion determined from SLR tracking', *Eos, Tranactions, American Geophysical Union,* 78(46).

Eubanks, T. M. (1993) 'Variations in the Orientation of the Earth', *Contributions of Space Geodesy to Geodynamics: Earth Dynamics,* Geodynamics 24.

Eubanks, T. M., Steppe, J. A., Dickey, J. and Callahan, P. S. (1985) 'A Spectral Analysis of the Earth's Angular Momentum Budget', *J. Geophys. Res,* 90, pp. 6859-6872.

Eubanks, T. M., Steppe, J. A. and Dickey, J. O. (1986) 'The El Nino, The Southern Oscillation and the Earth Rotation', *Earth Rotation: Solved and Unsolved Problems,* pp. 163-168.

Eubanks, T. M., Steppe, J. A., Dickey, J. O., Rosen, R. D. and Salstein, D. A. (1988) 'Causes of rapid motions of the Earth's pole', *Nature,* 334, (6178), pp. 115-119.

Farrell, W. E. (1972) 'Deformation of the Earth by surface loads', *Rev. Geophys.,* 10, (3), pp. 761-797.

Feissel-Vernier, M., Bail, K., Berio, P., Coulot, D., Ramillien, G. and Valette, J. (2006) 'Geocentre motion measured with DORIS and SLR, and predicted by geophysical models', *Journal of Geodesy,* 80, (8), pp. 637-648.

Gasperini, P., Sabadini, R. and Yuen, D. A. (1986) 'Excitation of the Earth's Rotational Axis by Recent Glacial Discharges', *Geophys. Res. Letts.,* 13, pp. 533-536.

Gill, A. (1982) *Atmosphere-Ocean Dynamics.* Elsevier.

Gipson, J. M. (1996) 'Very long baseline interferometry determination of neglected tidal terms in high-frequency Earth orientation variation', *Journal of Geophysical Research B: Solid Earth,* 101, (12), pp. 28051-28064.

Gross, R. S. (1986) 'The influence of earthquakes on the Chandler wobble during 1977-1983', *Geophysical Journal - Royal Astronomical Society,* 85, (1), pp. 161-177.

Gross, R. S. (1996) 'Combinations of Earth orientation measurements: SPACE94, COMB94, and POLE94', *Journal of Geophysical Research B: Solid Earth,* 101, (4), pp. 8729-8740.

Gross, R. S. (2000) 'The excitation of the Chandler wobble', *Geophysical Research Letters,* 27, (15), pp. 2329-2332.

Gross, R. S., Blewitt, G., Clarke, P. J. and Lavallee, D. (2004) 'Degree-2 harmonics of the Earth's mass load estimated from GPS and Earth rotation data', *Geophysical Research Letters,* 31, (7), pp. L07601 1-4.

Gross, R. S. and Chao, B. F. (1990) 'The global geodynamic effect of the MacQuarie Ridge Earthquake', *Geophys. Res. Lett.,* 17, (7), pp. 1009-1012.

Gross, R. S., Chao, B. F. and Desai, S. D. (1997) 'Effect of long-period ocean tides on the Earth's polar motion', *Progress In Oceanography,* 40, (1-4), pp. 385-397.

Gross, R. S., Fukumori, I. and Menemenlis, D. (2005) 'Atmospheric and oceanic excitation of decadal-scale Earth orientation variations', *Journal of Geophysical Research B: Solid Earth,* 110, (9), pp. 1-15.

Gross, R. S. and Lindqwister, U. J. (1992) 'Atmospheric excitation of polar motion during the GIG '91 measurement campaign', *Geophysical Research Letters,* 19, (9), pp. 849-852.

Hancock, C. M. and Moore, P. (2007) 'On the usefulness of atmospheric and oceanic angular momentum in recovering polar motion and gravity field variations in a unified process', *Advances in Space Research,* 39, (10), pp. 1648-1655.

Heiskanen, W. A. and Moritz, H. (1967) *Physical geodesy* W. H. Freeman.

Herring, T. A., Dong, D. and King, R. W. (1991) 'Sub-milliarcsecond determination of pole position using global positioning system data', *Geophysical Research Letters*, 18, (10), pp. 1893-1896.

Hide, R., Birch, N. T., Morrison, L. V., Shea, D. J. and White, A. A. (1980) 'Atmospheric angular momentum fluctuations and changes in the length of the day', *Nature*, 286, (5769), pp. 114-117.

Hide, R. and Dickey, J. O. (1991) 'Earth's variable rotation', *Science*, 253, (5020), pp. 629-637.

ILRS (2007) *ILRS Global Performance Report Card 2007*. Available at: http://ilrs.gsfc.nasa.gov/stations/site_info/global_report_cards/perf_2007q3_wLLR.html (Accessed: Oct 2011).

ILRS (2011) *ILRS Station Map*. Available at: http://ilrs.gsfc.nasa.gov/stations/index.html (Accessed: Oct 2011).

ILRS (2012) *Description of the MERIT II data format*. Available at: http://ilrs.gsfc.nasa.gov/products_formats_procedures/fullrate/index.html (Accessed: Jan 2012).

Jault, D. and Le Mouel, J. L. (1991) 'Exchange of angular momentum between the core and the mantle', *Journal of Geomagnetism & Geoelectricity*, 43, (2), pp. 111-129.

Jin, S., Chambers, D. P. and Tapley, B. D. (2010) 'Hydrological and oceanic effects on polar motion from GRACE and models', *Journal of Geophysical Research B: Solid Earth*, 115, (2).

Johnson, T. J. (1999) 'Oceanic angular momentum variability estimated from the Parallel Ocean Climate Model, 1988-1998', *Journal of Geophysical Research B: Solid Earth*, 104, (B11), pp. 25183-25195.

Kalnay, E., Kanamitsu, M., Kistler, R., Collins, W., Deaven, D., Gandin, L., Iredell, M., Saha, S., White, G., Woollen, J., Zhu, Y., Chelliah, M., Ebisuzaki, W., Higgins, W., Janowiak, J., Mo, K. C., Ropelewski, C., Wang, J., Leetmaa, A., Reynolds, R., Jenne, R. and Joseph, D. (1996) 'The NCEP/NCAR 40-year reanalysis project', *Bulletin of the American Meteorological Society*, 77, (3), pp. 437-471.

Kang, Z., Tapley, B., Chen, J., Ries, J. and Bettadpur, S. (2009) 'Geocenter variations derived from GPS tracking of the GRACE satellites', *Journal of Geodesy*, 83, (10), pp. 895-901.

Kaula, W. M. (1966) *Theory of satellite geodesy: Applications of satellites to geodesy*. Blaisdell Pub Co, Waltham, Mass.

Kay, S. M. (1988) *Modern Spectral Estimation*. Prentice-Hall, Englewood Cliffs, NJ.

Khrgian, A. K. (1985) 'The Hohenpeissenberg Obsesrvatory and Its Contribution to the Developemnt of the Climatology and Aerology', *Izvestiya Atm and Ocean. Phys*, 21, pp. 524-526.

Kinoshita, H. (1977) 'Theory of the Rotation of the Rigid Earth', *Clestial Mech.*, 15, pp. 277-326.

Kuehne, J. and Wilson, C. R. (1991) 'Terrestrial water storage and polar motion', *Journal of Geophysical Research*, 96, (B3), pp. 4337-4345.

Lambeck, K. (1980a) 'Changes in length-of-day and atmospheric circulation', *Nature*, 286, (5769), pp. 104-105.

Lambeck, K. (1980b) *The earth's variable rotation: Geophysical causes and consequences*. Cambridge University Press.

Lambeck, K. and Cazenave, A. (1973) 'The Earth's Rotation and Atmospheric Circulation. I, Seasonal Variations', *Geophys. J.*,, 32, pp. 79-93.

Lambeck, K. and Cazenave, A. (1977) 'The Earth's Variable Rotation: A Discussion of some Meteorological and Oceanic Causes and Consequences', *Phil. Trans. R. Soc. Lond.*, (A 284), pp. 495-506.

Lavallee, D. A., van Dam, T., Blewitt, G. and Clarke, P. J. (2006) 'Geocenter motions from GPS: A unified observation model', *Journal of Geophysical Research B: Solid Earth*, 111, (5).

Lichten, S. M., Marcus, S. L. and Dickey, J. O. (1992) 'Sub-daily resolution of Earth rotation variations with Global Positioning System measurements', *Geophysical Research Letters*, 19, (6), pp. 537-540.

MacMillan, W. D. (1958) *The Theory of the Potential.* Dover reprint, New York.

Marcus, S. L., Chao, Y., Dickey, J. O. and Gegout, P. (1998) 'Detection and Modeling of Nontidal Oceanic Effects on Earth's Rotation Rate', *Science*, 281, (5383), pp. 1656-1659.

Marini, J. W. and Murray, C. W. (1973) 'Correction of Laser Range Tracking Data for Atmospheric Refraction at Elevations Above 10 Degrees', *NASA Goddard Space Flight Center*, Greenbelt MD (1973) Preprint X-591-73-351.

Marotzke, J., Giering, R., Zhang, K. Q., Stammer, D., Hill, C. and Lee, T. (1999) 'Construction of the adjoint MIT ocean general circulation model and application to Atlantic heat transport sensitivity', *Journal of Geophysical Research C: Oceans*, 104, (C12), pp. 29529-29547.

McCarthy, D. D. and Petit, G. (2003) 'IERS Conventions 2003'.

Melbourne, W. (1983) 'MERIT Standards', *UNSO Circular* (167).

Milly, P. C. D. and Shmakin, A. B. (2002) 'Global modeling of land water and energy balances. Part I: The land dynamics (LaD) model', *Journal of Hydrometeorology*, 3, (3), pp. 283-299.

Ming, Z. and Danan, D. (1987) 'A new investigation of the secular drift of the Earth's pole', *Chin. Astron. Astrophys.*, 11, pp. 149-154.

Montenbruck, O. and Gill, E. (2000) *Satellite orbits : models, methods, and applications.* Springer.

Moore, P., Boomkamp, H. J., Carnochan, S. and Walmsley, R. J. (1999) 'FAUST: Multi-satellite orbital dynamics software', *Advances in Space Research*, 23, (4), pp. 785-795.

Moore, P. and Wang, J. (2003) 'Geocentre variation from laser tracking of LAGEOS1/2 and loading data', *Advances in Space Research*, 31, (8), pp. 1927-1933.

Moore, P., Zhang, Q. and Alothman, A. (2005) 'Annual and semiannual variations of the Earth's gravitational field from satellite laser ranging and CHAMP', *Journal of Geophysical Research B: Solid Earth*, 110, (6), pp. 1-14.

Mueller, I. (1969) *Spherical and Practical Astronomy.* Fredrick Ungar, New York.

Munk, W. and MacDonald, G. J. F. (1960) *The Rotation of the Earth: A Geophysical Discussion.* Cambridge University Press.

NASA (2010) *http://space.jpl.nasa.gov/msl/QuickLooks/lageosQL.html*. Available at: http://space.jpl.nasa.gov/msl/QuickLooks/lageosQL.html (Accessed: 02/09/2010).

Nastula, J., Ponte, R. M. and Salstein, D. A. (2002) 'Regional high-frequency signals in atmospheric and oceanic excitation of polar motion', *Advances in Space Research*, 30, (2), pp. 369-374.

Nerem, R. S., Eanes, R. J., Thompson, P. F. and Chen, J. L. (2000) 'Observations of annual variations of the earth's gravitational field using satellite laser ranging and geophysical models', *Geophysical Research Letters*, 27, (12), pp. 1783-1786.

Nikolaidis, R. (2002) *Observation of geodetic and seismic deformation with the Global Positioning System.* Ph.D thesis. Univ. of Calif., San Diego, San Diego.

Peltier, W. R. (1998) 'Postglacial variations in the level of the sea: Implications for climate dynamics and solid-earth geophysics', *Reviews of Geophysics,* 36, (4), pp. 603-689.

Philander, S. G. (1990) 'El Nino, La Nina and the Southern Oscillation', *Academic Press*, pp. 286.

Plag, H.-P., Altamimi, Z., Bettadpur, S., Beutler, G., Beyerle, G., Cazenave, A., Crossley, D., Donnellan, A., Forsberg, R., Gross, R. S., Hinderer, J., Komjathy, A., Ma, C., Mannucci, A. J., Noll, C., Nothnagel, A., Pavlis, E. C., Pearlman, M. R., Poli, P., Schreiber, U., Senior, K., Woodworth, P. L., Zerbini, S. and Zuffada, C. (2009) 'The goals, achievements, and tools of modern geodesy', in *in Global Geodetic Observing System: Meeting the Requirements of a Global Society on a Changing Planet.* Springer, pp. 15-87.

Ponte, R. M. and Stammer, D. (1999) 'Role of ocean currents and bottom pressure variability on seasonal polar motion', *Journal of Geophysical Research C: Oceans,* 104, (C10), pp. 23393-23409.

Ponte, R. M., Stammer, D. and Marshall, J. (1998) 'Oceanic signals in observed motions of the Earth's pole of rotation', *Nature,* 391, (6666), pp. 476-479.

Robertson, D. S. (1991) 'Geophysical applications of very-long-baseline interferometry', *Reviews of Modern Physics,* 63, (4), pp. 899-918.

Rosen, R. D. and Salstein, D. A. (1985) 'Contributions of stratospheric winds to annual and semiannual fluctuations in atmospheric angular momentum and the length of day', *J. Geophys. Res.*, 90, pp. pp 8033-8041.

Rosen, R. D., Salstein, D. A., Eubanks, T. M., Dickey, J. O. and Steppe, J. A. (1984) 'An El Nino signal in atmospheric angular momentum and earth rotation', *Science,* 225, (4660), pp. 411-414.

Rummel, R., Beutler, G., Dehant, V., Gross, R. S., Plag, H.-P., Poli, P., Rothacher, M., Stein, S., Thomas, R., Woodworth, P. L., Zerbini, S. and Zlotnicki, V. (2009) 'Understanding a dynamic planet: Earth science requirements for geodesy', in *Global Geodetic Observing System: Meeting the Requirements of a Global Society on a Changing Planet in 2020.*

Rutherford, D. E. (1964) *Classical mechanics / by D.E. Rutherford.* Oliver and Boyd.

Salstein, D. A. (1993) 'Monitoring atmospheric winds and pressures for Earth orientation studies', *Advances in Space Research,* 13, (11), pp. 175-184.

Salstein, D. A. and Rosen, R. D. (1989) 'Regional contributions to the atmospheric excitation of rapid polar motions', *Journal of Geophysical Research,* 94, (D7), pp. 9971-9978.

Salstein, D. A. and Rosen, R. D. (1997) 'Global momentum and energy signals from reanalysis systems', *7th Conference on Climate Variations, American Meteorological Society*, pp. 344-348.

Seeber, G. (2003) *Satellite Geodesy.* Walter de Gruyter.

Stepanick, M. (1982) 'Interannual atmospheric angular momentum variability 1963-1973 and the Southern Oscillation', *Journal of Geophysical Research,* 87, (C1), pp. 428-432.

Stephenson, F. R., Morrison, L. V. and Whitrow, G. J. (1984) 'Long Term Changes in the Rotation of the Earth', *Philosophical. Trans. Royal. Soc. Lond.*, 351, (1524), pp. 47-70.

Tapley, B. D., Chambers, D. P., Bettadpur, S. and Ries, J. C. (2003) 'Large scale ocean circulation from the GRACE GGM01 Geoid', *Geophysical Research Letters*, 30, (22), pp. OCE 6-1 - OCE 6-4.

Tapley, B. D., Schutz, B. E. and Eanes, R. J. (1985) 'Station coordinates, baselines, and Earth rotation from LAGEOS laser ranging: 1976-1984', *Journal of Geophysical Research*, 90, (B11), pp. 9235-9248.

Torge, W. (2001) *Geodesy*. de Gruyter.

Trupin, A. and Wahr, J. (1990) 'Spectroscopic analysis of global tide gauge sea level data', *Geophysical Journal International*, 100, (3), pp. 441-453.

Trupin, A. S., Meier, M. F. and Wahr, J. M. (1992) 'Effect of melting glaciers on the Earth's rotation and gravitational field: 1965-1984', *Geophysical Journal International*, 108, (1), pp. 1-15.

Vanâiécek, P. and Krakiwsky, E. J. (1986) *Geodesy : the concepts / Petr Vanâiécek, Edward J. Krakiwsky*. North Holland Pub. Co.

Wahr, J., Molenaar, M. and Bryan, F. (1998) 'Time variability of the Earth's gravity field: Hydrological and oceanic effects and their possible detection using GRACE', *Journal of Geophysical Research B: Solid Earth*, 103, (B12), pp. 30205-30229.

Wahr, J. M. (1982) 'The effects of the atmosphere and oceans on the Earth's wobble - I. Theory', *Geophysical Journal, Royal Astronomical Society*, 70, (2), pp. 349-372.

Wang, J. (2004) *Precise orbit determination and altimeter calibration for altimetric satellites* thesis. University of Newcastle.

Wilson, C. A. (1993) 'Contribution of Water Storage to the Excitation of Polar Motion', *Contributions of Space Geodesy to Geodynamics: Earth Dynamics*, Geodynamics 24.

Wilson, C. R. and Haubrich, R. A. (1976) 'Meteorological Excitation of the Earth's Wobble', *Geophys. J. R. Astr. Soc.*, 46, pp. pp 707-743.

Woolard, E. W. (1953) 'Theory of the Rotation of the Earth Around its Center of Mass', *Astron. Papers Amer.*, (15), pp. p1.

Wu, P. and Peltier, W. R. (1984) 'Pleistocene deglaciation and the Earth's rotation: a new analysis', *Geophys. J. R. Astr. Soc.*, 76, pp. 753-791.

Wunsch, C. and Stammer, D. (1997) 'Atmospheric loading and the oceanic "Inverted barometer" effect', *Reviews of Geophysics*, 35, (1), pp. 79-107.

Yoder, C. F., Williams, J. G. and Parke, M. E. (1981) 'Tidal variations of earth rotation', *Journal of Geophysical Research*, 86, (B2), pp. 881-891.